

國立臺灣大學醫學院解剖學暨細胞生物學研究所



博士論文

Graduate Institute of Anatomy and Cell Biology

College of Medicine

National Taiwan University

Doctoral Dissertation

微膠細胞在*NR2E3*基因缺陷小鼠視網膜退化

扮演角色之探討

The Role of Microglia in Retinal Degeneration of

Mice with Defective *NR2E3* Gene

王南凱

Wang, Nan-Kai

指導教授：錢宗良 教授

Advisor: Chien, Chung-Liang, Ph.D.

中華民國 102 年 7 月

July, 2013

國立臺灣大學博士學位論文
口試委員會審定書

論文中文題目：微膠細胞在NR2E3基因缺陷小鼠
視網膜退化扮演角色之探討

論文英文題目：The Role of Microglia in Retinal
Degeneration of Mice with Defective NR2E3 Gene

本論文係王南凱君（學號 D95446004）在國立臺灣大學醫學院
解剖學暨細胞生物學研究所，所完成之博士學位論文，於民國一〇
二年七月二十日承下列考試委員審查通過及口試及格，特此證明

口試委員：

錢宗良 教授

錢宗良 (簽名)

(指導教授)

盧國賢 教授

盧國賢

呂俊宏 教授

呂俊宏

賴旗俊 教授

賴旗俊

楊長豪 教授

楊長豪

系主任、所長

許松蒼

(簽名)

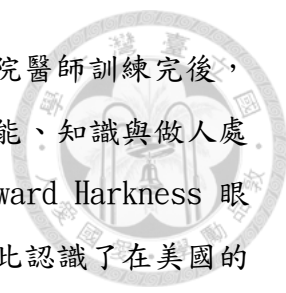
誌謝

從 2006 年 9 月入學至今(2013 年 6 月)已經過了七年，其中休學兩年(2007-2009)得到國科會補助「博士生出國進修」到美國紐約哥倫比亞大學進修。這七年的心情歷經高興、猶豫、難過、掙扎、挫折、絕望，直到論文被接受後，心中才鬆了一口氣，多年的努力終於獲得肯定。一路走來有太多的人要感謝，因為有您們，讓我終於可以順利完成博士學位。

首先感謝啟蒙恩師錢宗良教授的苦心栽培與細心指導，引領我進入基礎醫學研究的殿堂。錢老師是我在台大醫學系就讀三年級時的解剖學課程老師，錢老師教學嚴謹，對於實驗之結果、圖片的品質與資料的呈現要求甚高，使我獲得不少寶貴知識與研究方法，也學到演講的技巧。而且錢老師有時也像朋友一樣，時常替我著想，多方面提供幫助，尤其在我一邊臨床工作，一邊還要到臺大研究所唸書，有時甚至差點趕不上老師的實驗室進度報告，常常要利用晚上或假日來做實驗，錢老師仍然不辭辛勞的教導我多項能力包括嚴謹的研究態度，獨立思考，論文寫作的邏輯觀念，也進一步培養出與同儕或是其他研究機構及跨院區合作的能力。感謝前所長盧國賢老師的從旁指導與包容，尤其對電子顯微鏡之教學讓我獲益良多，也要感謝所內王老師、尹老師、謝老師、陳老師、呂老師、黃老師、賴老師與李老師的教導，每位老師教授的知識與方法，使我在實驗上獲益頗多。另外也要感謝所內老師的大度包涵，能讓我在解剖研究所安心就讀，能回到學校重新當一個學生，這是之前從未想過的事也沒有勇氣去嘗試。感謝論文考試委員：錢老師、盧老師、呂俊宏老師、賴旗俊醫師與楊長豪醫師，對於實驗與論文的指導與幫助甚大，提供許多的寶貴意見，使論文能更加完整。在此同時要感謝解剖所內提供了一個非常優良的研究環境及充沛的研究資源，使我可以多方擴展學習領域，激發自己之潛能。

要感謝的人還包括所內的所有學長姐的指導與學弟妹們的分享激勵，謝謝電顯室的阿美學姐，已畢業的景中醫師、廣文學長、龍坤醫師、旭照醫師，650 實驗室的成員們：玫青與昀佑、娟娟學姐、珮珊、宇立醫師、紀秀、偉君、翠薇、孟琳、喻惠、依雯、宜津、惠敏、佳徽、琬汝、寬誼。因為有你們的幫助與鼓勵，使得這段重回當學生的日子，倍感溫馨，特別感謝紀秀提醒我選課及註冊時間。

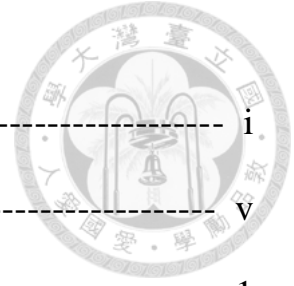
另外要感謝的是長庚醫院眼科部副主任賴旗俊教授，沒有他的提攜收我當



長庚醫院視網膜科臨床研究員，從南部北上來求學的我，在住院醫師訓練完後，可能已經回南部開業去了。賴教授對我亦師亦友，教我臨床技能、知識與做人處事的態度，惠我良多。感謝賴教授派我去美國哥倫比亞大學 Edward Harkness 眼科中心進修，學習國外醫師做事的態度、與專業的知識，也因此認識了在美國的指導老師曾慶齡教授(Stephen H. Tsang)，曾老師照顧我們一家生活的點點滴滴我永遠銘記在心，也一點一點教授視網膜退化基礎與臨床知識，在此期間也認識了林全勝教授(哥倫比亞大學醫學院基因轉殖動物核心負責人)，教授我胚胎幹細胞及轉殖基因鼠技術，由於他們的鼓勵與指導，使我回國後繼續視網膜退化方面之研究；感謝他們的指引，在我遇到困難時，給予我協助，使得研究過程與論文發表得以順利進行並完成。感謝視網膜科內同仁在我博士班時給予臨床上的協助讓我在進修時無後顧之憂。也要感謝眼科前部長林耕國醫師與現任視網膜科主任吳為吉醫師的支持與鼓勵，也要感謝實驗室的聖傑、彩伶、佳穎、品靜。

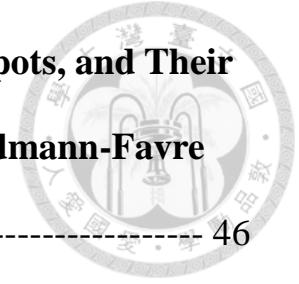
感謝父母的栽培、鼓勵，感謝哥哥王榮礪骨科醫學博士、姐姐王敏姿教育博士在研究的過程中提供我寶貴的經驗；當然也要感謝內人曾韻如醫師的支持，辛苦持家、大兒子紘熙與小兒子紘軒的乖巧聽話，體諒我犧牲家庭生活的時間，使我無後顧之憂；感謝岳父、岳母的支持。在此感謝所有曾經幫助過我的人，也在這一刻終於可以與你們分享我的喜悅。在未來，我會更努力為眼科臨床及基礎研究盡心盡力！

Contents



Acknowledgement-----	i
Abbreviation -----	v
Summary of Dissertation in Chinese -----	1
Summary of Dissertation in English -----	3
Chapter I. General Introduction -----	5
Enhanced S-Cone Syndrome -----	6
Retinal Degeneration 7 (<i>rd7</i>) Mice -----	6
Retinal Pigment Epithelium and Photoreceptor -----	8
Autofluorescent Spot in Retina -----	8
Microglia in Retinal Degeneration -----	9
Transgenic Mice for Macrophage Fas-Induced Apoptosis (Mafia) ----	10
Specific Aims of Current Study -----	11
Figure legends and Figures -----	15
Chapter II. Cellular Origin of Fundus Autofluorescence in Patients	
and Mice with Defective NR2E3 Gene -----	17
Abstract -----	18
Introduction -----	19
Materials and Methods -----	21
Results -----	25
Discussion -----	29
Figure legends and Figures -----	34

**Chapter III. Origin of Fundus Hyperautofluorescent Spots, and Their
Role in Retinal Degeneration in a Mouse Model of Goldmann-Favre**



Syndrome	46
Abstract	47
Introduction	49
Materials and Methods	52
Results	60
Discussion	67
Figure legends and Figures	75
Chapter IV. Conclusion and Future Prospective	93
Bibliography	97
Appendix	104



Abbreviation

AF: autofluorescence, autofluorescent

AMD: age-related macular degeneration

BM: bone marrow

EGFP: enhanced green fluorescent protein

ERG: electroretinogram

ESCS: enhanced S-cone syndrome

IHC: immunohistochemistry

IL-: interleukin-

INL: inner nuclear layer

IPL: inner plexiform layer

GCL: ganglion cell layer

Mafia: macrophage Fas-induced apoptosis

OCT: optical coherence tomography

ONL: outer nuclear layer

OPL: outer plexiform layer

OS: outer segment

RD7: retinal degeneration 7

RPE: retinal pigment epithelium

RT: room temperature

TEM: transmission electron microscop

Tg: transgene

TGF: transforming growth factor

TNF: tumor necrosis factor



中文摘要：

Goldmann-Favre徵候症，也稱為增強型 S-圓錐 (enhanced S-cone) 徵候症，是一個遺傳性視網膜退化疾病，這個退化疾病主要是由感光細胞增加所導致視網膜發育不良和變性。我們先前已經證明在 *rd7* 小鼠 (enhanced S-cone 徵候症小鼠模式) 視網膜中自發性螢光 (AF) 點是來自於微膠細胞，而不是視網膜色素上皮 (RPE) 細胞，這些微膠細胞呈現 F4/80 陽性。大多數微膠細胞出現在視網膜皺褶內 (retinal rosette)，推測這些微膠細胞的出現是幫助視網膜色素上皮細胞吞噬在視網膜皺褶內部分非接觸的感光細胞外節 (outer segment) 的碎片。雖然微膠細胞被認為參與許多神經退化性疾病，然而微膠細胞和導致視網膜退化之間的關係是未知的。

在此次研究中，連續分析視網膜皺褶及視網膜自發性螢光點，我們發現視網膜皺褶出現時間點較自發性螢光點早，這表示微膠細胞是在外核層折疊後被招募來的。我們推測微膠細胞在初期是扮演幫忙的角色，主要是在維護感光細胞和視網膜色素上皮細胞之間的環境並清理感光細胞外節的碎片。

利用轉殖基因小鼠 (Mafia) 的優勢，我們藉由二代交叉繁殖成功配種出 *rd7/rd7;Tg/Tg* 小鼠。這種小鼠體內的微膠細胞都表現綠色螢光及自殺基因，它可以藉由 AP20187 (FA506 dimerizer 的) 引發 Fas 所導致的細胞凋亡。我們發現這些 80% 綠色螢光細胞同時表現 Iba-1 (常駐微膠細胞標記)。我們發現在剔除全身血液循環中的微膠細胞後，視網膜中仍然可以偵測到綠色螢光細胞，依此推測 AP20187 無法通過血液-視網膜屏障；所以只有血液循環中的微膠細胞可以被殺死。我們更發現在剔除全身血液循環中的微膠細胞後，小鼠呈現後期視網膜退化的徵兆。

視網膜中自發性螢光 (AF) 點的增加和常駐微膠細胞的複製增生有關。常駐微膠細胞的複製增生伴隨著發炎細胞因子 (cytokine) 的表達增加 (如 IL-1 β , IL-6, and TNF- α)。這種發炎細胞因子的增加可能加速視網膜變性。這項研究不只確定發炎

在視網膜退化中發病機制的角色，也可以利用參與其中的細胞因子作為今後治療視網膜退化的方向。

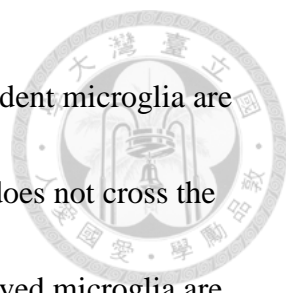




Abstract:

Goldmann-Favre Syndrome, also known as enhanced S-cone syndrome, is an inherited retinal degeneration in which a gain of photoreceptor cell types results in retinal dysplasia and degeneration. We demonstrated previously that microglia that are stained positively for F4/80, rather than retinal pigment epithelium (RPE) cells, may contribute to the hyper-autofluorescent (AF) spots observed in the retina of *rd7* mice, which are a mouse model of enhanced S-cone syndrome (ESCS). Most of these cells were present inside retinal rosettes and presumably help RPE cells to phagocytose the noncontact outer segment debris located within the rosettes. Although microglia have been implicated in the pathogenesis of many neurodegenerative diseases, the fundamental role of these cells in this disease is unknown.

In the current study, sequential analyses suggest that microglia are recruited and appear after outer nuclear layer folding. Using mice with the macrophage Fas-induced apoptosis (Mafia) transgene, we generated double-mutant mice and studied the role of the resident retinal microglia. Microglial cells in these double-mutant mice express enhanced green fluorescent protein (EGFP) and a suicide gene, which can trigger Fas-mediated apoptosis via systemic treatment with AP20187 (FA506 dimerizer). We demonstrated that more than 80% of the EGFP⁺ cells in *rd7/rd7;Tg/Tg* mice retina



expressed Iba-1, which is a resident microglia marker. We found resident microglia are still present in the retina after applying AP20187 because AP20187 does not cross the blood-retina barrier. Hence, only circulating bone marrow (BM)-derived microglia are depleted. In addition, depletion of circulating BM-derived microglia accelerates retinal degeneration in *rd7* mice. An increased number of autofluorescent (AF) spots are a consequence of resident microglia proliferation which in turn establishes an inflammatory cytokine milieu via the upregulation of *IL-1 β* , *IL-6*, and *TNF- α* expression. This inflammation likely accelerates retinal degeneration. This study has identified not only inflammation as a critical step in the pathogenesis of retinal degeneration, but also the involvement of specific cytokine genes that could serve as future treatment targets in retinal degenerations.

Chapter I

General Introduction

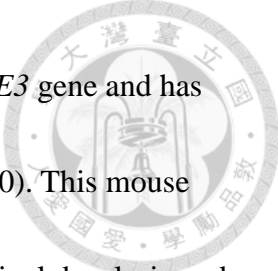




Enhanced S-Cone Syndrome

Most hereditary retinal degeneration disorders affect the mature photoreceptor topography by reducing the number of rod and cone photoreceptor neurons through apoptotic mechanisms. Enhanced S-cone syndrome (ESCS; OMIM 268100; <http://www.ncbi.nlm.nih.gov/omim/> Online Mendelian Inheritance in Man; NCBI, Bethesda, MD) is a relatively slowly progressive autosomal recessive rod-cone degeneration caused by mutations in the orphan nuclear receptor transcription factor NR2E3 (OMIM: 604485). ESCS is the only known retinal dystrophy to date that appears to manifest as a gain in the function of cone photoreceptor subtype (Smith 2001). *NR2E3* mutations were first identified in patients with ESCS, but more recent studies have demonstrated that mutations in *NR2E3* are also common causes of clumped pigmentary changes in Goldmann-Favre syndrome, clumped pigmentary retinal degenerations, autosomal recessive retinitis pigmentosa and autosomal dominant retinitis pigmentosa (Gerber et al. 2000; Haider et al. 2001; Milam et al. 2002; Sharon et al. 2003; Wright et al. 2004; Chavala et al. 2005; Hayashi et al. 2005; Coppieters et al. 2007).

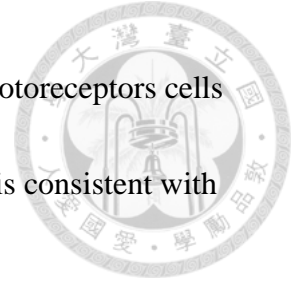
Retinal degeneration 7 (rd7) mice



The spontaneous mutant *Nr2e3^{rd7}(rd7)* mice carry a mutation in *NR2E3* gene and has been used to study as a mouse model for ESCS (Akhmedov et al. 2000). This mouse serves as model where a gain of photoreceptor cell types results in retinal dysplasia and degeneration. At weaning age, fundus examination demonstrates numerous white dots throughout the retina. However, as time progresses, the dots decrease in number while becoming larger and irregular in shape. By 16 months, retinal vessels are attenuated and there is pigment mottling, but the spots disappear (Akhmedov et al. 2000). The morphological changes correlate well with the clinical findings. The spots are due to the widespread occurrence of prominent folds in the outer nuclear layer that create pseudorosettes reminiscent of those seen in retinal dysplasia. These folds occur as early as P14 (Haider et al. 2001). One or more lightly pigmented cells that contain cellular debris are usually present in the center of each pseudorosette (Akhmedov et al. 2000). It has not been determined whether these cells are mobilized RPE cells or macrophages. Therefore, recognizing these cells and investigating the origin of these cells are interesting and important issues.

By 5 months of age, the outer retinal folds begin disappear, coincident with the disease in spot number on clinical examination. By 16 months of age, the folds disappear concurrent with a thinning of the outer nuclear layer and outer segments, although neither layer disappears as they do in other retinal degenerations. Electron

microscopy demonstrates that the inner and outer segments of the photoreceptors cells seen on light microscopy contain pigment granules and cellular debris consistent with phagocytosis.



Retinal pigment epithelium and photoreceptor

The retinal pigment epithelium (RPE) is the pigmented cell layer just outside the neurosensory retina that nourishes retinal visual cells, and is firmly attached to the underlying choroid and overlying retinal visual cells. Daily phagocytosis of photoreceptor outer segments is a critical maintenance function performed by the RPE to preserve vision. RPE is also involved in the vitamin A cycle where it isomerizes all trans retinol to 11-cis retinal.

Autofluorescent spot in retina


Aging RPE accumulates lipofuscin, which includes

N-retinylidene-*N*-retinylethanolamine (A2E) as the major autofluorescent component.

Excessive accumulation of lipofuscin granules in the lysosomal compartment of retinal

pigment epithelium cells (RPE) is considered a common downstream pathogenetic

pathway in many hereditary and complex retinal diseases, including age-related macular



degeneration (Schmitz-Valckenberg et al. 2008). Fundus autofluorescence imaging has been shown to be useful with regard to understanding of pathophysiologic mechanisms, diagnostics, phenotype-genotype correlation, identification of predictive markers for disease progression, and monitoring of novel therapies. Although we can use the characteristics of spectral wavelength of A2E to investigate if the autofluorescence in patient's retina originated from RPE or not, there is no available machine to do this *in vivo* study on patients. Therefore, recognizing autofluorescent material containing cells and investigating the origin of these cells in disease mutant mice can provide more information when we would like to apply this technique on patients.

Microglia in retinal degeneration

Microglia, which are part of the mononuclear phagocytic system, act as the first and main form of active immune defense in the central nervous system, including the retina.

Microglia are the tissue-infiltrating counterpart to monocyte, a subset representing 5% of circulating leukocytes. Microglia are known to exist in various states of activation.

Resting or scavenging microglia are nature's garbage disposal, entering tissue for the purpose of safe removal of debris and repair of damaged extracellular matrix.

Accumulation of outer segment debris and microglia infiltration has been associated

with the development of age-related macular degeneration (AMD) (Wenzel et al. 2005).

In photoreceptor damage or degeneration, microglia invade the retina to support the role of RPE in phagocytosing outer segment debris (Hoppeler et al. 1988; Gordon et al.

2002). Thus, infiltration of microglia can be used as a marker for early phases of various

degenerative conditions, and their subsequent disappearance correlates with loss of

hyperautofluorescent spots in later stages of retinal degeneration. However, the

activated microglia produce pro-inflammatory and angiogenic factors which are

potential candidates for regulators of photoreceptor apoptosis. These cells can damage

photoreceptors by production of oxidants, cytokines, and prostaglandins. They can also

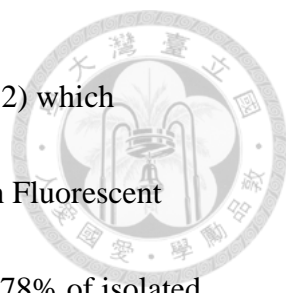
induce neovascularization by release of angiogenic stimuli, including vascular

endothelial growth factor and tumor necrosis factor.

Interestingly, it has not been determined whether these cells are pathological or protective roles in retinal degeneration. To investigate the role of macrophage can help us to develop new therapies in retinal degeneration patients.

Transgenic mice for macrophage Fas-induced apoptosis (Mafia)

These transgenic mice have an inducible Fas suicide/ apoptotic system driven by the mouse *Csf1r*, colony stimulating factor 1 receptor promoter. The transgene insert



contains a mutant human FK506 binding protein 1A, 12kDa (FKBP12) which preferentially binds the dimerization drug AP20187. Enhanced Green Fluorescent Protein (EGFP) fluorescence and transgene expression is detected in 78% of isolated peritoneal cells. EGFP fluorescence is variable among tissues (B- and T-cells do not express EGFP). Administration of the dimerizing reagent, AP20187, induces apoptosis in macrophages and dendritic cells (intravenous injection of dimerizer is recommended, since the intraperitoneal route can elicit peritoneal adhesions). In treated mice, EGFP fluorescing peritoneal and bone marrow macrophage numbers are depleted by more than 90%, and macrophage numbers in blood, spleen, lung and thymus by more than 70% (Burnett et al. 2004). Seven days after cessation of treatment, the EGFP fluorescing macrophage and dendritic cell populations rebound. Homozygous mutant mice are viable, fertile, normal in size and do not display any gross physical or behavioral abnormalities. With these mice, we can investigate the possible physiology change after depleting the macrophages. From now on, we will use “*Tg/Tg*” to refer mice with this transgene.

Specific aims of current study

In *rd7* mice, abnormal retinal morphology (retinal rosette) appears as early as P14, and

begins to disappear at 5 months old (Akhmedov et al. 2000). By 16 months of age, these folds disappear concurrent with a thinning of the outer nuclear layer and outer segments.

The concordance of the appearance and disappearance of the white spots observed over entire retina with the waves seen under histology suggests that these spots are associated with the retinal rosettes (Akhmedov et al. 2000). To investigate the relationship between retinal degeneration, autofluorescence and macrophage infiltration, we will need to establish the sequence of appearance of autofluorescent material, macrophages, and retinal rosettes by performing immunohistochemical staining on serial sections and flat mount retina of *rd7/rd7* mice at different time points.

The second purpose is to identify autofluorescent cells and investigate the origin of these cells containing autofluorescence in retinal degeneration mouse retina by two generation backcrossing *rd7/rd7* mice with *Tg/Tg* mice. With serial sections on transgenic *Tg/Tg; rd7/rd7* mice retina at different time point, we will know whether BM-macrophage contributes to these autofluorescence. Our study will demonstrate that macrophages in the degenerated retina are from bone marrow instead of local tissue. If we can detect EGFP positive cells in the retinal section, then we assume these macrophages are from bone marrow rather than local tissue. Some studies used the advantage of bone marrow transplantation and showed that these macrophages are from bone marrow in some photoreceptor damage (Hoppeler et al. 1988; Gordon et al. 2002;

Wenzel et al. 2005). Due to limitation of equipment and facility, we will use the advantage of *Tg/Tg* mice.



The third purpose is to determine if macrophages serve a pathological or protective role in a mouse retinal degeneration model by applying AP20187 on *Tg/Tg; rd7/rd7* mice. We will take advantage of the *Tg/Tg; rd7/rd7* mice to determine if genetic ablation of macrophages will accelerate or delay the retinal degeneration.

From our preliminary study in *rd7* mice, we believe that photoreceptor outer segments within the rosettes are inefficiently phagocytosized by RPE and the accumulation of outer segment debris may in turn trigger macrophage infiltration to remove the accumulating outer segment waste, and thus explain the increased autofluorescence within macrophage cytoplasm. However, the activated macrophages produce pro-inflammatory and angiogenic factors. Macrophages can damage photoreceptors by production of oxidants, cytokines, and prostaglandins. Whether the activated macrophage is helping or damaging the retina is not known.

In addition, because inflammation in retinal degeneration leads to retinal fibrosis and severe vision loss, it is important to understand the factors that regulate macrophage activity and determine their control of inflammation. *Rd7/rd7* mice are a good model of studying retinal degeneration with macrophage. By using the advantage of *Tg/Tg* mice, we can explore the underlying mechanism between inflammation and retinal

degeneration.

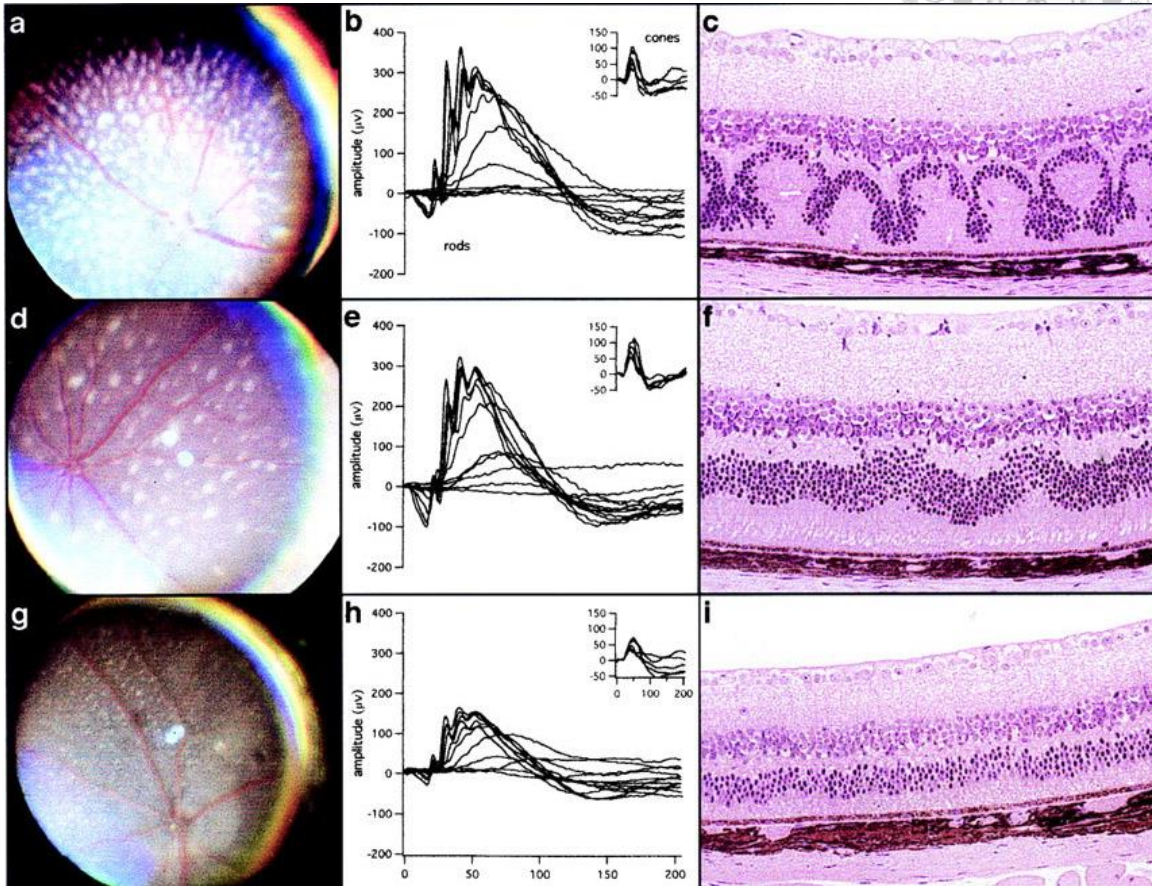


Chapter 1, Figure 1.



Figure 1. Light microscopic examination of histological preparations shows outer nuclear layer waves, whorls, and rosettes in the retinas of homozygous *rd7* mutants by 1 mo of age (**C**). These waves flatten out by 5 mo and are gone by 16 mo (**f and i**). Flattening of the waves is concordant with disappearance of the retinal spots. Late-onset progressive retinal degeneration is also observed. Photoreceptor cells degenerate as evidenced by the reduction of the outer nuclear layer from the normal thickness of 10 rows of nuclei to only 4 or 5 rows by 16 mo. Histological changes correlate directly with functional changes, as shown by electroretinography (**b,e, and h**). (Akhmedov et al. 2000)

Chapter 1, Figure 1.



(Akhmedov et al. 2000)

Chapter II



Cellular Origin of Fundus Autofluorescence in Patients and Mice with Defective *NR2E3* Gene



Abstract

Aim: To characterize new clinical features in a family with enhanced S-cone syndrome (ESCS) and investigate the pathogenesis of these clinical features in the homozygous

Nr2e3^{rd7rd7} (*rd7*) mutant mice.

Methods: Four patients from an affected family were included for genotypic and phenotypic study. Eye tissues from *rd7* mice were used to detect a possible relationship between macrophages and autofluorescent material by immunohistochemistry (IHC) staining.

Results: Homozygous mutation in R311Q in *NR2E3* was detected in this family. Color photographs revealed that white dots do not correlate to hyperautofluorescent spots seen in autofluorescence imaging of the macula. OCT showed rosette-like lesions similar to those found in *rd7* mice histology sections. From IHC analysis, we observed that F4/80 (a pan macrophage marker), and autofluorescence were co-localized to the same cells within the retina rosettes.

Conclusions: Retinal structure of a young ESCS patient with homozygous R311Q mutation in the *NR2E3* gene is similar to that seen in the *rd7* mice. The macrophages were found to contain autofluorescent materials in the retinal rosettes of *rd7* mice. Our data are consistent with macrophage infiltration contributing to the hyper-autofluorescent spots found in our patients.



Introduction

Enhanced S-cone syndrome (ESCS; OMIM 268100; [http://](http://www.ncbi.nlm.nih.gov/omim/)

www.ncbi.nlm.nih.gov/omim/ Online Mendelian Inheritance in Man; NCBI, Bethesda,

MD) is a relatively slowly progressive autosomal recessive rod-cone degeneration

caused by mutations in the orphan nuclear receptor transcription factor *NR2E3* (OMIM:

604485). *NR2E3* encodes a retinal nuclear receptor that is a ligand-dependent

transcription repressor of cone-specific genes in rod photoreceptors (Chen et al. 2005).

The *NR2E3* protein is part of a large family of nuclear receptor transcription factors that

is homologous to an orphan nuclear receptor, *Nr2e1* (formerly known as *tailless* or

TLX), which is involved in the development and maintenance of normal function of the

central nervous system (CNS) in *Drosophila* and mammals. *NR2E3* is expressed in

mitotic progenitor cells during development and its increased expression in cone cells

may be due to a prolonged period of cone proliferation, which is followed by a gradual

increase in apoptosis. *NR2E3* appears to be a dual regulator, suppressing cone cell

proliferation in mitotic cells and promoting rod cell genesis in postmitotic cells. *NR2E3*

mutations were first identified in patients with ESCS, but more recent studies have

demonstrated that mutations in *NR2E3* are also common causes of clumped pigmentary

changes in Goldmann-Favre syndrome, clumped pigmentary retinal degenerations,

autosomal recessive retinitis pigmentosa and autosomal dominant retinitis pigmentosa (Gerber et al. 2000; Haider et al. 2000; Milam et al. 2002; Sharon et al. 2003; Wright et al. 2004; Chavala et al. 2005; Hayashi et al. 2005; Coppieters et al. 2007).

The spontaneous mutant *Nr2e3^{rd7}* (*rd7*) mice have a mutation in *NR2E3* gene (Akhmedov et al. 2000). This mutant mouse displays increased number and proportion of photoreceptors with S-cone phenotype and abnormal lamination of the outer nuclear layer (ONL) (Akhmedov et al. 2000; Haider et al. 2001).

With confocal scanning-laser ophthalmoscope and spectral domain optical coherence tomography we discovered similar features in a patient. In addition, we demonstrated the origin of these unique clinical features in the homozygous *Nr2e3^{rd7}* (*rd7*) mutant mice.



Materials and Methods

Phenotypic Studies


Four patients from an affected family (6, 8, 35, and 46 years of age) were enrolled with the approval of the institutional review board protocol #AAAB6560 at Columbia University. The tenets of the Declaration of Helsinki were followed.

All patients underwent complete ophthalmic evaluation after informed consent was obtained. Fundus photographs, retinal pigment epithelium (RPE) autofluorescence (AF), Fourier-domain optical coherence tomography (OCT) and electroretinogram (ERG) were performed in the two children.

Genetic Analyses

The coding region of *NR2E3* was sequenced for disease-causing mutations in all patients. DNA was extracted from peripheral blood with the QIAamp DNA Mini Kit (Qiagen Inc., Valencia, CA). Extracted genomic DNA was amplified by polymerase chain reaction (PCR) using primers and cycling temperature as previously described (Audo et al. 2008). The PCR products were purified (QIAquick PCR Purification Kit, Qiagen Inc., Valencia, CA) and sequenced.

Autofluorescence Imaging



Autofluorescence images were obtained using a confocal scanning-laser ophthalmoscope (cSLO, Heidelberg Retina Angiograph 2, Heidelberg Engineering, Dossenheim, Germany) by illuminating the fundus with argon laser light (488 nm) and viewing the resultant fluorescence through a band pass filter with a short wavelength cut-off at 495 nm (von Ruckmann et al. 1995; Robson et al. 2003; Robson et al. 2006; Tsang et al. 2007; Tsui et al. 2008; Tsui et al. 2008).

Optical Coherence Tomography (OCT)

Spectral domain optical coherence tomography (SD-OCT) images were obtained using the Cirrus Spectral Domain OCT from Zeiss (Carl Zeiss Meditec Inc., Dublin, CA, USA). The acquisition protocols included five-line raster scans. Three scans were performed on each eye, and the one with the best signal strength was selected for the final analysis.

Electroretinogram (ERG) Testing

Full-field ERG were performed with silver-impregnated fiber electrodes (DTL; Diagnosys LLC, Littleton, MA) and incorporated the ISCEV Standards (Holder et al. 2007). The minimum protocol incorporates the rod-specific and standard bright flash ERGs, both recorded after a minimum of 20 min dark adaptation. Following 10 min of light adaptation, the photopic 30 Hz flicker cone and transient photopic cone ERGs were recorded. S-cone ERGs used a blue stimulus (445 nm, 2-12 cd/m²) on an orange

background (620 nm, 100 cd/m²) (Audo et al. 2008).

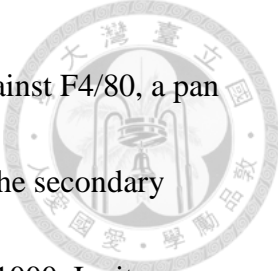


Whole Mount Eyecup

To better understand the mechanisms underlying the clinical findings in our patients, we acquired the *Nr2e3^{rd7}* mutant mice, a mouse model for ESCS, from Jackson laboratory (stock #004643, Bar Harbor, Maine, United States). Eyes from five week-old *Nr2e3^{rd7}* mice and eight week-old C57BL/6J mice (used as a control) were enucleated and placed in 4% paraformaldehyde for one hour at room temperature. The cornea and lens were removed from each eye under a surgical microscope. The whole eyecups were flattened by means of four radial cuts and mounted with mounting medium (VECTASHIELD, Burlingame, CA). Autofluorescence was detected by standard fluorescence microscopy.

Immunohistochemistry (IHC)

Whole eyecups were prepared as described above, and frozen in optimum cutting temperature compound (Tissue-Tek OCT, Miles Laboratories, Elkhart, IN). Frozen eyes were cryosectioned using a thickness of 10µm. Blocking was performed using 10% donkey serum in PBS with 0.3% Triton X-100 (blocking solution) for 30 min at room temperature (RT). The sections were then incubated with the primary antibodies diluted in 4% donkey serum in PBS with 0.1% Triton X-100 for 2 hours at RT. The samples were subsequently incubated for 40 minutes at RT with the secondary antibodies diluted



in PBS with 0.1% Triton. The primary antibody used was directed against F4/80, a pan macrophage marker, (dilution 1:500, eBioscience, San Diego, CA). The secondary antibody used was: Alexa Fluor 488 donkey anti-rat IgG (dilutions 1:1000, Invitrogen, Carlsbad, CA). After washing three times with PBS, the retinas were mounted with mounting medium containing the nuclear dye DAPI (VECTASHIELD, Burlingame, CA) and viewed under a fluorescence microscope (Leica DM 5000 B, Wetzlar, Germany). Images were digitally merged to assess for triple labeling.



Results

Genetic Studies


Direct sequencing of the *NR2E3* gene from the proband revealed a homozygous missense mutation 932G→A in exon 6 coding for the R311Q residue (fig 1). His asymptomatic elder brother (8 year old) and consanguineous parents (first cousins) were heterozygous for a mutation at the same DNA site.

Clinical Examination

Case 1

A 6-year-old boy presented with poor night vision since the age of 2. No history of prematurity or developmental abnormalities was noted, and past ocular history was also unremarkable. The patient is a product of consanguineous mating. Two months prior to presentation, the boy was suspected of having chorioretinitis after failing a standard vision screening at his elementary school. Serum examination was negative for inflammatory and infectious markers, including toxoplasmosis, toxocara, cat scratch disease, Lyme disease and syphilis.

On examination, visual acuity was 20/800 in the right eye and 20/40 in the left eye. The intraocular tension was 13 mmHg in the right eye and 15 mmHg in the left eye. The eye position was orthophoric with full motility. Biomicroscopy was unremarkable except for



1+ vitreous cells in both eyes. Dilated fundus examination of both eyes revealed multiple whitish subretinal deposits and several prominent lesions within the macula (fig 2A). Fundus autofluorescence imaging (FAF) showed hyperautofluorescence in the macula and mid-peripheral retina (fig 3A). Spectral-domain optical coherence tomography (OCT) showed intraretinal cystic changes surrounding the lesion and rosette-like lesions in the mid-peripheral retina, with loss of normal retinal lamination (fig 3B). There was no cystoid macular edema or foveal schisis in the left eye.

Fluorescein angiography showed hyperfluorescence that increased with time, suggesting chronic subretinal neovascularization and fibrosis. There was no peripheral vascular leakage. Full-field ERG shows three characteristic findings: 1). no rod responses; 2) the waveforms of scotopic maximal response are very identical to the transient photopic responses except the size (circles); 3) the amplitude of a wave in the transient photopic response is larger than amplitude of photopic 30 Hz flicker. S-cone-specific ERG was of remarkably high amplitude and confirmed the diagnosis of ESCS (fig 4).

Case 2

The proband's older brother was an asymptomatic 8-year-old boy. The best corrected visual acuity was 20/20 (OU) and biomicroscopy was unremarkable. Dilated fundus examination of both eyes revealed a normal retinal appearance without white dots (fig 2B). FAF showed several increased hyperautofluorescence spots around the disc and

arcades (fig 3C). OCT showed normal retinal lamination without rosette-like lesions (fig 3D). ERG results were normal (fig 4).



Case 3 & 4

The proband's parents were first cousins and both were beta-thalassemia carriers.

Comprehensive ophthalmic evaluation was unremarkable and there were no fundus white dots or hyper-autofluorescence spots in either parent.

Examination of $Nr2e3^{rd7}$ mutant mice

Dilated fundus photography from 5-week-old $Nr2e3^{rd7}$ mutant mice showed diffuse subretinal white dots (fig 5B), and whole mount eyecup from age-matched $Nr2e3^{rd7}$ mice demonstrated similar hyperautofluorescent spots (fig 5D). Images obtained from 8-week-old wild type C57BL/6J mice showed no white dots in the retina (fig 5A) and no hyperautofluorescent spots (fig 5C). Autofluorescence imaging of retina from $Nr2e3^{rd7}$ mice has chromophores with a wide spectrum of emission in the visible wavelengths with the highest intensity around 550 nm when excited at 436 nm (fig 5E).

DAPI staining of retina from $Nr2e3^{rd7}$ mice demonstrated rosette and whorl-like structures in the retina and the autofluorescent materials were localized to the region between the outer nuclear layer (ONL) and retinal pigment epithelium (RPE), and mostly within the rosettes (fig 6A). IHC performed with the macrophage marker F4/80 demonstrated that the macrophages were within the rosettes, and the autofluorescent

materials were in the cytoplasm of these macrophages (fig 6B).





Discussion

Fundus examination

Nummular pigment clumping along the vascular arcades, the classical retinal phenotype seen in adult ESCS patients, is not observed in our proband. Findings from recent reports of young ESCS patients suggest that subtle pigmentary changes with white dots represent an early stage of the disease process (Sharon et al. 2003; Khan et al. 2007), and these white dots progress to characteristic clumped retinopathy in late adulthood (Sharon et al. 2003). This phenomenon suggested why there were few reports described similar fundus white dots from the ESCS patients. Although a normal fundus appearance without subretinal white dots has been reported in some case series with 6-10 year-old patients (Audo et al. 2008; Vaclavik et al. 2008), those patients are homozygous for a missense mutation (R104W) that is different from the R311Q mutation seen in our case series. The R311Q substitution, the most common ESCS allele, is found in ~45% of patients (Haider et al. 2000). Whether there is genotype-phenotype correlation requires further studies to analyze younger ESCS patients to explain clinical characteristics variability.

Optical Coherence Tomography (OCT)

Foveal schisis has been reported in patients with ESCS (Haider et al. 2000; Audo

et al. 2008; Vaclavik et al. 2008). In case 1, there is no foveal schisis in the left eye, however, there are intraretinal cysts around the lesion in the macula of the right eye (fig 3B).



Patients with ESCS have histologically dysmorphic retinas in the ONL (Peyman et al. 1977; Milam & Jacobson 1990; Milam et al. 2002) and our results demonstrate that spectral-domain OCT can detect such rosette formation in the ONL and can be used to monitor photoreceptor loss as the disease progresses.

Autofluorescence imaging

The ring of increased AF in the macula area has been suggested to be associated with fundus white dots and retinal rosette (Audo et al. 2008). In case 1, hyperautofluorescent spots are not limited in the macula area but also extended beyond the arcades. The hyperautofluorescent spots outside the macula area correspond to the fundus white dots (fig 3A), whereas the hyperautofluorescent spots within the macula do not correspond to the white dots or pigmentary clumps. In addition, the heterozygous brother (case 2) does not have white dots visible funduscopically, but does have several hyperautofluorescent spots along the arcades. Thus, the hyperautofluorescent spots and fundus white dots may have different origins.

Figure 3C showed several hyperautofluorescence dots around the disc and arcades in case 2. Whether heterozygosity with the mutant *NR2E3* allele has any phenotypic

manifestation is unknown; the absence of these hyperautofluorescent dots in the asymptomatic consanguineous parents suggests that they may be transient in nature and only detectable in heterozygous children.




Fundus white dots and retinal rosettes of $Nr2e3^{rd7}$ mutant mice

Subretinal white dots (Akhmedov et al. 2000) and abnormal lamination of the ONL (Akhmedov et al. 2000; Haider et al. 2001) have been described in $Nr2e3^{rd7}$ mutant mice. The $Nr2e3^{rd7}$ mutant mice have numerous white dots over the entire retina at 1 month old that gradually decrease by five months of age, and disappear completely by 16 months (Akhmedov et al. 2000). The concordance of the appearance and disappearance of the white spots observed over entire retina with the waves seen under histology suggests that these spots are associated with the retinal rosettes (Akhmedov et al. 2000). Milam *et al* described an approximately 2-fold increase in total cones from a 70-year-old R311Q patient (Milam et al. 2002), and Haider *et al* described a 1.5-2.0 fold increase of S-cones in $Nr2e3^{rd7}$ mice (Haider et al. 2001). Whether the excessive numbers of S-cones contribute to rosette formation is uncertain.

Autofluorescent spots of $Nr2e3^{rd7}$ mutant mice

In $Nr2e3^{rd7}$ mice retina, we found that the autofluorescent materials were present in the cytoplasm of macrophages situated within and sometimes adjacent to the retinal rosettes (fig 6). Immunolocalization studies (fig 6) demonstrate that the chromophores



are found within macrophages instead of RPE. In addition, the multiple spectral wavelength (fig 5) of the hyperautofluorescent spots from *Nr2e3^{rd7}* mutant mice suggests that these spots contain chromophores in addition to A2E, which has an emission maxima of 565 to 570 nm (Sparrow et al. 1999). In a manner analogous to that seen in *Nr2e3^{rd7}* mutant mice, we can expect that hyperautofluorescent spots in our case may not from RPE cells, but macrophages. Further in vivo study on ESCS patient with different spectral wavelength can help to determine the origin of these hyperautofluorescent spots.

There are two probable explanations for the presence of macrophages in *Nr2e3^{rd7}* mice retina. First, the macrophages are recruited into the retina to remove apoptotic photoreceptors found as early as in P30 *Nr2e3^{rd7}* retina (Sparrow et al. 1999). Second, photoreceptor outer segments within the rosettes are inefficiently phagocytosized by RPE due to the abnormal retinal structure, and the accumulation of outer segment debris may in turn trigger macrophage infiltration to remove the waste. However, our IHC studies suggest that these fluorophores within macrophages are derived from the outer segment, rather than apoptotic photoreceptors.

Similar accumulation of outer segment debris and macrophage infiltration has been associated with the development of age-related macular degeneration (AMD) (Wenzel et al. 2005). In photoreceptor damage or degeneration, macrophages invade the

retina to support the role of RPE in phagocytosing outer segment debris (Hoppeler et al. 1988; Gordon et al. 2002). Thus, infiltration of macrophages can be used as a marker for early phases of various degenerative conditions, and their subsequent disappearance correlates with loss of hyperautofluorescent spots in later stages of retinal degeneration.

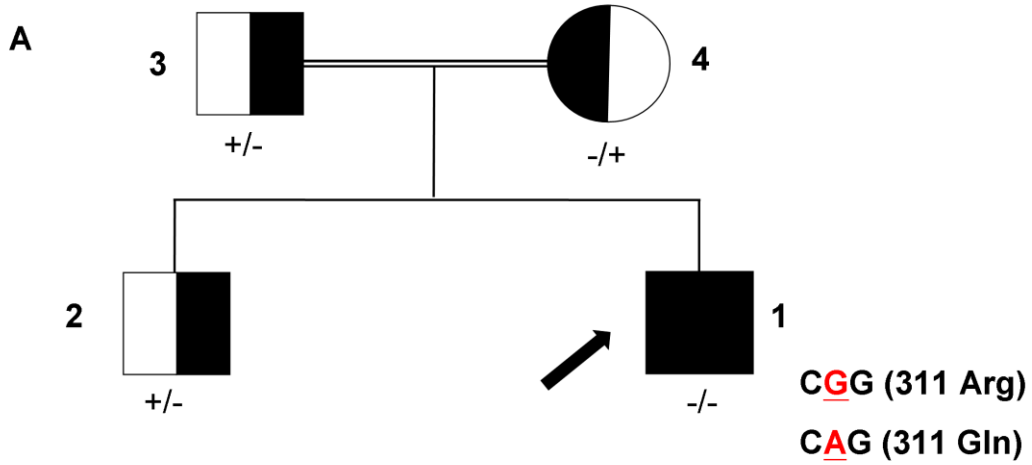
In summary, we discovered several novel features (fundus white dots, hyperautofluorescent spots and rosette-like retinal lesions) observed in a child homozygous for the R311Q allele in *NR2E3*. Findings from the *Nr2e3^{rd7}* mutant mice suggest that fundus hyperautofluorescent lesions are likely to be contributed by macrophages.

Chapter 2, Figure 1.

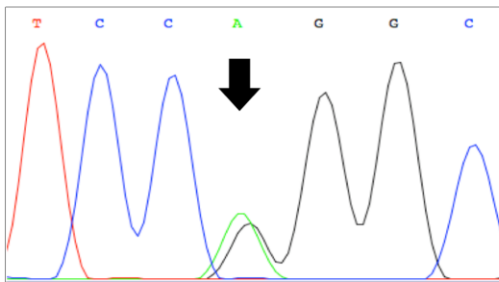


Figure 1. (A). Pedigree of a family in which mutation in the *NR2E3* gene were identified. A mutant allele is indicated by (-); a normal allele is indicated by (+). Arrow shows the proband (1, homozygous), and the other members are heterozygous. **(B).** Direct DNA sequencing from proband's consanguineous parents and brother showed heterozygous base-substitution at 932G→A in exon 6. **(C).** Direct sequencing from the proband revealed a homozygous base-substitution at 932G→A with a predicted missense mutation of R311Q (CGG to CAG).

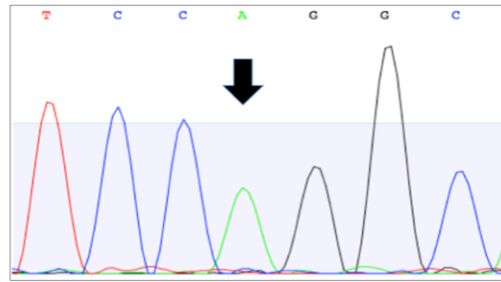
Chapter 2, Figure 1.



B Heterozygous sequence



C Homozygous sequence



Chapter 2, Figure 2.

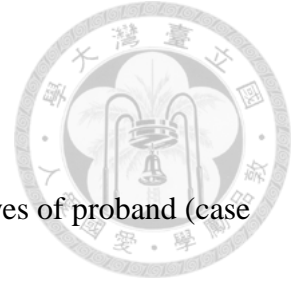
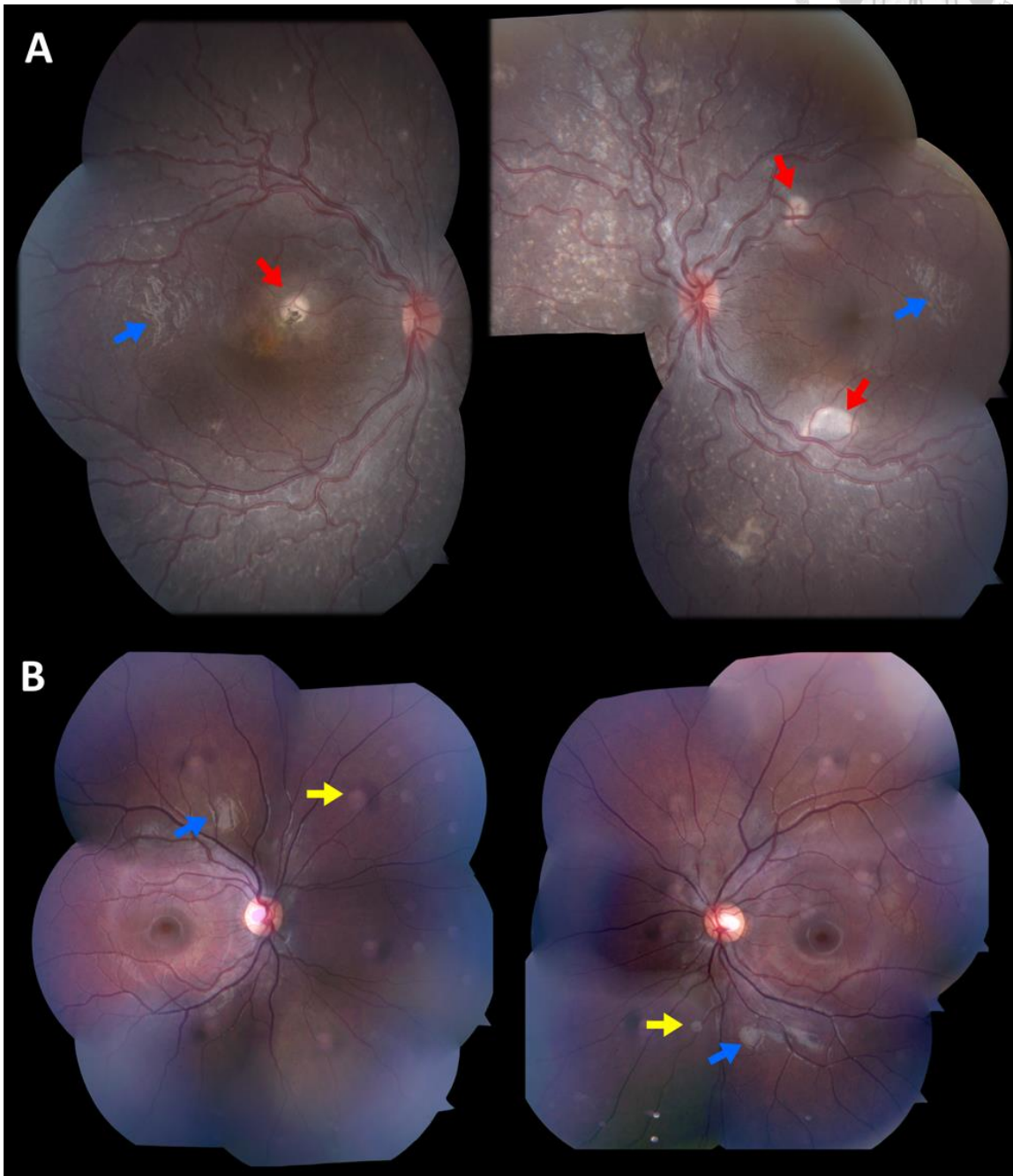


Figure 2. (A). Composite fundus photographs of the right and left eyes of proband (case 1) showing multiple subretinal white deposits and prominent lesions in the macula (red arrows). **(B).** Composite fundus imaging of the right and left eyes of case 2 exhibited a normal retina without subretinal deposit. There are some artifacts arising from photography (yellow arrows illustrate examples of artifacts from the camera lens, blue arrows show reflections of the nerve fiber layer).

Chapter 2, Figure 2.

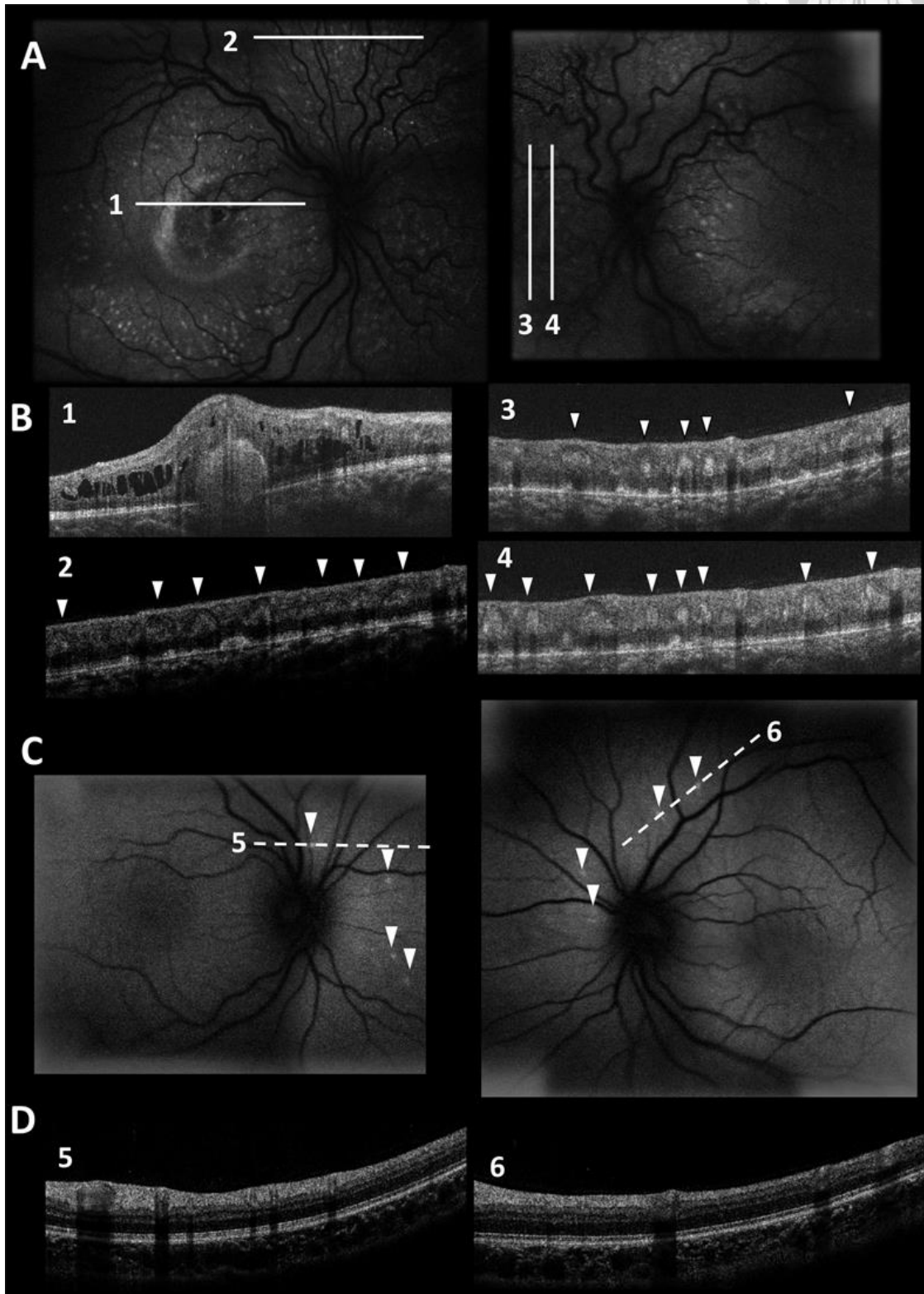


Chapter 2, Figure 3.



Figure 3. (A). Fundus autofluorescence exam (FAF) of proband (case 1) showed hyper-autofluorescent spots in the macular area and in the mid-peripheral retina. **(B).** Optical coherence tomography (OCT) 1, 2, 3, and 4 correspond to scanning sections in fig A. 1 showed cystic changes around the foveal lesion (OD). Note that the rosette-like lesions (arrow head) correspond to hyper-autofluorescent spots and loss of retinal lamination (2, 3 and 4). **(C).** FAF of case 2 showed several hyper-autofluorescent spots around the disc and arcades. **(D).** (5,6) OCT sectioning of case 2 (line 5 and 6 from fig C) showed normal retinal lamination without rosette-like lesions. Some shadows casted by retinal vessels are observed.

Chapter 2, Figure 3.

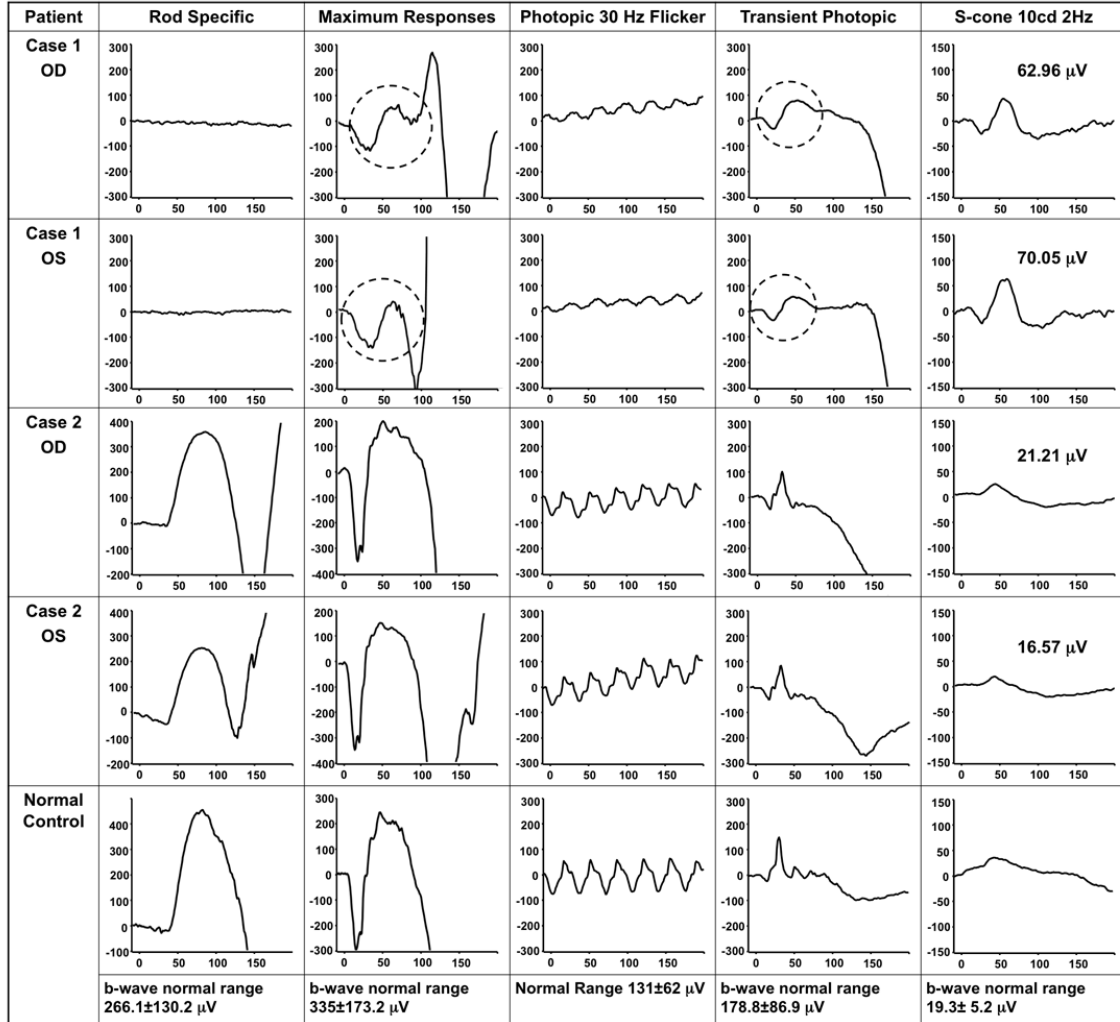


Chapter 2, Figure 4.



Figure 4. Electroretinogram (ERG) from case 1 revealed three characteristic findings: 1) no rod responses; 2) the waveforms of scotopic maximal response are very identical to the transient photopic responses except the size (circles); 3) the amplitude of a wave in the transient photopic response is larger than amplitude of photopic 30 Hz flicker. S-cone-specific ERG was of remarkably high amplitude (60-70 μV) and further confirmed the diagnosis of ESCS. ERG from case 2 was normal.

Chapter 2, Figure 4.



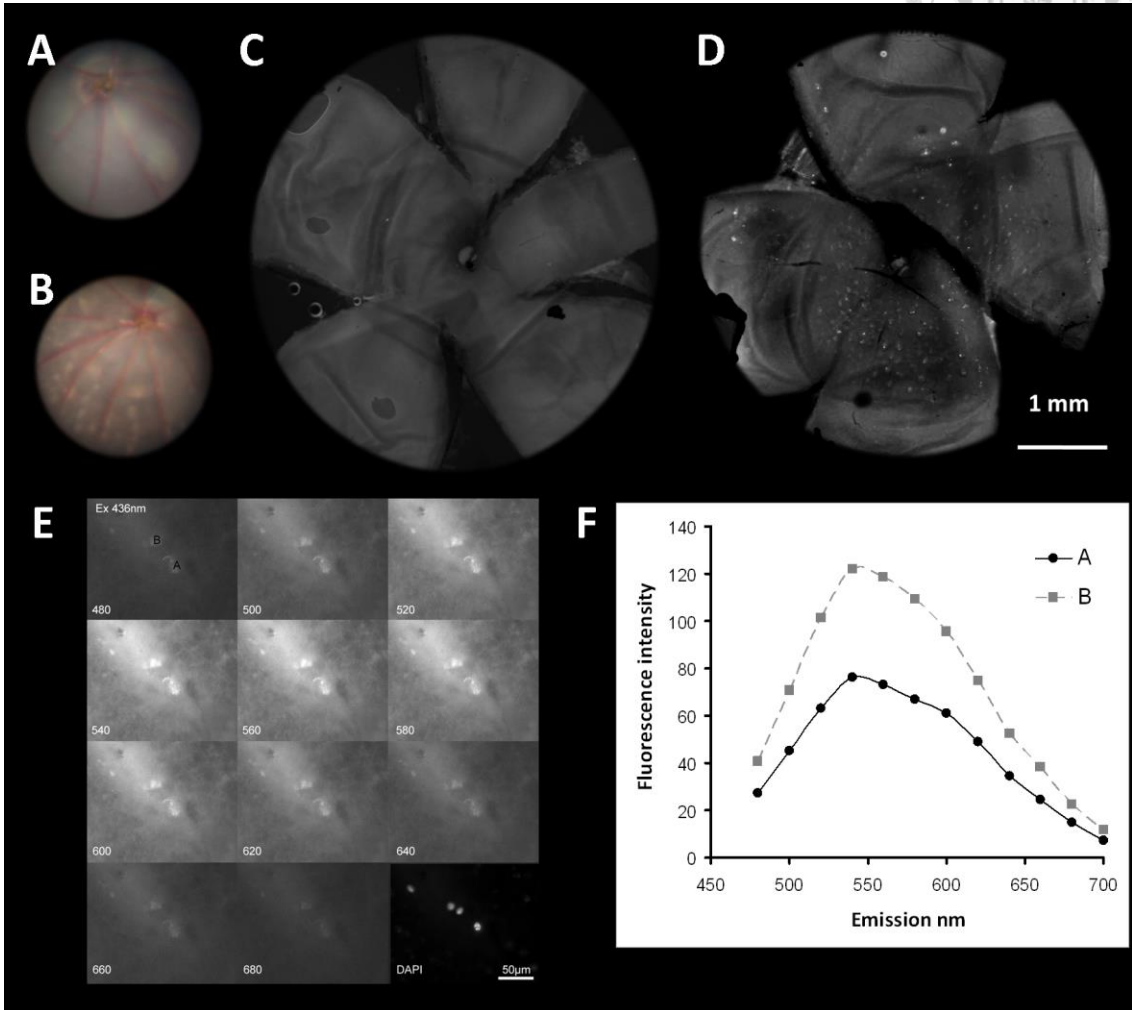
Chapter 2, Figure 5.



Figure 5. Color fundus photographs from wild type mouse (**A**) showed normal retina, whereas image from *rd7* mouse (**B**) showed numerous subretinal white dots. Whole mount eyecup from wild type mouse (**C**) did not reveal hyperautofluorescence spots whereas image from *rd7* mouse (**D**) showed hyperautofluorescence spots. (**E, F**).

Spectral fluorescence of hyperautofluorescence spots from *rd7* mouse retina demonstrated the wave length of highest fluorescence intensity was 540 nm to 560 nm when excited with light of 436 nm.

Chapter 2, Figure 5.

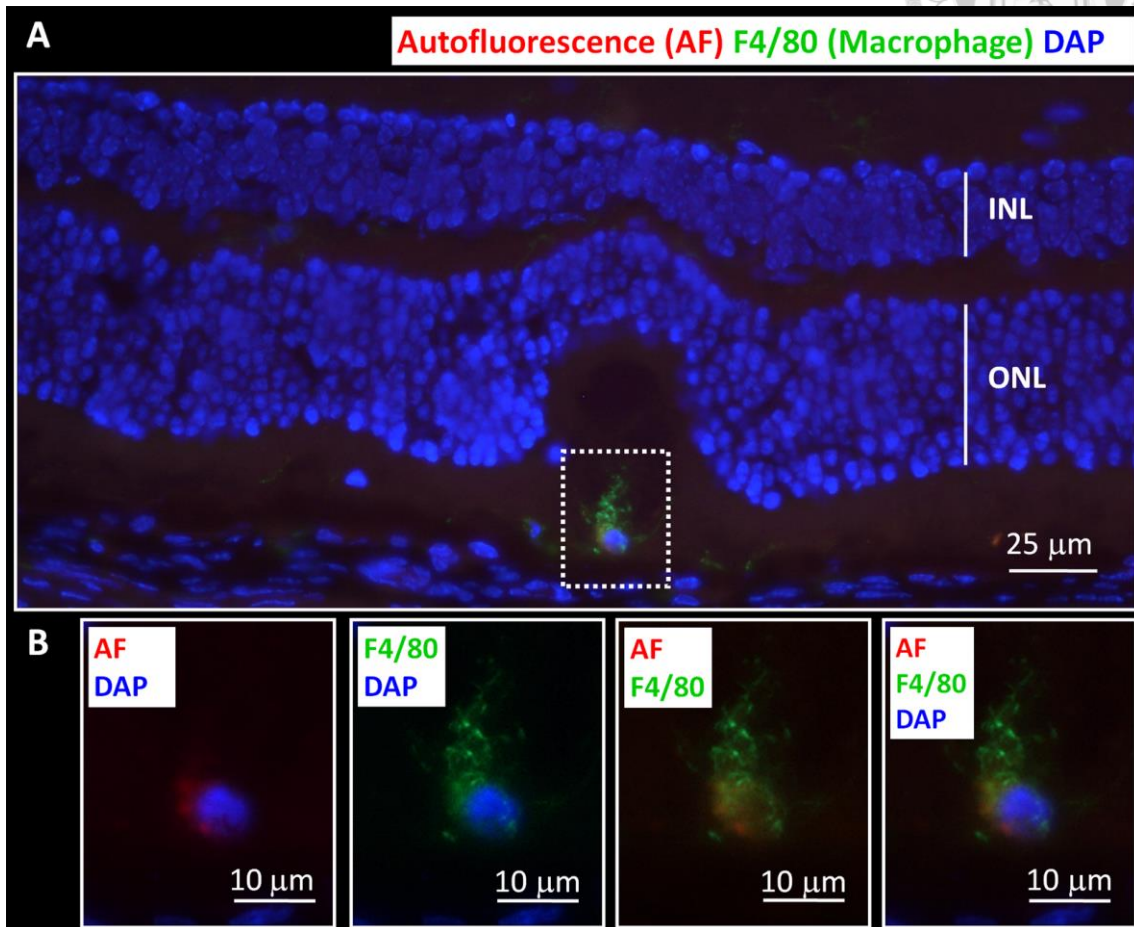
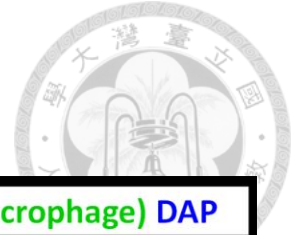


Chapter 2, Figure 6.



Figure 6. (A). Immunohistochemistry of a frozen section from *rd7* mouse retina using anti-F4/80 antibodies (macrophage marker) showed one macrophage in the retinal rosette, or whorl lesion. **(B).** High magnification of white dots lined area from (A) showed images merge from different fluorescence channels. The autofluorescence (red) was co-localized with macrophage marker (green). INL: inner nuclear layer; ONL: outer nuclear layer; AF: autofluorescence; F4/80: macrophage marker; DAP: DAPI staining.

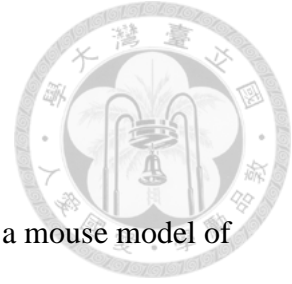
Chapter 2, Figure 6.



Chapter III



Origin of fundus hyperautofluorescent (AF) spots, and their role in retinal degeneration in a Mouse Model of Goldmann-Favre Syndrome



Abstract

Aim: To investigate the role of microglia in *rd7/rd7* mice, which are a mouse model of enhanced S-cone syndrome (ESCS).

Methods: Using mice with the macrophage Fas-induced apoptosis (Mafia) transgene, we generated double-mutant (*rd7/rd7;Tg/Tg*) mice and studied the role of the resident retinal microglia. Microglial cells in these double-mutant mice express enhanced green fluorescent protein (EGFP) and a suicide gene, which can trigger Fas-mediated apoptosis via systemic treatment with AP20187 (FK506 dimerizer). AP20187 was used to systemic ablation of bone marrow-derived microglia in *rd7/rd7;Tg/Tg* mice.

Immunohistochemical analysis, flow cytometry, electron microscopy, and western blot were used in this study.

Results: We demonstrated that more than 80% of the EGFP⁺ cells in *rd7/rd7;Tg/Tg* mice retina expressed Iba-1, and resident microglia are still present in the retina because AP20187 does not cross the blood-retina barrier. Hence, only circulating bone marrow (BM)-derived microglia are depleted. Depletion of circulating BM-derived microglia accelerates retinal degeneration in *rd7* mice. An increased number of autofluorescent (AF) spots is a consequence of resident microglia proliferation which in turn establishes an inflammatory cytokine milieu via the upregulation of *IL-1 β* , *IL-6*, and *TNF- α*

expression. This inflammation likely accelerates retinal degeneration.

Conclusions: This study has identified not only inflammation as a critical step in the pathogenesis of retinal degeneration, but also the involvement of specific cytokine genes that could serve as future treatment targets in retinal degenerations.






Introduction

Retinal degeneration in *rd7* mice is caused by a spontaneous mutation in the *Nr2e3* gene.

In addition, this mouse strain is a model for Goldmann-Favre Syndrome or enhanced S-cone syndrome (ESCS; OMIM 268100; <http://www.ncbi.nlm.nih.gov/omim/Online> Mendelian Inheritance in Man; NCBI, Bethesda, MD) (Akhmedov et al. 2000). In these mice, a gain of photoreceptor cell types results in retinal dysplasia and degeneration.

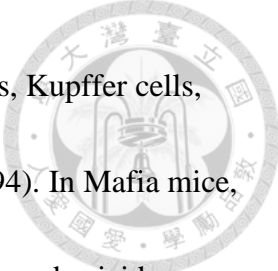
Recently, we described novel characteristics in a 6-year-old boy with ESCS who carried a homozygous R311Q mutation in the *Nr2e3* gene, including diffuse retinal white dots, hyperautofluorescent (AF) spots, and retinal rosettes (Wang et al. 2009). His phenotypic manifestations were similar to those of “young” *rd7* mice. We demonstrated that F4/80-positive microglia, rather than retinal pigment epithelium (RPE) cells, contributed to these AF spots. Most of these cells were present inside retinal rosettes and presumably helped RPE cells phagocytose this outer segment debris within the rosettes. Although these data demonstrated the presence of comparable retinal characteristics in human ESCS and a mouse model of the disease, the fundamental role of microglia in retinal degeneration is unknown.

Microglia, which are part of the mononuclear phagocytic system, act as the first and main form of active immune defense in the central nervous system, including the



retina (Kreutzberg 1996; Cuadros & Navascues 1998; Hanisch & Kettenmann 2007; Tambuyzer et al. 2009). Microglial activation is characterized by the expression of various microglial/macrophagic markers. In the retina, microglial activation has been demonstrated in injury (Ng & Streilein 2001; Langmann 2007; Joly et al. 2009), ischemia (Zhang et al. 2005; Ritter et al. 2006; Sivakumar et al. 2011), and degeneration (Langmann 2007; Sasahara et al. 2008; Arroba et al. 2011). Microglial cells consist of the two types of resident microglia and circulating bone marrow (BM)-derived microglia, with the former entering from hyaloid vessels and being thought to be associated with neuronal death in retinal histogenesis (Ashwell et al. 1989), whereas the latter entering from the optic nerve after retinal vascularization (Caicedo et al. 2005; Hou et al. 2006). Although BM transplantation approaches have the potential to systemically remove macrophages in order to study their function in vivo in normal or disease models, pre-BM-transplantation irradiation damages resident microglia, which may change the immune environment of the retina (Amoaku et al. 1992; Kaneko et al. 2008).

Burnett and colleagues generated transgenic mice for macrophage Fas-induced apoptosis (Mafia) (Burnett et al. 2004; Burnett et al. 2006). This transgene (Tg: Csf1r-EGFP-NGFR/FKBP1A/TNFRSF6) is under the control of the *c-fms* promoter, which drives the expression of the CSF-1 receptor in cells of the mononuclear



phagocytic system, including monocytes, macrophages, dendritic cells, Kupffer cells, Langerhans cells, osteoclasts, and microglial cells (Cecchini et al. 1994). In Mafia mice, cells of the macrophage lineage express the EGFP and a membrane-bound suicide protein that can be activated by the covalently linked dimerizing reagent AP20187. Henceforth, we will use “*Tg/Tg*” to refer to mice that are homozygous mice for this transgene.

In the current study, we took advantage of Mafia transgenic mice to mark the origin of hyperautofluorescent (AF) spots with the EGFP reporter in *rd7* mice.



Materials and Methods


Mouse Strains

All mice were handled in accordance with the Statement for the Use of Animals in Ophthalmic and Vision Research of the Association for Research in Vision and Ophthalmology, and all experiments were approved by the Institutional Animal Care and Use Committee of the Chang Gung Memorial Hospital.

C57BL/6, B6.Cg-*Nr2e3*^{rd7/rd7} (*rd7*), and Mafia (*Tg/Tg*) mice were purchased from the Jackson Laboratory (Bar Harbor, ME, USA) and were housed at a local animal facility under a 12 h light/12 h dark cycle. All mice used in this study were in the B6 background. The *rd7* mice were outcrossed to *Tg/Tg* mice, with F₁ offspring from each of these outcrosses being intercrossed to generate F₂ mice. The two-generation outcross-intercross series was used to generate *rd7/rd7;Tg/Tg* double homozygotes for the *Nr2e3*^{rd7/rd7} mutation and *Tg/Tg*, as described previously (Haider et al. 2001). The offspring from an intercross of *rd7/rd7;Tg/Tg* mice were used in this study.

Screening for the Transgene in Mafia Mice and for the Nr2e3 Gene in rd7 Mice

Genomic DNA was extracted from mouse tails using the QuickExtract kit (Epicentre, Madison, WI). To detect the transgene in Mafia mice, the following EGFP



primers were used: 52–AAGTTCATCTGCACCACCG–32 (forward) and 52–TCCTTGAAGAAGATGGTGCG–32 (reverse). Homozygous *rd7* animals were differentiated from heterozygous and wild-type controls via PCR analysis of genomic DNA using primers designed for the *Nr2e3* gene. A forward primer located in exon 4 (52–GTAGCCTCTCCTGCTCTGGCAG–32) and a reverse primer located in exon 5 (52–CAGGTTGGAAAACACAGGCAAG–32) were used to amplify a 339 bp fragment in wild-type animals and a 239 bp fragment in *rd7* mutants and in heterozygotes harboring the deletion. The fragments were amplified using 5 μl of DNA extract in a 50.0 μl PCR reaction. The cycling conditions were an initial 10 min incubation at 94°C, followed by 10 cycles of 94°C for 10 s, 60°C for 30 s, and 68°C for 60 s and 20 cycles of 94°C for 10 s, 55°C for 30 s, and 68°C for 60 s, and a final extension at 68°C for 7 min. PCR products were electrophoresed on 2% agarose gels (Seakem LE, Lonza Rockland, Rockland, ME) and visualized via ethidium bromide staining. The homozygosity of *Tg* mice was determined by calculating the ΔC_t using real-time PCR with primers for *EGFP* (test gene) and *Apo B* (reference gene).

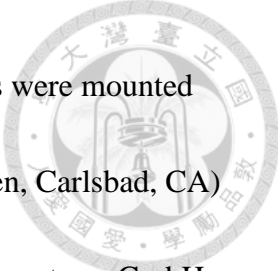
Cilioretinal Flatmount and Histochemical Analyses

Eyes were enucleated and placed in 4% paraformaldehyde for 1 h at room temperature (RT). The cornea and lens were removed from each eye under a surgical microscope.

Whole eyecups were flattened using four to eight radial cuts and mounted with mounting medium (VECTASHIELD, Burlingame, CA). Autofluorescence was detected using standard fluorescence microscopy, as described previously (Wang et al. 2009).

Immunostaining was performed as described previously (Wang et al. 2009; Wang et al. 2010).

After fixation as described above, eyes were frozen in optimum cutting temperature compound (Tissue-Tek OCT; Miles Laboratories, Elkhart, IN). Frozen eyes were cryosectioned at a thickness of 10 μm . Blocking was performed using 10% normal blocking serum in PBS with 0.3% Triton X-100 (blocking solution) for 30 min at RT. Sections were then incubated with primary antibodies diluted in 4% normal blocking serum in PBS with 0.1% Triton X-100 for 2 h at RT. The samples were subsequently incubated for 40 min at RT with secondary antibodies diluted in PBS with 0.1% Triton X-100. The primary antibodies used were anti-EGFP (1:2000, Novus Biologicals, Littleton, CO), anti-F4/80 (1:100, Abcam, Cambridge, MA), anti-CD68 (1:200, Abcam, Cambridge, MA), anti-ionized calcium-binding adaptor molecule 1 (Iba-1; 1:1000, Wako, Osaka, Japan), anti-major histocompatibility complex (MHC) class II (1:100, BD Pharmingen, San Jose, CA), anti-vimentin (1:200, Sigma-aldrich, Saint Louis, MO), and anti-active caspase 3 (1:200, BD Pharmingen, San Jose, CA). The secondary antibodies used were Alexa Fluor 488- or 555-conjugated antibodies (dilution, 1:1000; Invitrogen,

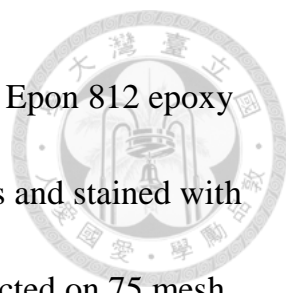


Carlsbad, CA). After being washed three times with PBS, the sections were mounted with mounting medium containing the nuclear dye Hoechst (Invitrogen, Carlsbad, CA) and viewed using a Leica TCS SP5 confocal microscope (Leica Microsystems GmbH, Wetzlar, Germany). Images were merged digitally to assess triple labeling.

The Click-iT 5-ethynyl-22-deoxyuridine (EdU) labeling kit was used to perform EdU labeling (Invitrogen, Carlsbad, CA). Timed, *rd7/rd7;Tg/Tg* mice were injected with EdU solution (30 μ g/g of body weight) continuously for 2 days, and then killed on the third day. Eyes were collected, fixed, and processed according to the immunostaining protocol mentioned above. EdU staining was performed according to the protocol provided by the kit.

Transmission Electron Microscopy


For transmission electron microscopy (TEM), P60 *rd7* and P60 wild-type (WT) mice were first perfused transcardially with 2% glutaraldehyde and 2% paraformaldehyde in phosphate buffer. Subsequently, the eyes of animals were enucleated and placed in 3% glutaraldehyde with 2% paraformaldehyde for 2 h at 4°C. The cornea was cut and the lens was removed, to allow further fixation for 1 h. After re-fixation in 1% osmium tetroxide for 4 h at room temperature, the eye samples were prepared as described previously (Yeh et al. 2008). After fixation, the eye samples



were washed in phosphate buffer, dehydrated, and embedded in Epon 812 epoxy resin. Serial semithin sections were obtained along the long axis and stained with toluidine blue. Ultrathin sections from selected areas were collected on 75 mesh copper grids and stained with uranyl acetate and lead citrate, and images were photographed with a Hitachi 7100 transmission electron microscope (Hitachi, Tokyo, Japan) equipped with an AMT digital camera.

Quantitative Real-Time RT-PCR (qRT-PCR)

Total mRNA was prepared from freshly dissected whole mouse retinas using the TRIzol reagent (Molecular Research Center, Cincinnati, OH). The mRNA was transcribed using SuperScript III Reverse Transcriptase (Invitrogen, Carlsbad, CA) and Q-PCR assays were performed using the KAPA SYBR[®] FAST qPCR Kit (Kapa Biosystems, Woburn, MA). Amplified products were run on the Mx3000P™ instrument (Stratagene) in a final reaction volume of 10 μL. The following thermocycling profile was used: denaturation at 95°C for 3 min and 40 cycles of 95°C for 3 s, 55°C for 20 s, and 72°C for 1 s. The MxPro software was used to set baselines and CT values according to the guidelines provided by Stratagene. The expression levels of each gene were normalized to the PCR products of *β-actin*. The following primers were used for Q-PCR: *IL-1β*, 52-TGTGAAATGCCACCTTTTGA-32 and



52-CTGCCTGAAGCTCTTGTTGA-32; *IL-6*, 52-TGTGCAATGGCAATTCTGAT-32
and 52-CTCTGAAGGACTCTGGCTTTG-32; *IL-10*,
52-TGGCCCAGAAATCAAGGAGC-32 and 52-CAGCAGACTCAATACACACT-32;
TNF- α , 52-CCACCACGCTCTTCTGTCTA-32 and
52-CACTTGGTGGTTTGCTACGA-32; *TFG- β 1*,
52-TTGCTTCAGCTCCACAGAGA-32 and 52-TGGTTGTAGAGGGCAAGGAC-32;
MCP-1, 52-TCTCTTCCTCCACCACTATGCA-32 and
52-GGCTGAGACAGCACGTGGAT-32; *β -actin*,
52-TCATGAAGTGTGACGTTGACATCCGT-32 and
52-CCTAGAAGCATTGCGGTGCAGGATG-32.

Ablation of BM-Derived Microglia in Transgenic Mice

The depletion protocol used here was as described previously (Burnett et al. 2004; Qualls et al. 2006). AP20187 (Ariad Pharmaceuticals, Cambridge, MA) was injected (i.v.) into the P14 *rd7/rd7;Tg/Tg* mice once daily at a dose of 10 mg/kg of body weight for 5 consecutive days, for initial cell depletion. This depletion protocol has been shown to cause 80–95% depletion of monocytes, macrophages, and dendritic cells in many tissues (Burnett et al. 2004). Depletion can be prolonged by subsequent injection of AP20187 twice weekly at a reduced dose of 1 mg/kg of body weight (Qualls et al.

2006).



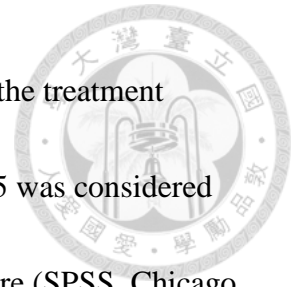
Flow Cytometry to Determine Macrophage/DC Depletion

Flow cytometric analysis and sorting were performed on a BD FACSCalibur flow cytometer (BD Biosciences, San Jose, CA) and the data collected were analyzed using the Flowjo software. Peritoneal lavage was performed under anesthesia using 5 mL of PBS and peripheral blood was collected from the tail vein. The preparations were resuspended in 10-fold ACK lysis buffer (Lonza Walkersville, Walkersville, MD), spun, and processed using flow cytometry. Histograms were graphed from events gated by forward and side scatter (FSC and SSC, respectively) to the region where macrophages and lymphocytes would be found.

Quantification and Statistical Analyses

In Fig. 1H, the number of AF spots and rosettes within fields of 200 x 200 μm (the average of four fields from the central retina and eight fields from the peripheral retina) was determined and processed statistically from montage images of the cilioretinal flatmounts. To compare the EdU-labeled cells in the *rd7/rd7;Tg/Tg* mice injected with AP20187 and vehicle, the number of EdU-labeled cells was counted and averaged from 15 serial sections cut around the optic nerve head in each mouse (n=3 in each group).

All experimental data were assessed by an operator blinded to the treatment condition. Significance was determined using a paired *t* test. $P < 0.05$ was considered significant. All analyses were performed using the SPSS 15.0 software (SPSS, Chicago, IL).





Results

Spatial and Temporal Distribution of Autofluorescent (AF) Spots and Rosettes in rd7

Mice

Our previous study showed that retinal rosettes corresponded to retinal folds, and that AF spots corresponded to microglial cells located between the neural retina and the RPE (Wang et al. 2009). To investigate the relationship between autofluorescence, microglial infiltration, and retinal degeneration, we counted the AF spots and rosettes in the cilioretinal flatmounts of the *rd7* mice between P14 and P720 (Fig. 1). Figs 1A and B show the cilioretinal flatmounts of the P21 wild type (A) and P19 *rd7* mice (B). Fig. 1C shows examples of AF spots (arrows) and rosettes (circular halos). Although the number of retinal rosettes increased from P14 to P21, the number of rosettes decreased progressively from P21 through P720. In contrast, AF spots that were absent at P14, were first detected as early as P21 (Fig. 1G), and increased gradually with age (Figs 1, F–K). We found that the AF spots were not distributed along the retinal vessels, but rather were correlated with rosettes between P21 and P60.

Abnormal Accumulation of Material in the Outer Segment of rd7 Mice



Previously, abnormal accumulation of material at the photoreceptor–RPE interface was documented in *Nrl*^{-/-} mice, another mouse model of ESCS (Mustafi et al. 2011). In addition, in our previous study, we found cells that were stained positively for F4/80 inside the retinal rosettes (Wang et al. 2009). To characterize these cells further, we performed an immunochemical analysis of retinas in *rd7* mice. Confocal images taken from the cilioretinal flatmounts of 2-month-old *rd7* mouse retinas probed with anti-F4/80 antibodies revealed the presence of ramified microglia “lying” above the RPE layer (Fig. 2). These cells were colocalized with F4/80 (green, Fig. 2B) and autofluorescent material (red, Fig. 2C). Crosshairs and high-magnification viewing revealed the presence of autofluorescent materials within the cytoplasm of an F4/80-positive cell (Fig. 2E).

To characterize the autofluorescent material further, we performed a histological analysis of *rd7* and wild-type (WT, C57BL/6) mouse photoreceptors. Abnormal folding at the outer nuclear layer and outer and inner segment was noted in P60 *rd7* mice (Fig. 3A), whereas this folding was not found in P60 WT mouse retinas (Fig. 3B). To confirm this finding, we examined the retinas of *rd7* and WT mice using transmission electron microscope (TEM) (Figs. 3C–H). In *rd7* mouse retinas, some microglia (different from RPE cells) were detected between the OS and the RPE (asterisks in Figs.

3E and F). A higher magnification of TEM images showed the accumulation of lysosomes inside a microglial cell (arrow in Fig. 3G), which was more likely to be found under retinal rosettes (Figs. 3E and F). No microglia were found in WT mouse retinas (Fig. 3D).

Distribution of Microglia in rd7/rd7;Tg/Tg Mice

To investigate the role of circulating BM-derived microglia in *rd7* mice, we generated *rd7/rd7;Tg/Tg* double homozygotes via a two-generation outcross–intercross series.

Theoretically, the transgene is under the control of the *c-fms* promoter and is expressed in macrophages, monocytes, microglia, and dendritic cells (Burnett et al. 2004; Burnett et al. 2006). Previously, microglia were classified into various subtypes (Zhang et al.

2005). To investigate further whether EGFP was expressed in these microglia and whether they colocalized with microglial markers, we performed an

immunohistochemical analysis of the retinas of the *rd7/rd7;Tg/Tg* mice. Among the

EGFP⁺ cells, 45.4 ± 9.5% expressed F4/80, 47.7 ± 10.4% expressed CD68, 84.2 ± 8.0% expressed Iba-1, and 39.7 ± 7.7% expressed MHC class II. Less than 10% of the EGFP⁺

cells expressed vimentin. We also found that the EGFP⁺ cells were distributed in the

ganglion cell layer (GCL), inner plexiform layer (IPL), inner nuclear layer (INL), outer

plexiform layer (OPL), and between the OS and the RPE (Fig. 4). In summary, the

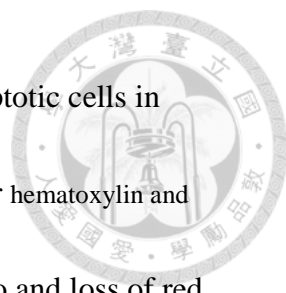
majority of EGFP⁺ cells (>80%) in *rd7/rd7;Tg/Tg* mice expressed Iba-1, and few EGFP⁺ cells were labeled by vimentin.



Circulating BM-derived Microglia Deficiency in rd7 Mice

We introduced inducible circulating BM-derived microglia deficiency into the mouse model of ESCS by crossbreeding *rd7* onto the Mafia mice. The *rd7/rd7;Tg/Tg* mice had similar physical characteristics as those of *rd7* mice and survived more than 1 year, when allowed. The growth of *rd7/rd7;Tg/Tg* mice was similar to that of *rd7* mice. However, after circulating BM-derived microglia ablation using AP20187, the body weight in the AP20187 mice did not increase as fast as in the vehicle treated animal (Fig. S1).

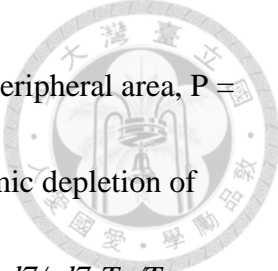
To investigate whether AP20187 can systemically deplete circulating BM-derived microglia in *rd7/rd7;Tg/Tg* mice, we injected AP20187 intravenously at a dose of 10 mg/kg of body weight for 5 consecutive days, and then twice weekly at a reduced dose of 1 mg/kg of body weight. We found a marked decrease in EGFP expression in peritoneal cells, suggesting that AP20187 can deplete circulating BM-derived microglia in *rd7/rd7;Tg/Tg* mice (Fig. S2, A). An enlarged spleen was noted in *rd7/rd7;Tg/Tg* mice injected with AP20187 compared with the vehicle-injected mice (Figs S2, G and D). We stained apoptotic cells selectively in the spleen section using an anti-active



caspase 3 antibody and TUNEL and found a marked increase in apoptotic cells in AP20187-injected *rd7/rd7;Tg/Tg* mice (Figs S2, B, C, E, and F). Our hematoxylin and eosin analysis demonstrated an increase in the nucleus/cytoplasm ratio and loss of red pulp in the spleen (data not shown), suggesting the presence of extramedullary hematopoiesis in the *rd7/rd7;Tg/Tg* mice after long-term depletion of circulating BM-derived microglia.

Acceleration of Retinal Degeneration in *rd7/rd7;Tg/Tg* Mice after Systemic Depletion of Circulating BM-Derived Microglia

To confirm the role of circulating BM-derived microglia in the *rd7/rd7;Tg/Tg* mice, we investigated the morphological changes in the retinal rosettes and AF spots after the AP20187 injection (Figs 5, A–G). We found a marked and rapid decrease in the number of retinal rosettes, which was accompanied by an increase in the number of AF spots (Figs 5, I and J). As mentioned above, increasing numbers of AF spots and decreased numbers of rosettes resemble the characteristics found in older *rd7* mice, suggesting an acceleration of retinal degeneration. For this reason, we counted the number of nuclei in the photoreceptors of the *rd7/rd7;Tg/Tg* mice after 5 months of AP20187 injections, as well as that for the vehicle-injected mice (Fig. 5L). There was a significant decrease in the number of nuclei in the ONL in the *rd7/rd7;Tg/Tg* mice injected with AP20187



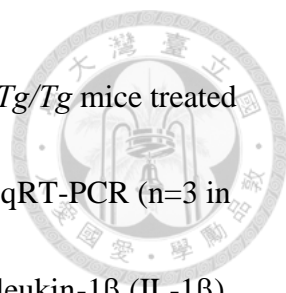
compared with vehicle-injected mice (posterior pole, $P = 0.022$; midperipheral area, $P = 0.031$; $n = 3$) (Figs 5, D, H, and K). These data suggest that the systemic depletion of circulating BM-derived microglia accelerates retinal degeneration in *rd7/rd7;Tg/Tg* mice.

Changes in the Number of Proliferative Cells after Systemic Depletion of Circulating BM-Derived Microglia in *rd7/rd7;Tg/Tg* Mice

To investigate whether retinal resident microglia proliferation accounts for the significantly increased number of AF spots observed in the *rd7/rd7;Tg/Tg* mice injected with AP20187, we performed EdU labeling and Iba-1 immunostaining in the *rd7/rd7;Tg/Tg* mice 1 month after treatment with AP20187 and vehicle. Compared with the retinas from the vehicle-injected *rd7/rd7;Tg/Tg* mice, there were significantly more labeled dividing resident microglial cells in the retinas after 1 month of AP20187 injection in the *rd7/rd7;Tg/Tg* mice (Fig. 6), demonstrating an essential role for the resident microglia after the systemic depletion of circulating BM-derived microglia.

Changes in the Expression of Retinal Cytokines/Chemokines after Systemic Depletion of Circulating BM-Derived Microglia in *rd7/rd7;Tg/Tg* Mice

Next, we investigated the mechanism underlying the retinal degeneration observed after circulating BM-derived microglia depletion. Retinas from the WT mice



(C57BL/6), *rd7/rd7;Tg/Tg* mice treated with AP20187, and *rd7/rd7;Tg/Tg* mice treated with vehicle, were extracted using lysis buffer and were subjected to qRT-PCR (n=3 in each group). The genes that encode the inflammatory cytokines interleukin-1 β (IL-1 β), IL-6, tumor necrosis factor- α (TNF- α), and monocyte chemotactic protein (MCP-1) were upregulated after systemic depletion of circulating BM-derived microglia; however, the gene that encodes the anti-inflammatory cytokine TGF β 1 was downregulated (Fig. 7). TNF was chosen for its role as the classical activator and initiator of cytotoxicity, as well as a sustainer of macrophage responses. We thus concluded that resident microglia play an essential role, and that their proliferation upregulates the expression of the *IL-1 β* , *IL-6*, and *TNF- α* genes in the retina, after circulating BM-derived microglia depletion.




Discussion

Microglia have been reported to play a central role in the chronic degenerative conditions of CNS, including Alzheimer and Parkinson diseases, and Amyotrophic Lateral Sclerosis (Block et al. 2007; Gentleman 2013). In the present study, we reported the opposing roles of resident microglia and circulating BM-derived microglia in retinal degeneration.

Sequential Appearance of AF Spots, Rosettes, and Microglial Cells


In a previous study, we found microglia inside the outer nuclear layer folding, which appeared as white dots in funduscopy and retinal rosettes in cilioretinal flatmounts (Wang et al. 2009). In the current study, TEM and immunochemical analyses demonstrated the presence of lysosomes inside these microglia, which appeared as AF spots in the cilioretinal flatmounts. Sequential analyses of the retinal rosettes and AF spots indicated that the retinal rosettes appeared earlier than the AF spots, suggesting that microglia are recruited and appear after outer nuclear layer folding. The increased number of AF spots found in the older *rd7* mice may be related to an increase in activated-lysosome-laden microglia, which represent a later stage of retinal degeneration.



Based on the spatial and temporal distribution of the AF spots and rosettes, we found that microglial cells are not simply bystanders in *rd7* mice, but may contribute to the degenerative process. We hypothesize that microglia play a positive role in maintaining the environment of photoreceptors by initially cleaning up debris between photoreceptors and the RPE. A similar symbiosis between microglia and photoreceptors was found in other studies (Banerjee & Lund 1992; Ritter et al. 2006; Sasahara et al. 2008; Joly et al. 2009; Arroba et al. 2011). Another study demonstrated that BM-derived cells can eliminate amyloid deposits in Alzheimer disease via a cell-specific phagocytic mechanism (Simard et al. 2006).


Advantages of Mafia Mice Compared with BM Chimeric Mice

An advantage of our murine model of circulating BM-derived microglia deficiency in retinal degeneration is that, in contrast to most published macrophage-deficiency models on which BM transplantations were performed after systemic irradiation, in our model, the resident microglia are not ablated after systemic depletion of BM-derived microglia. This helped us investigate the role of resident and circulating BM-derived microglia in retinal degeneration. Although many researchers have used BM transplantation to investigate the role of BM-derived microglia, the number of migrating BM-derived cells in normal retinas remains controversial. Xu et al. reported that a



majority of retinal microglia/macrophages are replenished from circulating BM-derived cells over 6 months, with very little *in situ* proliferation (i.e., insufficient to account for renewal) (Xu et al. 2007). Kaneko et al. observed bulk BM-derived cell migration to the retina only after the induction of retinal damage (Kaneko et al. 2008). Conversely, systemic irradiation before BM transplantation may ablate resident microglia in the retina, thereby inducing additional BM-derived cell migration. In the current study, we demonstrated that AP20187 efficiently depleted circulating EGFP⁺ BM-derived cells in *rd7/rd7;Tg/Tg* mice (Fig. S2), thus providing better results than BM transplantation, without damaging resident retinal microglial cells. However, we only injected AP20187 after P14 because injection is technically easier at the tail vein after this stage; as such, we could not determine the number of circulating BM-derived cells that migrated to the retina before P14 in the *rd7/rd7;Tg/Tg* mice. It is noteworthy that the variance in the AF spots in *rd7* mice (Fig. 1E) and *rd7/rd7;Tg/Tg* mice treated with vehicle (Fig. 5J) may not be identical because of an effect of the genetic background and/or the use of ethanol as a vehicle for AP20187 intraperitoneal injection.

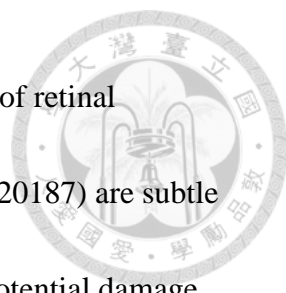
In this study, we demonstrated the presence of heterogeneous populations of microglia in the retina that exhibited distinct morphological characteristics, location, and distribution in the *rd7/rd7;Tg/Tg* mice. Iba-1⁺ ramified cells have been observed to have delicate processes, have been located in the inner layers of the retina, and have



been considered to be a marker of resident microglia (Sasahara et al. 2008; Joly et al. 2009). CD68 is a cytoplasmic lysosomal antigen and CD68+ amoeboid cells may represent blood-borne macrophages (Milligan et al. 1991). MHC class II+ spindle cells are regarded as antigen-presenting cells and are not present in the normal retina (Zhang et al. 2005). The intermediate filament vimentin is expressed ubiquitously in Müller cells of many mammalian species (Kivela et al. 1986). However, although different subgroups of microglia may express different markers, we found that not only are more than 80% of the EGFP+ cells expressed Iba-1 in the *rd7/rd7;Tg/Tg* mice, but also that these EGFP+ cells are different from Müller cells.

Distribution of Microglia in rd7/rd7;Tg/Tg Mice

BM-derived cells have been observed along optic nerves and retinal vessels, where activated astrocytes are present, after 24 h of retinal degeneration induced by *N*-methyl-*N*-nitrosourea (MNU) (Kaneko et al. 2008). Similar findings of the presence of BM-derived cells in the ciliary body and in the optic nerve have also been reported in other studies that used BM transplantation (Hou et al. 2006; Xu et al. 2007). In the present study, microglial cells in the *rd7* and *rd7/rd7;Tg/Tg* mice were distributed throughout the retina. And we also did not find the pattern that was observed during retinal development (i.e., waves of radial migration) in the *rd7/rd7;Tg/Tg* mice treated



with AP20187. One explanation for this finding is that the processes of retinal degeneration in the *rd7* and *rd7/rd7;Tg/Tg* mice (with or without AP20187) are subtle and are different from the abrupt degeneration induced by drugs or potential damage during pre-BM-transplantation irradiation. Another explanation is that AP20187 depleted most of the circulating BM-derived cells, resulting in few cells being left in circulation.

In the *rd7/rd7;Tg/Tg* mice injected with AP20187, we observed the presence of EGFP+ ramified microglial cells distributed evenly and superficially in the cilioretinal flatmounts. Burnett et al. found no significant EGFP+ cell depletion in brain tissues after AP20187 injection in Mafia mice, and assumed that AP20187 cannot cross the blood-brain barrier (Burnett et al. 2004). Our immunohistochemical findings that Iba-1+ cells were distributed in the GCL, and the residual ramified microglial cells that remained in the cilioretinal flatmounts after AP20187 injection suggest that these EGFP+ ramified cells are resident microglia and that the dimerizing reagent AP20187 cannot effectively penetrate the blood-retina barrier. However, it should be noted that we could only inject AP20187 through the tail vein or intraperitoneally because AP20187 powder needs to dissolve in ethanol during preparation, which may cause retinal toxicity if injected intravitreally. We attempted retrobulbar injection of AP20187, but injections repeatedly resulted in eyeball ischemia and fibrosis. Additional studies

are needed to optimize the dimerizer-treatment protocol to achieve depletion of microglial cells in the CNS and in the retina.



Inflammation was Seen after Systemic Depletion of Circulating BM-Derived Microglia

Unexpectedly, accelerated retinal degeneration occurred after the observation of the systemic depletion of circulating BM-derived microglia in the ESCS model (Fig. 5). Macrophages and microglial cells become classically activated (M1) or alternatively activated (M2) when affected by Th1- and Th2-derived cytokines, respectively. Several studies have indicated that M1 cells have strong cytotoxic activity, whereas M2 cells promote cell survival, angiogenesis, and suppress destructive immunity (Gratchev et al. 2001; Gratchev et al. 2005; Kzhyshkowska et al. 2006; Kigerl et al. 2009; Seledtsov & Seledtsova 2012). In the retina, M2 cells may secrete neurotrophic factors that promote the survival of neurons during retinal degeneration (Carwile et al. 1998; Harada et al. 2002; Arroba et al. 2011) and promote vascular repair in a model of ischemic retinopathy (Ritter et al. 2006). Conversely, M1 cells can induce ganglion cell and photoreceptor death by releasing cytotoxic factors (Roque et al. 1999; Zeng et al. 2005; Sivakumar et al. 2011). Inflammatory cytokines related to M1 cells include TNF- α , IL-1 β , and IL-6, whereas cytokines related to M2 cells include IL-10 and TGF β 1. In *rd* mice, the TNF- α produced by activated microglia has been found to be neurotoxic

(Zeng et al. 2005). In hypoxic neonatal retinas, TNF- α and IL-1 β also appear to induce retinal ganglion cell death (Sivakumar et al. 2011).



Joly et al. have shown that both resident and BM-derived microglia cooperate to remove dead photoreceptors from retinal lesions (Joly et al. 2009). Therefore, resident microglia initially play a positive role in maintaining the environment of photoreceptors by cleaning up debris between photoreceptors and the RPE. Without the cooperation of circulating BM-derived microglia, resident microglia secrete a monocyte chemotactic protein to try to recruit additional monocytes, as seen in Fig. 7. In addition, resident microglia may proliferate and produce high levels of TNF- α and IL-1 β , which subsequently lead to the acceleration of retinal degeneration.

In summary, our study demonstrated the sequence of events during the retinal degenerative process of *rd7* mice. Taking advantage of the unique characteristics of Mafia mice, we demonstrated that more than 80% EGFP⁺ cells in the retina of the *rd7/rd7;Tg/Tg* mice expressed Iba-1, and that resident microglia are still present in the retina because AP20187 does not cross blood-brain barrier. For this reason, only circulating BM-derived microglia are depleted. After the systemic depletion of circulating BM-derived microglia, the cilioretinal flatmounts from the *rd7/rd7;Tg/Tg* mice exhibited characteristics that mimicked those of later stages of retinal degeneration in *rd7* mice. Moreover, outer nuclear layer analyses confirmed the decrease in the

number of nuclei in the *rd7/rd7;Tg/Tg* mice. Our finding suggests that the increased number of AF spots are related to resident microglia proliferation, which established a cytokine milieu that was skewed to inflammation by upregulating the expression of the *IL-1 β* , *IL-6*, and *TNF- α* genes, which subsequently accelerated retinal degeneration.

Future studies dedicated to the search for therapeutic agents to intervene in the inflammatory processes involved in retinal degeneration should investigate the molecular signals that act between microglial activation and photoreceptor loss.



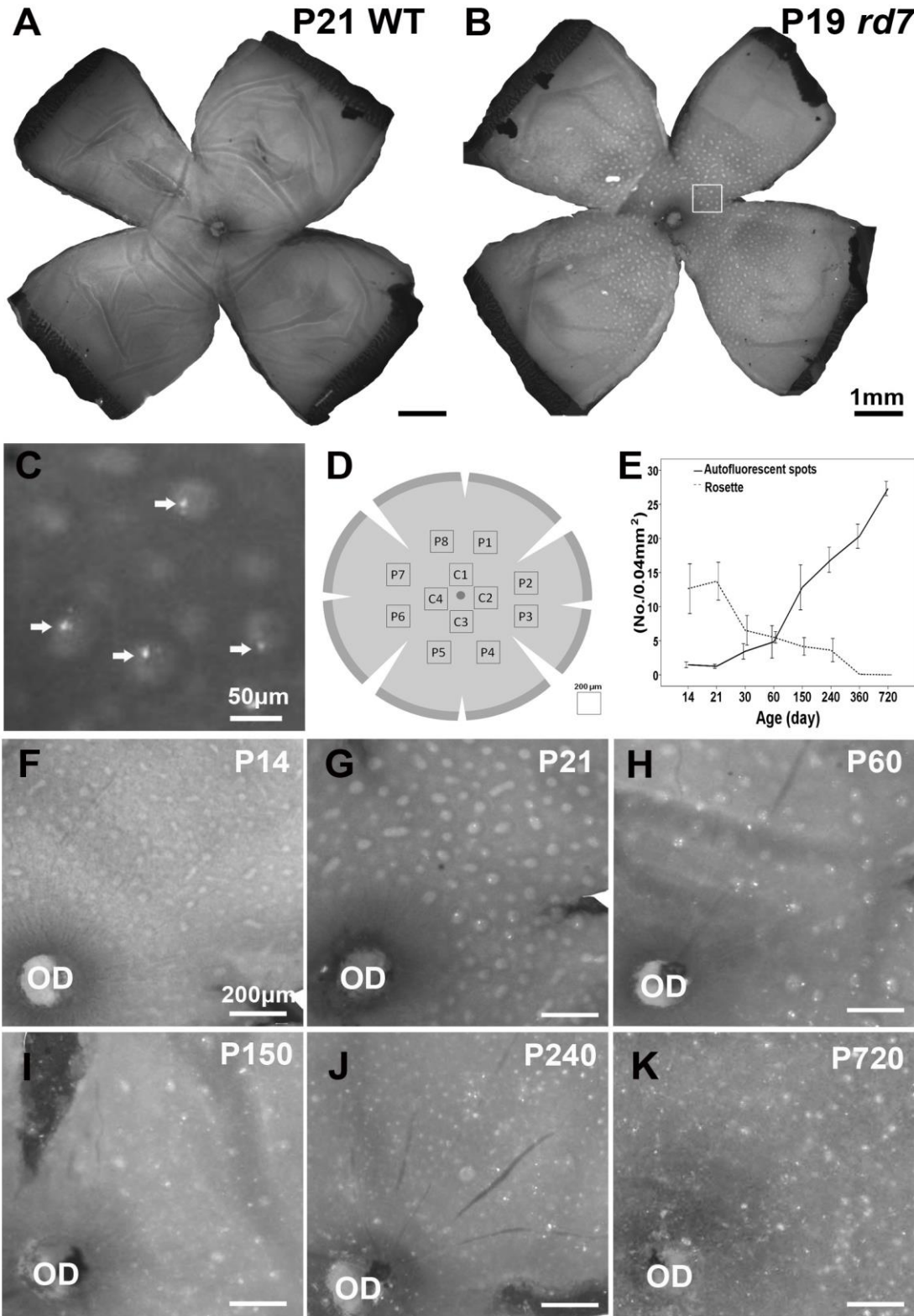
Chapter 3, Figure 1.



Figure 1. Spatial and temporal distribution of autofluorescent (AF) spots and rosettes in *rd7* mice.

A-B: Cilioretinal flatmount of P21 wild type (**A**) and P19 *rd7* mice (**B**). **C:** Higher magnification of the white-lined areas from panels (**B**) showed example of AF spots (arrows) and rosettes (circular halos). Note that the AF spots were located inside the rosettes. **D:** Scheme of a cilioretinal flatmount showing the area in which the AF spots and rosettes were counted. **E:** The number of AF spots and rosettes in the cilioretinal flatmount (mean \pm SD) was determined at P14 (n = 4), P21 (n = 3), P30 (n = 3), P60 (n = 4), P150 (n = 3), P240 (n = 3), P360 (n = 2), and P720 (n = 2). **F:** By P14, rosettes were distributed throughout the cilioretinal flatmount. Note that AF spots were absent. **G:** By P21, some AF spots were located inside rosettes; the AF spots were not distributed along the retinal vessels. **H-K** and **E:** The number of rosettes decreased gradually, whereas the number of AF spots increased. OD, optic disc; C, central; P, peripheral; WT: wild type. Scale bar: (**A, B**) 1 mm, (**C**) 50 μ m, (**F-K**) 200 μ m.

Chapter 3, Figure 1.



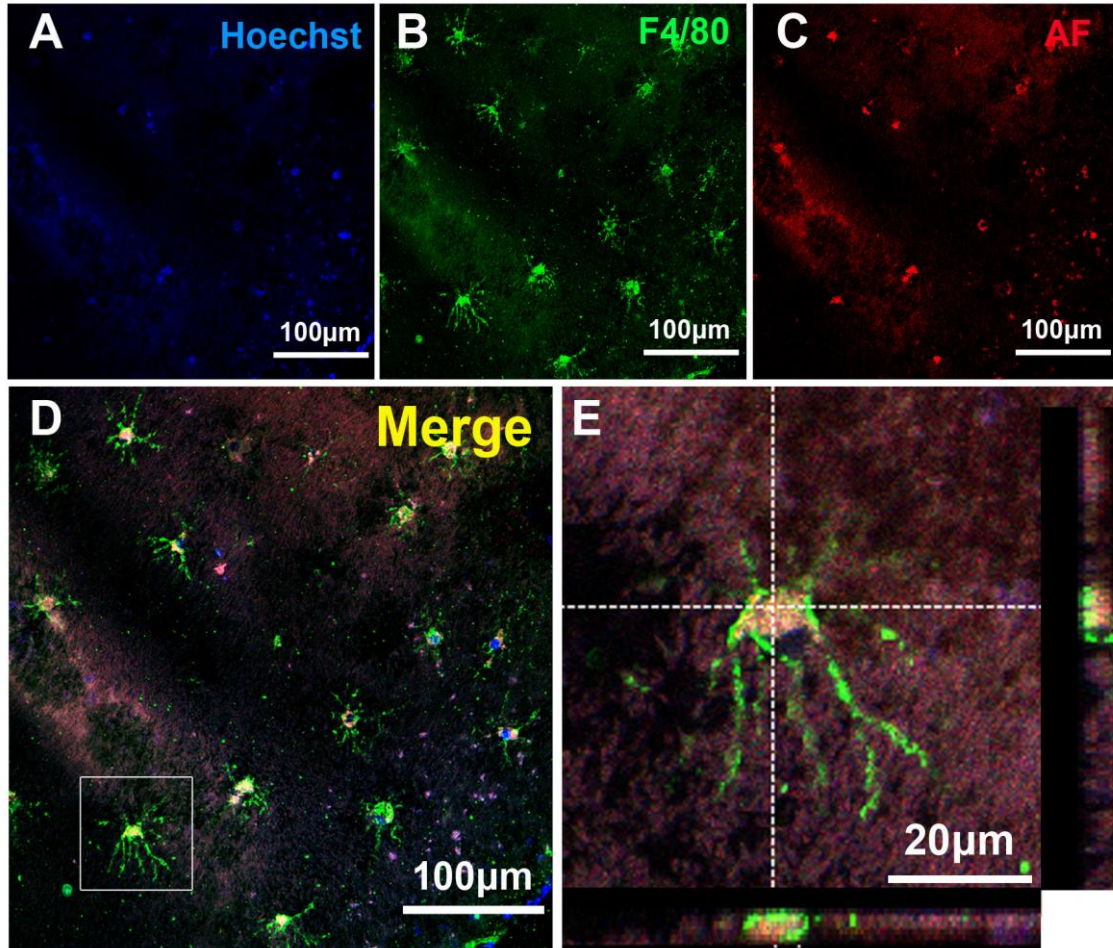
Chapter 3, Figure 2.



Figure 2. Immunohistochemistry of the cilioretinal flatmounts from 2-month-old *rd7* mouse retinas using anti-F4/80 antibodies.

A–D: Confocal images taken from the cilioretinal flatmounts showed the presence of several ramified microglia “lying” above the RPE layer. These cells were colocalized with F4/80 (green) and autofluorescent material (red). **E:** Crosshairs and high-magnification viewing of single cells located inside the white-lined area from **(D)** showed the presence of autofluorescent material within the cytoplasm of an F4/80-positive cell. F4/80, microglial marker; AF, autofluorescence. Scale bar: **(A–D)** 100 μm , **(E)** 20 μm .

Chapter 3, Figure 2.



Chapter 3, Figure 3.



Figure 3. Histology and electron microscopy of P60 *rd7* mouse retinas compared with P60 wild-type mouse retinas.

A: Semi-thin section of an *rd7* mouse retina showing outer nuclear layer foldings. **B:**

Control: semi-thin section of a *WT* mouse retina. **C and D:** Ultra-thin section of retinas

of *rd7* and *WT* mice showing the junction between the outer segment and RPE. **E and F:**

The ultrastructural analysis of the retina of *rd7* mice revealed the presence of microglial

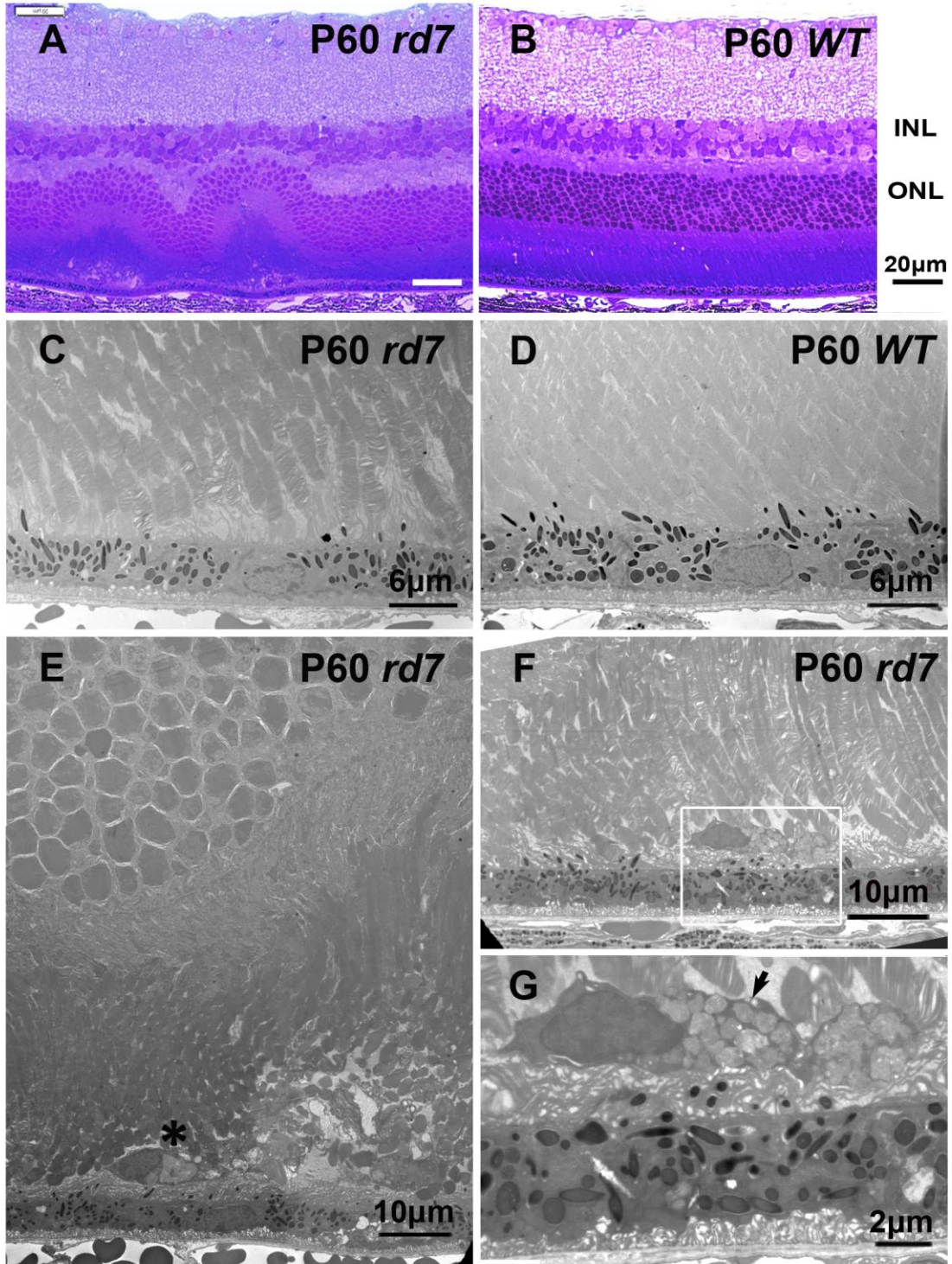
cells between the outer segment and the RPE. **G:** Higher magnification of the

white-lined area from panel F showing the accumulation of lysosomes inside a

microglial cell (**G**). INL, inner nuclear layer; ONL, outer nuclear layer; OS, outer

segment. Scale bar: (**A, B**) 20 μm , (**C, D**) 6 μm , (**E, F**) 10 μm , and (**G**) 2 μm .

Chapter 3, Figure 3.



Chapter 3, Figure 4.



Figure 4. Confocal images showing the distribution of EGFP, F4/80, CD68, MHC

Class II, Iba-1, and vimentin labeling in the retina of a 3-month-old *rd7/rd7;Tg/Tg*

mouse.

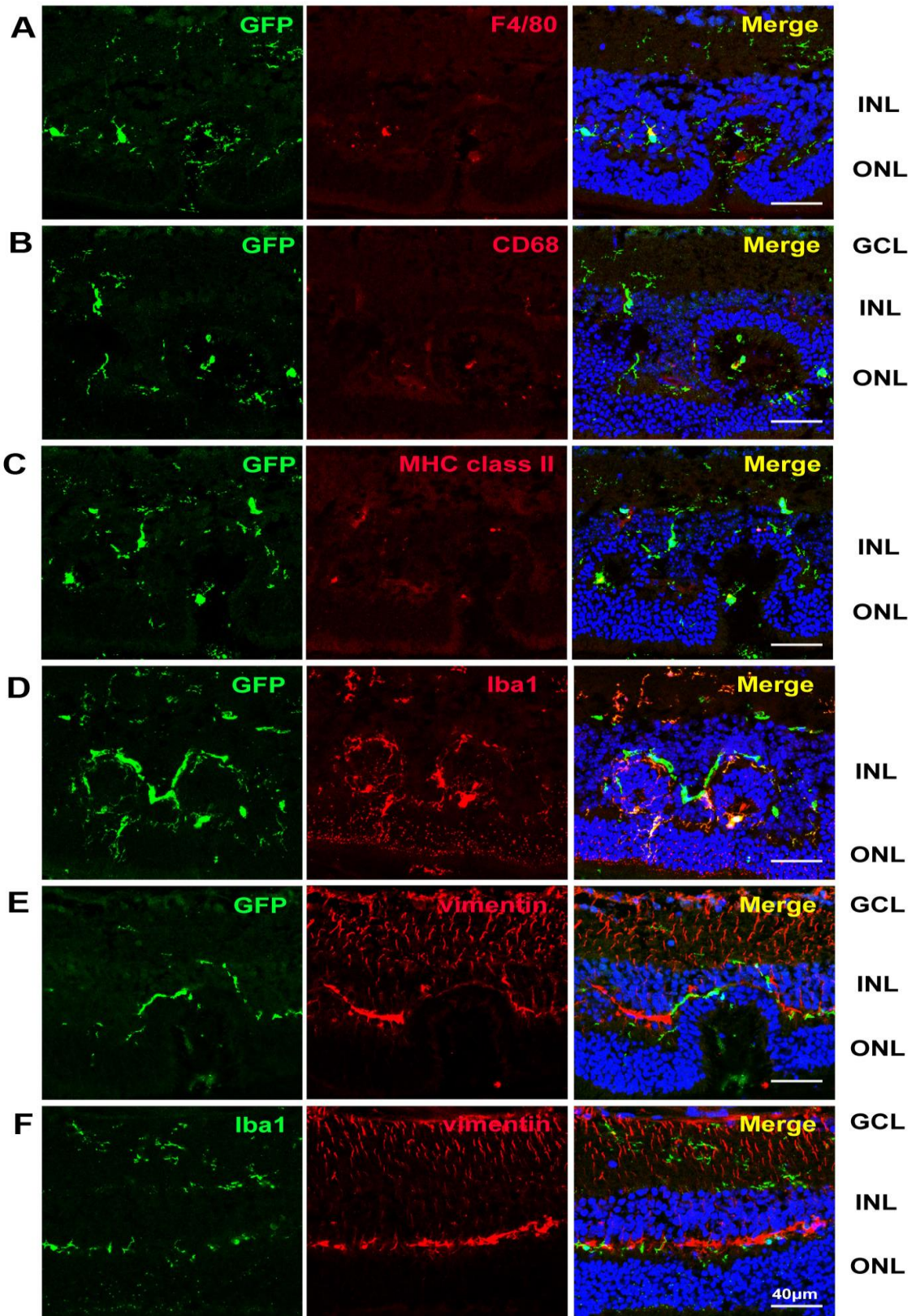
Of the EGFP+ cells, $45.4 \pm 9.5\%$ expressed F4/80 (A), $47.7 \pm 10.4\%$ expressed CD68

(B), $84.2 \pm 8.0\%$ expressed Iba-1(D), and $39.7 \pm 7.7\%$ expressed MHC class II (C).

Less than 10% of the EGFP+ cells expressed vimentin (E). GCL, ganglion cell layer,

INL, inner nuclear layer, ONL, outer nuclear layer. Scale bar: 40 μm .

Chapter 3, Figure 4.



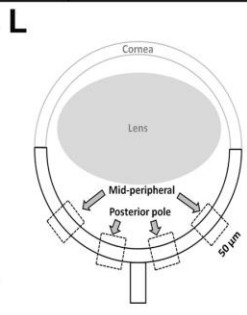
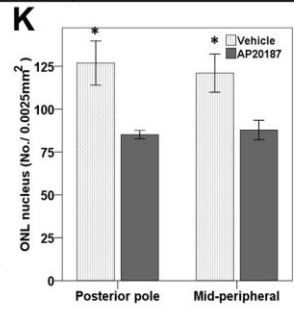
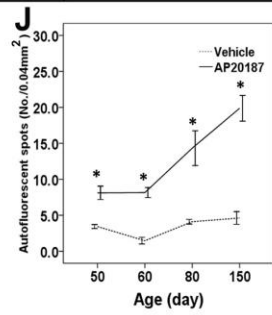
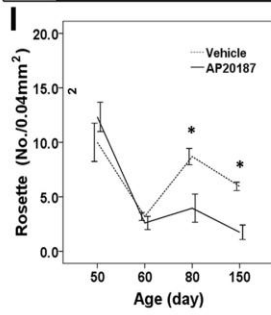
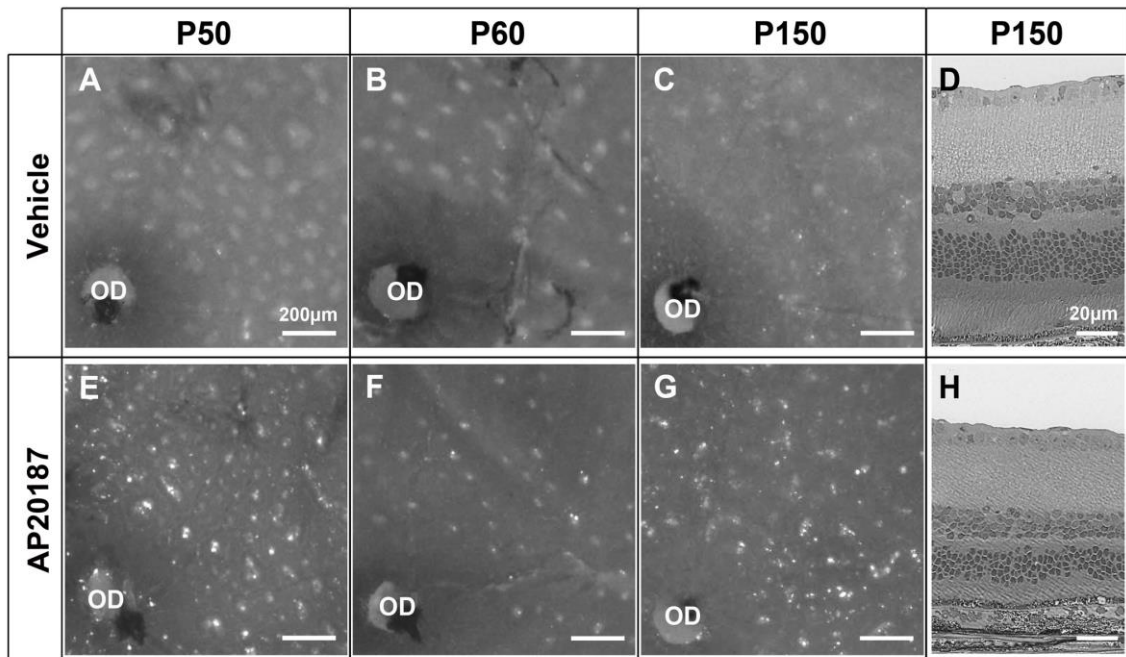
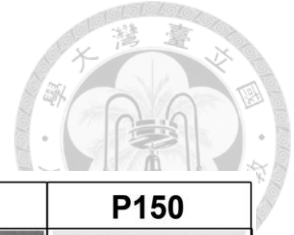
Chapter 3, Figure 5.



Figure 5. Accelerated retinal degeneration after systemic depletion of circulating BM-derived microglia in *rd7/rd7;tg/tg* mice.

A-D: The cilioretinal flatmounts and histology from the *rd7/rd7;Tg/Tg* mice treated with vehicle at P50 (**A**), P60 (**B**), and P150 (**C, D**). **E-H:** The cilioretinal flatmounts and histology from the *rd7/rd7;Tg/Tg* mice treated with AP20187 at P50 (**E**), P60 (**F**), and P150 (**G, H**). **I:** The number of rosettes in the cilioretinal flatmounts (mean \pm SD) was determined at P50 (n = 8), P60 (n = 11), P80 (n = 3), and P150 (n = 4). **J:** The number of AF spots in the cilioretinal flatmounts (mean \pm SD) was determined at P50 (n = 8), P60 (n = 11), P80 (n = 3), and P150 (n = 4). **K:** The number of nuclei in the outer nuclear layer was significantly decreased in mice injected with AP20187 for 5 months compared with mice injected with vehicle. **L:** Scheme of an eye section showing the area in which the outer nuclear layer nuclei were counted (**A**). ONL, outer nuclear layer. OD, optic disc. Scale bar: (**A-C, E-G**) 200 μ m, (**E, H**) 20 μ m. * $P < 0.05$.

Chapter 3, Figure 5.



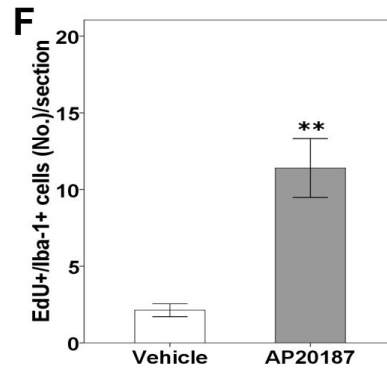
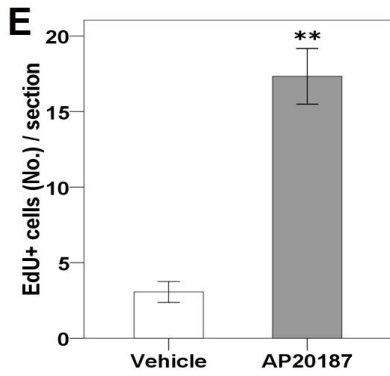
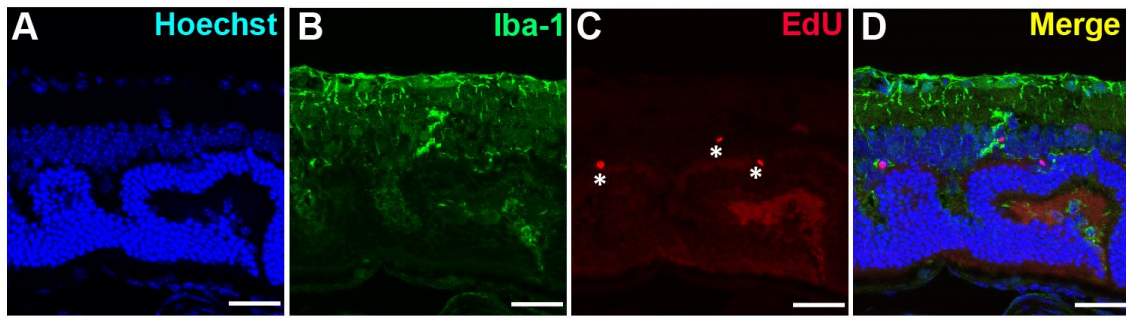
Chapter 3, Figure 6.



Figure 6. Confocal images showing proliferative resident microglia in the retina of *rd7/rd7;tg/tg* mice after 4 weeks of injection of AP20187.

A–D: Proliferative cells located in the outer plexiform layer, outer nuclear layer, or ganglion cell layer exhibited EdU labeling (asterisks in **C**). Colocalized labeling of EdU and Iba-1 was detected in (**D**). **E and F:** The number of EdU-labeled cells was significantly increased in mice injected with AP20187 for 1 month compared with mice injected with vehicle (n=3 in each group). The majority of the EdU-labeled cells were colocalized with Iba-1 (**F**). Asterisks indicate significant difference. Scale bar: (**A–D**) 30 μm . **** $P < 0.001$**

Chapter 3, Figure 6.



Chapter 3, Figure 7.

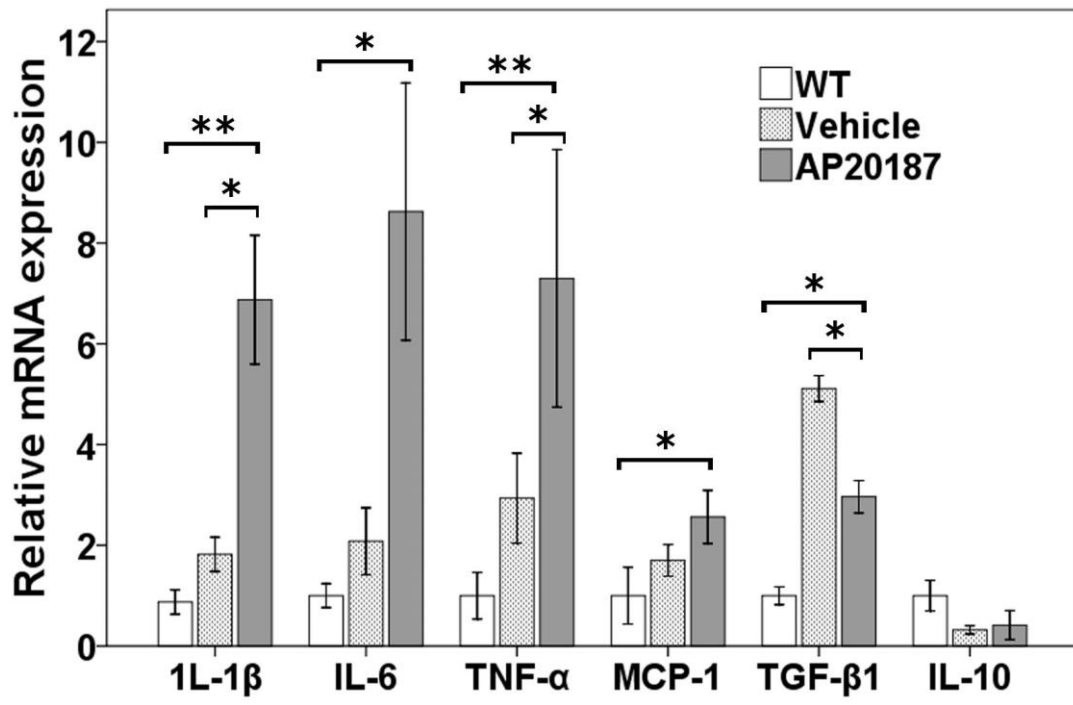


Figure 7. Relative gene expression after systemic depletion of circulating

BM-derived microglia.

Quantification of gene expression changes by qRT-PCR at P60 (4 weeks after being treated with AP20187 and vehicle, n=3 in each group), expressed as mean fold change in comparison with wild type \pm 1 s.d., showing a trend of downregulation of the gene encoding the anti-inflammatory cytokine TGF β 1, and upregulation in genes encoding the inflammatory cytokines IL-1 β , IL-6, TNF- α , and monocyte chemotactic protein (MCP-1). Asterisks indicate significant difference. WT: wild type. * P < 0.05, ** P < 0.001.

Chapter 3, Figure 7.



Chapter 3, Figure S1.



Figure S1. Body weight changes after systemic depletion of circulating BM-derived microglia.

A and B: After systemic macrophage ablation using AP20187, body weight didn't increase as fast in the AP20187 mice than in the vehicle treated animal.

Chapter 3, Figure S1.

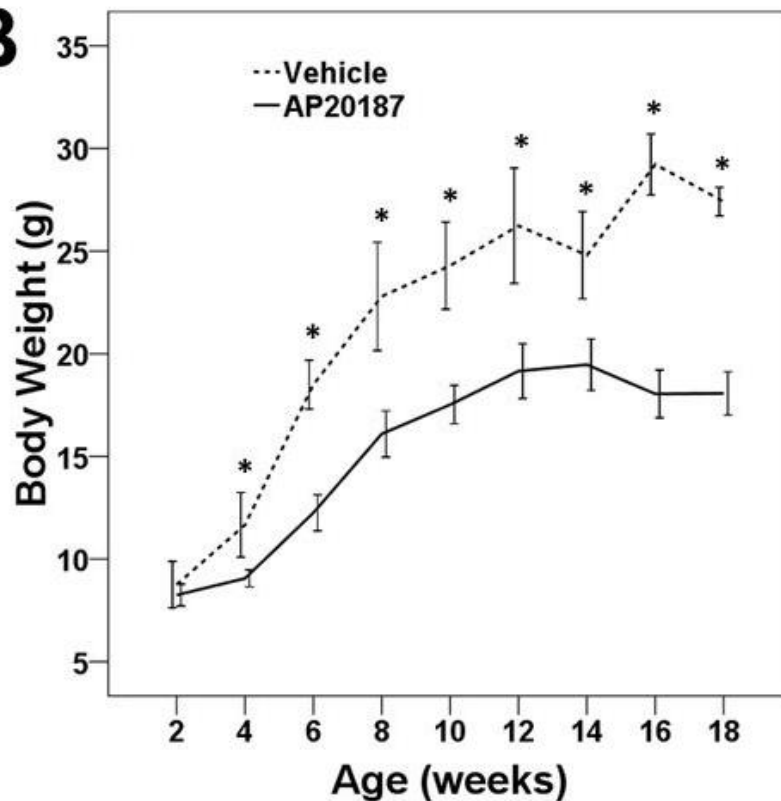


A

	AP20187 (No.)	Vehicle (No.)	P Value
BW 2 wks, gm	8.25 ± 1.02 (15)	8.76 ± 1.79 (10)	0.375
BW 4 wks, gm	9.06 ± 0.80 (15)	11.67 ± 2.49 (10)	0.009
BW 6 wks, gm	12.25 ± 1.70 (15)	18.50 ± 1.88 (10)	<0.001
BW 8 wks, gm	16.10 ± 2.18 (15)	22.80 ± 4.17 (10)	0.001
BW 10 wks, gm	17.52 ± 1.75 (14)	24.30 ± 3.36 (10)	<0.001
BW 12 wks, gm	19.15 ± 2.31 (12)	26.24 ± 3.97 (8)	0.001
BW 14 wks, gm	19.47 ± 1.98 (10)	24.80 ± 2.81 (7)	<0.001
BW 16 wks, gm	18.04 ± 1.53 (7)	29.22 ± 1.82 (6)	<0.001
BW 18 wks, gm	18.07 ± 1.18 (5)	27.42 ± 0.86 (6)	<0.001

BW: body weight; No.: number.

B



Chapter 3, Figure S2.

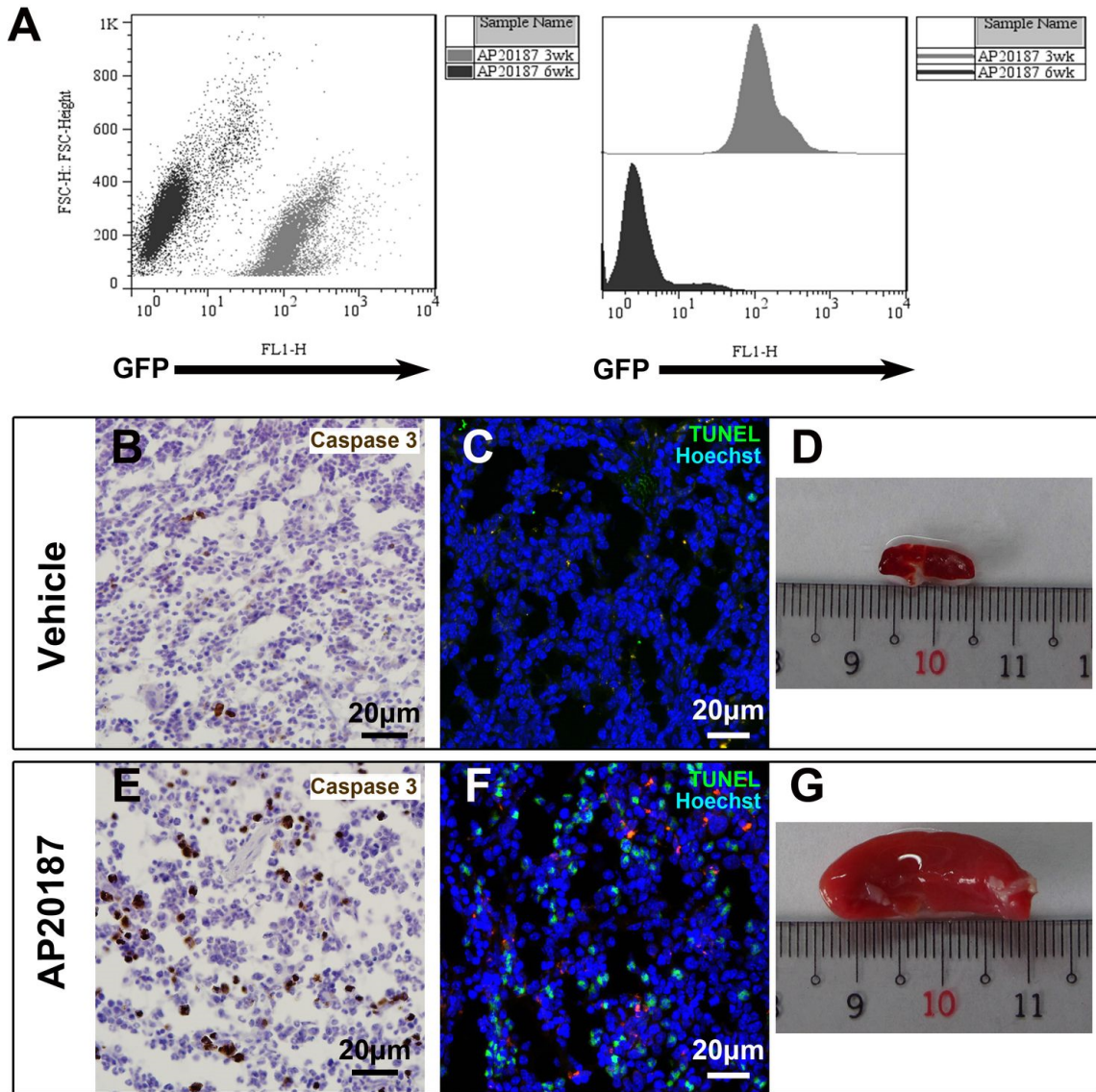


Figure S2. Systemic Depletion of Circulating BM-derived Microglia

A: Peritoneal cells from an *rd7/rd7;Tg/Tg* mouse were analyzed for EGFP expression using cytometric analysis after treatment with AP20187 (i.v.) for 3 weeks and 6 weeks. Histograms were graphed from events gated by forward and side scatter (FSC and SSC, respectively) to the region where macrophages and lymphocytes would be found.

Immunostaining of spleens of *rd7/rd7;Tg/Tg* mice 8 weeks after being injected with vehicle (**B** and **C**) and AP20187 (**E** and **F**) showed more apoptotic cells (brown, active caspase 3; green, TUNEL) in AP20187-injected groups. Nuclei are stained with Hoechst (**C** and **F**). Enlarged spleens were noted in *rd7/rd7;Tg/Tg* mice 8 weeks after injection with AP20187 (**G**) compared with animals injected with vehicle (**D**). Scale bar: (**B**, **C**, **E**, **F**) 20 μm .

Chapter 3, Figure S2.



Chapter IV

Conclusion and Future Perspectives





Conclusion

On funduscopy, the appearance of diffuse retinal white dots, hyperautofluorescent (AF) spots, and retinal rosettes in young patients with Goldmann-Favre Syndrome were similar to those seen in young *rd7* mice. We showed that microglia, rather than retinal pigment epithelium (RPE) cells, contributed to these AF spots (Wang et al. 2009).

Temporal control of a circulating BM-derived microglia population was achieved by introducing the *Mafia* transgene into the *rd7* mouse model of Goldmann-Favre Syndrome. Since the *Mafia* inducer AP20187 does not cross the blood-brain barrier, resident retinal microglia are spared but circulating BM-derived microglia are ablated after AP20187 administration. After systemic depletion of circulating BM-derived microglia in young mice, cilioretinal flatmounts exhibited characteristics that mimicked those of later stages of retinal degeneration in *rd7* mice, and outer nuclear layer analyses showed decreased nuclei count. Inflammatory cytokines IL-1 β , IL-6, TNF- α , and monocyte chemotactic protein (MCP-1) were upregulated, whereas the anti-inflammatory cytokine TGF- β 1 was downregulated in the retina. Circulating BM-derived microglia appear to have a role in suppressing intraocular inflammation, and its loss can promote retinal degeneration. These results highlight the opposing roles of resident microglia and circulating BM-derived microglia in retinal degeneration.

Perspective I



Microglia reacts not only to inflammation, but to signals from damaged neurons.

Once they receive the signal, an autocrine signal function activates itself to fully activate macrophages. Besides, microglia receives signals from astrocytes (e.g., pro-inflammatory cytokines such as TNF alpha, IL-6 and nitric oxide). Microglia also has a phagocytic function and has been implicated in wound healing, angiogenesis, and extracellular matrix formation (Ellis-Behnke et al. 2013). Although we found microglial proliferation in our study, we still don't know which factor or cytokines has triggered the activation of microglia.

Kohno et al. (2013) found photoreceptor proteins initiate microglial activation via Toll-like receptor 4. In their study, bone marrow-derived microglia from *Tlr4*-deficient mice does not increase Ccl2 (MCP-1) after coincubation with photoreceptor proteins. Our research results indicate that photoreceptor proteins from noncontact outer segment debris locate in the rosettes that could not be phagocytosed by retinal pigment epithelium may trigger the inflammation, and thus activate the microglia. If we want to test the hypothesis that microglial activation is related to Toll-like receptor 4, we can further generate *Tlr4*^{-/-} *rd7/rd7;Tg/Tg* mice. In briefly, retina from *Tlr4*^{-/-} *rd7/rd7;Tg/Tg* mice were harvested and assayed by quantitative real-time PCR (qRT-PCR), western blots and immunohistochemistry after treated with AP20187 or

vehicle.



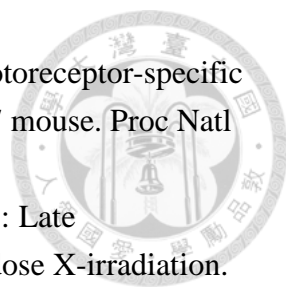
Perspective II


Microglial activation has been reported in different retinal degenerations (Langmann 2007; Sasahara et al. 2008; Arroba et al. 2011). However, our results suggest opposing roles of resident microglia and BM-derived microglia in only *rd7* mice. We use the advantage of *Mafia* mice to investigate whether these opposing roles between resident and BM-derived microglia exist in other retinal degenerations.

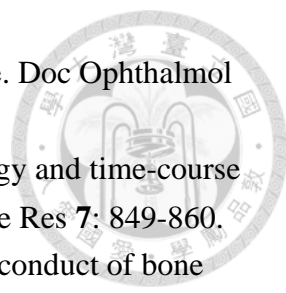
In the present study, the expression of TNF- α and IL-1 β was increased in mice injected with AP20187 compared to vehicle-injected and WT mice, suggesting a possible causal role for these cytokines in photoreceptor loss. It is important to investigate the mechanism of photoreceptor loss after systemic depletion of BM-derived microglia in *rd7/rd7;Tg/Tg* mice. We find that the resident microglia proliferation accounts for not only the increase in AF spots observed in cilioretinal flatmounts, but increased cytotoxic substances aggravate inflammatory processes. This finding suggest that future research should focus on the search for therapeutic agents to intervene the inflammatory processes involved in retinal degeneration, and investigate the molecular signals that act between microglial activation and photoreceptor loss. These therapeutic agents include cell replacement, cytokines, growth factors, and gene therapy with or without cell therapy.


Bibliography



- 
- Akhmedov NB, Piriev NI, Chang B, et al. (2000): A deletion in a photoreceptor-specific nuclear receptor mRNA causes retinal degeneration in the rd7 mouse. *Proc Natl Acad Sci U S A* **97**: 5551-5556.
- Amoaku WM, Mahon GJ, Gardiner TA, Frew L & Archer DB (1992): Late ultrastructural changes in the retina of the rat following low-dose X-irradiation. *Graefes Arch Clin Exp Ophthalmol* **230**: 569-574.
- Arroba AI, Alvarez-Lindo N, van Rooijen N & de la Rosa EJ (2011): Microglia-mediated IGF-I neuroprotection in the rd10 mouse model of retinitis pigmentosa. *Invest Ophthalmol Vis Sci* **52**: 9124-9130.
- Ashwell KW, Hollander H, Streit W & Stone J (1989): The appearance and distribution of microglia in the developing retina of the rat. *Vis Neurosci* **2**: 437-448.
- Audo I, Michaelides M, Robson AG, et al. (2008): Phenotypic variation in enhanced S-cone syndrome. *Invest Ophthalmol Vis Sci* **49**: 2082-2093.
- Banerjee R & Lund RD (1992): A role for microglia in the maintenance of photoreceptors in retinal transplants lacking pigment epithelium. *J Neurocytol* **21**: 235-243.
- Block ML, Zecca L & Hong JS (2007): Microglia-mediated neurotoxicity: uncovering the molecular mechanisms. *Nature reviews. Neuroscience* **8**: 57-69.
- Burnett SH, Beus BJ, Avdiushko R, Qualls J, Kaplan AM & Cohen DA (2006): Development of peritoneal adhesions in macrophage depleted mice. *J Surg Res* **131**: 296-301.
- Burnett SH, Kershen EJ, Zhang J, et al. (2004): Conditional macrophage ablation in transgenic mice expressing a Fas-based suicide gene. *J Leukoc Biol* **75**: 612-623.
- Caicedo A, Espinosa-Heidmann DG, Pina Y, Hernandez EP & Cousins SW (2005): Blood-derived macrophages infiltrate the retina and activate Muller glial cells under experimental choroidal neovascularization. *Exp Eye Res* **81**: 38-47.
- Carwile ME, Culbert RB, Sturdivant RL & Kraft TW (1998): Rod outer segment maintenance is enhanced in the presence of bFGF, CNTF and GDNF. *Exp Eye Res* **66**: 791-805.
- Cecchini MG, Dominguez MG, Mocchi S, et al. (1994): Role of colony stimulating factor-1 in the establishment and regulation of tissue macrophages during postnatal development of the mouse. *Development* **120**: 1357-1372.
- Chavala SH, Sari A, Lewis H, et al. (2005): An Arg311Gln NR2E3 mutation in a family with classic Goldmann-Favre syndrome. *Br J Ophthalmol* **89**: 1065-1066.
- Chen J, Rattner A & Nathans J (2005): The rod photoreceptor-specific nuclear receptor Nr2e3 represses transcription of multiple cone-specific genes. *J Neurosci* **25**: 118-129.

- 
- Coppieters F, Leroy BP, Beysen D, et al. (2007): Recurrent mutation in the first zinc finger of the orphan nuclear receptor NR2E3 causes autosomal dominant retinitis pigmentosa. *Am J Hum Genet* **81**: 147-157.
- Cuadros MA & Navascues J (1998): The origin and differentiation of microglial cells during development. *Prog Neurobiol* **56**: 173-189.
- Ellis-Behnke RG, Jonas RA & Jonas JB (2013): The microglial system in the eye and brain in response to stimuli in vivo. *Journal of glaucoma* **22 Suppl 5**: S32-35.
- Gentleman SM (2013): Review: Microglia in protein aggregation disorders: friend or foe? *Neuropathol Appl Neurobiol* **39**: 45-50.
- Gerber S, Rozet JM, Takezawa SI, et al. (2000): The photoreceptor cell-specific nuclear receptor gene (PNR) accounts for retinitis pigmentosa in the Crypto-Jews from Portugal (Marranos), survivors from the Spanish Inquisition. *Hum Genet* **107**: 276-284.
- Gordon WC, Casey DM, Lukiw WJ & Bazan NG (2002): DNA damage and repair in light-induced photoreceptor degeneration. *Invest Ophthalmol Vis Sci* **43**: 3511-3521.
- Gratchev A, Guillot P, Hakiy N, et al. (2001): Alternatively activated macrophages differentially express fibronectin and its splice variants and the extracellular matrix protein betaIG-H3. *Scand J Immunol* **53**: 386-392.
- Gratchev A, Kzhyshkowska J, Utikal J & Goerdts S (2005): Interleukin-4 and dexamethasone counterregulate extracellular matrix remodelling and phagocytosis in type-2 macrophages. *Scand J Immunol* **61**: 10-17.
- Haider NB, Jacobson SG, Cideciyan AV, et al. (2000): Mutation of a nuclear receptor gene, NR2E3, causes enhanced S cone syndrome, a disorder of retinal cell fate. *Nat Genet* **24**: 127-131.
- Haider NB, Naggert JK & Nishina PM (2001): Excess cone cell proliferation due to lack of a functional NR2E3 causes retinal dysplasia and degeneration in rd7/rd7 mice. *Hum Mol Genet* **10**: 1619-1626.
- Hanisch UK & Kettenmann H (2007): Microglia: active sensor and versatile effector cells in the normal and pathologic brain. *Nat Neurosci* **10**: 1387-1394.
- Harada T, Harada C, Kohsaka S, et al. (2002): Microglia-Muller glia cell interactions control neurotrophic factor production during light-induced retinal degeneration. *J Neurosci* **22**: 9228-9236.
- Hayashi T, Gekka T, Goto-Omoto S, Takeuchi T, Kubo A & Kitahara K (2005): Novel NR2E3 mutations (R104Q, R334G) associated with a mild form of enhanced S-cone syndrome demonstrate compound heterozygosity. *Ophthalmology* **112**: 2115.
- Holder GE, Brigell MG, Hawlina M, Meigen T, Vaegan & Bach M (2007): ISCEV

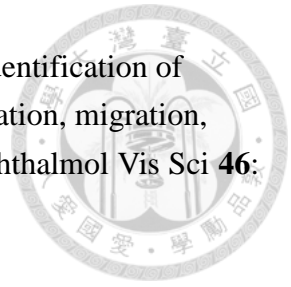
- 
- standard for clinical pattern electroretinography--2007 update. *Doc Ophthalmol* **114**: 111-116.
- Hoppeler T, Hendrickson P, Dietrich C & Reme C (1988): Morphology and time-course of defined photochemical lesions in the rabbit retina. *Curr Eye Res* **7**: 849-860.
- Hou HY, Wang YS, Xu JF, Wang YC & Liu JP (2006): The dynamic conduct of bone marrow-derived cells in the choroidal neovascularization microenvironment. *Curr Eye Res* **31**: 1051-1061.
- Joly S, Francke M, Ulbricht E, et al. (2009): Cooperative phagocytes: resident microglia and bone marrow immigrants remove dead photoreceptors in retinal lesions. *Am J Pathol* **174**: 2310-2323.
- Kaneko H, Nishiguchi KM, Nakamura M, Kachi S & Terasaki H (2008): Characteristics of bone marrow-derived microglia in the normal and injured retina. *Invest Ophthalmol Vis Sci* **49**: 4162-4168.
- Khan AO, Aldahmesh M & Meyer B (2007): The enhanced S-cone syndrome in children. *Br J Ophthalmol* **91**: 394-396.
- Kigerl KA, Gensel JC, Ankeny DP, Alexander JK, Donnelly DJ & Popovich PG (2009): Identification of two distinct macrophage subsets with divergent effects causing either neurotoxicity or regeneration in the injured mouse spinal cord. *J Neurosci* **29**: 13435-13444.
- Kivela T, Tarkkanen A & Virtanen I (1986): Intermediate filaments in the human retina and retinoblastoma. An immunohistochemical study of vimentin, glial fibrillary acidic protein, and neurofilaments. *Invest Ophthalmol Vis Sci* **27**: 1075-1084.
- Kreutzberg GW (1996): Microglia: a sensor for pathological events in the CNS. *Trends Neurosci* **19**: 312-318.
- Kzhyshkowska J, Workman G, Cardo-Vila M, et al. (2006): Novel function of alternatively activated macrophages: stabilin-1-mediated clearance of SPARC. *J Immunol* **176**: 5825-5832.
- Langmann T (2007): Microglia activation in retinal degeneration. *J Leukoc Biol* **81**: 1345-1351.
- Milam AH & Jacobson SG (1990): Photoreceptor rosettes with blue cone opsin immunoreactivity in retinitis pigmentosa. *Ophthalmology* **97**: 1620-1631.
- Milam AH, Rose L, Cideciyan AV, et al. (2002): The nuclear receptor NR2E3 plays a role in human retinal photoreceptor differentiation and degeneration. *Proc Natl Acad Sci U S A* **99**: 473-478.
- Milligan CE, Cunningham TJ & Levitt P (1991): Differential immunochemical markers reveal the normal distribution of brain macrophages and microglia in the developing rat brain. *J Comp Neurol* **314**: 125-135.
- Mustafi D, Kevany BM, Genoud C, et al. (2011): Defective photoreceptor phagocytosis

- 
- in a mouse model of enhanced S-cone syndrome causes progressive retinal degeneration. *FASEB J* **25**: 3157-3176.
- Ng TF & Streilein JW (2001): Light-induced migration of retinal microglia into the subretinal space. *Invest Ophthalmol Vis Sci* **42**: 3301-3310.
- Peyman GA, Fishman GA, Sanders DR & Vlcek J (1977): Histopathology of Goldmann-Favre syndrome obtained by full-thickness eye-wall biopsy. *Ann Ophthalmol* **9**: 479-484.
- Qualls JE, Kaplan AM, van Rooijen N & Cohen DA (2006): Suppression of experimental colitis by intestinal mononuclear phagocytes. *J Leukoc Biol* **80**: 802-815.
- Ritter MR, Banin E, Moreno SK, Aguilar E, Dorrell MI & Friedlander M (2006): Myeloid progenitors differentiate into microglia and promote vascular repair in a model of ischemic retinopathy. *J Clin Invest* **116**: 3266-3276.
- Robson AG, Egan C, Holder GE, Bird AC & Fitzke FW (2003): Comparing rod and cone function with fundus autofluorescence images in retinitis pigmentosa. *Adv Exp Med Biol* **533**: 41-47.
- Robson AG, Saihan Z, Jenkins SA, et al. (2006): Functional characterisation and serial imaging of abnormal fundus autofluorescence in patients with retinitis pigmentosa and normal visual acuity. *Br J Ophthalmol* **90**: 472-479.
- Roque RS, Rosales AA, Jingjing L, Agarwal N & Al-Ubaidi MR (1999): Retina-derived microglial cells induce photoreceptor cell death in vitro. *Brain Res* **836**: 110-119.
- Sasahara M, Otani A, Oishi A, et al. (2008): Activation of bone marrow-derived microglia promotes photoreceptor survival in inherited retinal degeneration. *Am J Pathol* **172**: 1693-1703.
- Schmitz-Valckenberg S, Holz FG, Bird AC & Spaide RF (2008): Fundus autofluorescence imaging: review and perspectives. *Retina* **28**: 385-409.
- Seledtsov VI & Seledtsova GV (2012): A balance between tissue-destructive and tissue-protective immunities: a role of toll-like receptors in regulation of adaptive immunity. *Immunobiology* **217**: 430-435.
- Sharon D, Sandberg MA, Caruso RC, Berson EL & Dryja TP (2003): Shared mutations in NR2E3 in enhanced S-cone syndrome, Goldmann-Favre syndrome, and many cases of clumped pigmentary retinal degeneration. *Arch Ophthalmol* **121**: 1316-1323.
- Simard AR, Soulet D, Gowing G, Julien JP & Rivest S (2006): Bone marrow-derived microglia play a critical role in restricting senile plaque formation in Alzheimer's disease. *Neuron* **49**: 489-502.
- Sivakumar V, Foulds WS, Luu CD, Ling EA & Kaur C (2011): Retinal ganglion cell

- death is induced by microglia derived pro-inflammatory cytokines in the hypoxic neonatal retina. *J Pathol* **224**: 245-260.
- Smith RS (2001): *Systematic Evaluation of the Mouse Eye: Anatomy, Pathology, and Biomethods*. Boca Raton, Florida. CRC Press.
- Sparrow JR, Parish CA, Hashimoto M & Nakanishi K (1999): A2E, a lipofuscin fluorophore, in human retinal pigmented epithelial cells in culture. *Invest Ophthalmol Vis Sci* **40**: 2988-2995.
- Tambuyzer BR, Ponsaerts P & Nouwen EJ (2009): Microglia: gatekeepers of central nervous system immunology. *J Leukoc Biol* **85**: 352-370.
- Tsang SH, Vaclavik V, Bird AC, Robson AG & Holder GE (2007): Novel phenotypic and genotypic findings in X-linked retinoschisis. *Arch Ophthalmol* **125**: 259-267.
- Tsui I, Casper D, Chou CL & Tsang SH (2008): Electronegative electroretinogram associated with topiramate toxicity and vitelliform maculopathy. *Doc Ophthalmol* **116**: 57-60.
- Tsui I, Fuchs BS, Chou CL, Chang S & Tsang SH (2008): Non-vascular vision loss in pseudoxanthoma elasticum. *Doc Ophthalmol* **117**: 65-67.
- Vaclavik V, Chakarova C, Bhattacharya SS, et al. (2008): Bilateral giant macular schisis in a patient with enhanced S-cone syndrome from a family showing pseudo-dominant inheritance. *Br J Ophthalmol* **92**: 299-300.
- von Ruckmann A, Fitzke FW & Bird AC (1995): Distribution of fundus autofluorescence with a scanning laser ophthalmoscope. *Br J Ophthalmol* **79**: 407-412.
- Wang NK, Fine HF, Chang S, et al. (2009): Cellular origin of fundus autofluorescence in patients and mice with a defective NR2E3 gene. *Br J Ophthalmol* **93**: 1234-1240.
- Wang NK, Tosi J, Kasanuki JM, et al. (2010): Transplantation of reprogrammed embryonic stem cells improves visual function in a mouse model for retinitis pigmentosa. *Transplantation* **89**: 911-919.
- Wenzel A, Grimm C, Samardzija M & Reme CE (2005): Molecular mechanisms of light-induced photoreceptor apoptosis and neuroprotection for retinal degeneration. *Prog Retin Eye Res* **24**: 275-306.
- Wright AF, Reddick AC, Schwartz SB, et al. (2004): Mutation analysis of NR2E3 and NRL genes in Enhanced S Cone Syndrome. *Hum Mutat* **24**: 439.
- Xu H, Chen M, Mayer EJ, Forrester JV & Dick AD (2007): Turnover of resident retinal microglia in the normal adult mouse. *Glia* **55**: 1189-1198.
- Yeh LK, Liu CY, Chien CL, et al. (2008): Molecular analysis and characterization of zebrafish keratocan (zKera) gene. *J Biol Chem* **283**: 506-517.

Zeng HY, Zhu XA, Zhang C, Yang LP, Wu LM & Tso MO (2005): Identification of sequential events and factors associated with microglial activation, migration, and cytotoxicity in retinal degeneration in rd mice. *Invest Ophthalmol Vis Sci* **46**: 2992-2999.

Zhang C, Lam TT & Tso MO (2005): Heterogeneous populations of microglia/macrophages in the retina and their activation after retinal ischemia and reperfusion injury. *Exp Eye Res* **81**: 700-709.



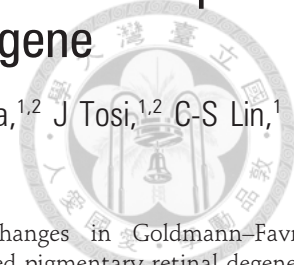
Appendix



1. **Cellular origin of fundus autofluorescence in patients and mice with a defective NR2E3 gene** – published in *British Journal Ophthalmology* 2009;93:1234-40.
2. **Origin of fundus hyperautofluorescent (AF) spots, and their role in retinal degeneration in a Mouse Model of Goldmann-Favre Syndrome** – accepted in *Disease Models & Mechanisms*. 2013 Jul 4.
[Epub ahead of print]

Cellular origin of fundus autofluorescence in patients and mice with a defective *NR2E3* gene

N-K Wang,^{1,2,3} H F Fine,¹ S Chang,¹ C L Chou,^{1,2} W Cella,^{1,2} J Tosi,^{1,2} C-S Lin,¹ T Nagasaki,¹ S H Tsang^{1,2}



¹ Bernard & Shirlee Brown Glaucoma Laboratory, Edward S Harkness Eye Institute, New York, USA; ² Department of Pathology & Cell Biology, Columbia University, New York, USA; ³ Department of Ophthalmology, Chang Gung Memorial Hospital, Linkou, Taiwan

Correspondence to: Dr S Tsang, Edward Harkness Eye Institute, 160 Fort Washington Ave, Research Annex, Room 513, New York, NY 10032, USA; sht2@columbia.edu

Accepted 23 April 2009
Published Online First 2 July 2009

ABSTRACT

Aim: To characterise new clinical features in a family with enhanced S-cone syndrome (ESCS) and investigate the pathogenesis of these clinical features in the homozygous *Nr2e3^{rd7}* (*rd7*) mutant mice.

Methods: Four patients from an affected family were included for genotypic and phenotypic study. Eye tissues from *rd7* mice were used to detect a possible relationship between macrophages and autofluorescent material by immunohistochemistry (IHC) staining.

Results: Homozygous mutation in R311Q in *NR2E3* was detected in this family. Colour photographs revealed that white dots do not correlate to hyperautofluorescent spots seen in autofluorescence imaging of the macula. OCT showed rosette-like lesions similar to those found in *rd7* mice histology sections. From IHC analysis, we observed that F4/80 (a pan macrophage marker) and autofluorescence were colocalised to the same cells within the retina rosettes.

Conclusions: The retinal structure of a young ESCS patient with homozygous R311Q mutation in the *NR2E3* gene is similar to that seen in the *rd7* mice. The macrophages were found to contain autofluorescent materials in the retinal rosettes of *rd7* mice. These data are consistent with macrophage infiltration contributing to the hyperautofluorescent spots found in our patients.

Enhanced S-cone syndrome (ESCS; OMIM 268100; <http://www.ncbi.nlm.nih.gov/omim/> Online Mendelian Inheritance in Man; NCBI, Bethesda, Maryland) is a relatively slowly progressive autosomal recessive rod–cone degeneration caused by mutations in the orphan nuclear receptor transcription factor *NR2E3* (OMIM: 604485). *NR2E3* encodes a retinal nuclear receptor that is a ligand-dependent transcription repressor of cone-specific genes in rod photoreceptors.¹ The NR2E3 protein is part of a large family of nuclear receptor transcription factors that is homologous to an orphan nuclear receptor, Nr2e1 (formerly known as *tailless* or *TLX*), which is involved in the development and maintenance of normal function of the central nervous system (CNS) in *Drosophila* and mammals. NR2E3 is expressed in mitotic progenitor cells during development, and its increased expression in cone cells may be due to a prolonged period of cone proliferation, which is followed by a gradual increase in apoptosis. NR2E3 appears to be a dual regulator, suppressing cone cell proliferation in mitotic cells and promoting rod cell genesis in postmitotic cells. *NR2E3* mutations were first identified in patients with ESCS, but more recent studies have demonstrated that mutations in *NR2E3* are also common causes of clumped

pigmentary changes in Goldmann–Favre syndrome, clumped pigmentary retinal degenerations, autosomal recessive retinitis pigmentosa and autosomal dominant retinitis pigmentosa.^{2–9}

The spontaneous mutant *Nr2e3^{rd7}* (*rd7*) mice have a mutation in *NR2E3* gene.¹⁰ This mutant mouse displays increased number and proportion of photoreceptors with S-cone phenotype and abnormal lamination of the outer nuclear layer (ONL).^{10 11}

With confocal scanning-laser ophthalmoscope and spectral domain optical coherence tomography, we discovered similar features in a patient. In addition, we demonstrated the origin of these unique clinical features in the homozygous *Nr2e3^{rd7}* (*rd7*) mutant mice.

MATERIALS AND METHODS

Phenotypic studies

Four patients from an affected family (6, 8, 35 and 46 years of age) were enrolled with the approval of the institutional review board protocol #AAAB6560 at Columbia University. The tenets of the Declaration of Helsinki were followed.

All patients underwent complete ophthalmic evaluation after informed consent was obtained. Fundus photographs, retinal pigment epithelium (RPE) autofluorescence (AF), Fourier-domain optical coherence tomography (OCT) and electroretinography (ERG) were performed in the two children.

Genetic analyses

The coding region of *NR2E3* was sequenced for disease-causing mutations in all patients. DNA was extracted from peripheral blood with the QIAamp DNA Mini Kit (Qiagen, Valencia, California). Extracted genomic DNA was amplified by polymerase chain reaction (PCR) using primers and cycling temperature as previously described.¹² The PCR products were purified (QIAquick PCR Purification Kit, Qiagen, Valencia, California) and sequenced.

Autofluorescence imaging

Autofluorescence images were obtained using a confocal scanning-laser ophthalmoscope (cSLO, Heidelberg Retina Angiograph 2, Heidelberg Engineering, Dossenheim, Germany) by illuminating the fundus with argon laser light (488 nm) and viewing the resultant fluorescence through a band pass filter with a short wavelength cut-off at 495 nm.^{13–18}

Optical coherence tomography (OCT)

Spectral domain optical coherence tomography (SD-OCT) images were obtained using the Cirrus Spectral Domain OCT from Zeiss (Carl Zeiss Meditec, Dublin, California). The acquisition protocols included five-line raster scans. Three scans were performed on each eye, and the one with the best signal strength was selected for the final analysis.

Electroretinogram (ERG) testing

Full-field ERG were performed with silver-impregnated fibre electrodes (DTL; Diagnosys LLC, Littleton, Massachusetts) and incorporated the ISCEV Standards.¹⁹ The minimum protocol incorporates the rod-specific and standard bright flash ERGs, both recorded after a minimum of 20 min dark adaptation. Following 10 min of light adaptation, the photopic 30 Hz flicker cone and transient photopic cone ERGs were recorded. S-cone ERGs used a blue stimulus (445 nm, 2–12 cd/m²) on an orange background (620 nm, 100 cd/m²).¹²

Whole mount eyecup

To better understand the mechanisms underlying the clinical findings in our patients, we acquired the *Nr2e3*^{rd7} mutant mice, a mouse model for ESCS, from Jackson laboratory (stock #004643, Bar Harbor, Maine). Eyes from 5-week-old *Nr2e3*^{rd7} mice and 8-week-old C57BL/6J mice (used as a control) were enucleated and placed in 4% paraformaldehyde for 1 h at room temperature. The cornea and lens were removed from each eye under a surgical microscope. The whole eyecups were flattened by means of four radial cuts and mounted with mounting medium (VECTASHIELD, Burlingame, California). Autofluorescence was detected by standard fluorescence microscopy.

Immunohistochemistry (IHC)

Whole eyecups were prepared as described above, and frozen in optimum cutting temperature compound (Tissue-Tek OCT, Miles Laboratories, Elkhart, Indiana). Frozen eyes were cryosectioned using a thickness of 10 µm. Blocking was performed using 10% donkey serum in PBS with 0.3% Triton X-100 (blocking solution) for 30 min at room temperature (RT). The sections were then incubated with the primary antibodies diluted in 4% donkey serum in PBS with 0.1% Triton X-100 for 2 h at RT. The samples were subsequently incubated for 40 min at RT with the secondary antibodies diluted in PBS with 0.1% Triton. The primary antibody used was directed against F4/80, a pan macrophage marker (dilution 1:500, eBioscience, San Diego, California). The secondary antibody used was: Alexa Fluor 488 donkey antirat IgG (dilutions 1:1000, Invitrogen, Carlsbad, California). After washing three times with PBS, the retinas were mounted with mounting medium containing the nuclear dye DAPI (VECTASHIELD, Burlingame, California) and viewed under a fluorescence microscope (Leica DM 5000 B, Wetzlar, Germany). Images were digitally merged to assess for triple labelling.

RESULTS

Genetic studies

Direct sequencing of the *NR2E3* gene from the proband revealed a homozygous missense mutation 932G→A in exon 6 coding for the R311Q residue (fig 1). His asymptomatic elder brother (8 year old) and consanguineous parents (first cousins) were heterozygous for a mutation at the same DNA site.

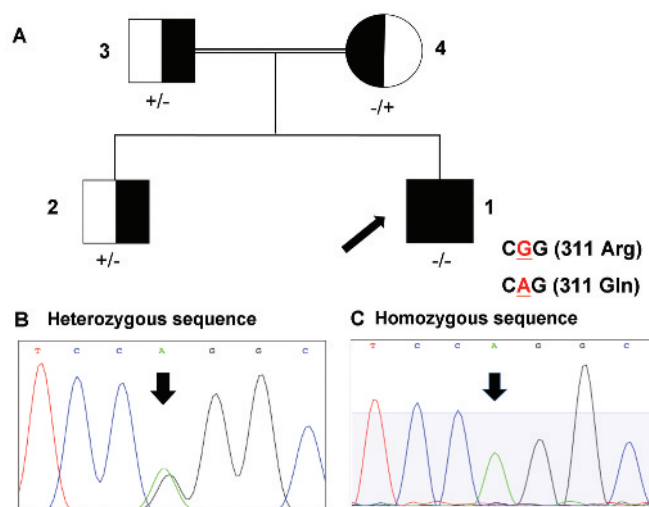


Figure 1 (A) Pedigree of a family in which mutation in the *NR2E3* gene were identified. A mutant allele is indicated by (-); a normal allele is indicated by (+). The arrow shows the proband (1, homozygous), and the other members are heterozygous. (B) Direct DNA sequencing from proband's consanguineous parents and brother showing heterozygous base-substitution at 932G→A in exon 6. (C) Direct sequencing from the proband revealing a homozygous base substitution at 932G→A with a predicted missense mutation of R311Q (CGG to CAG).

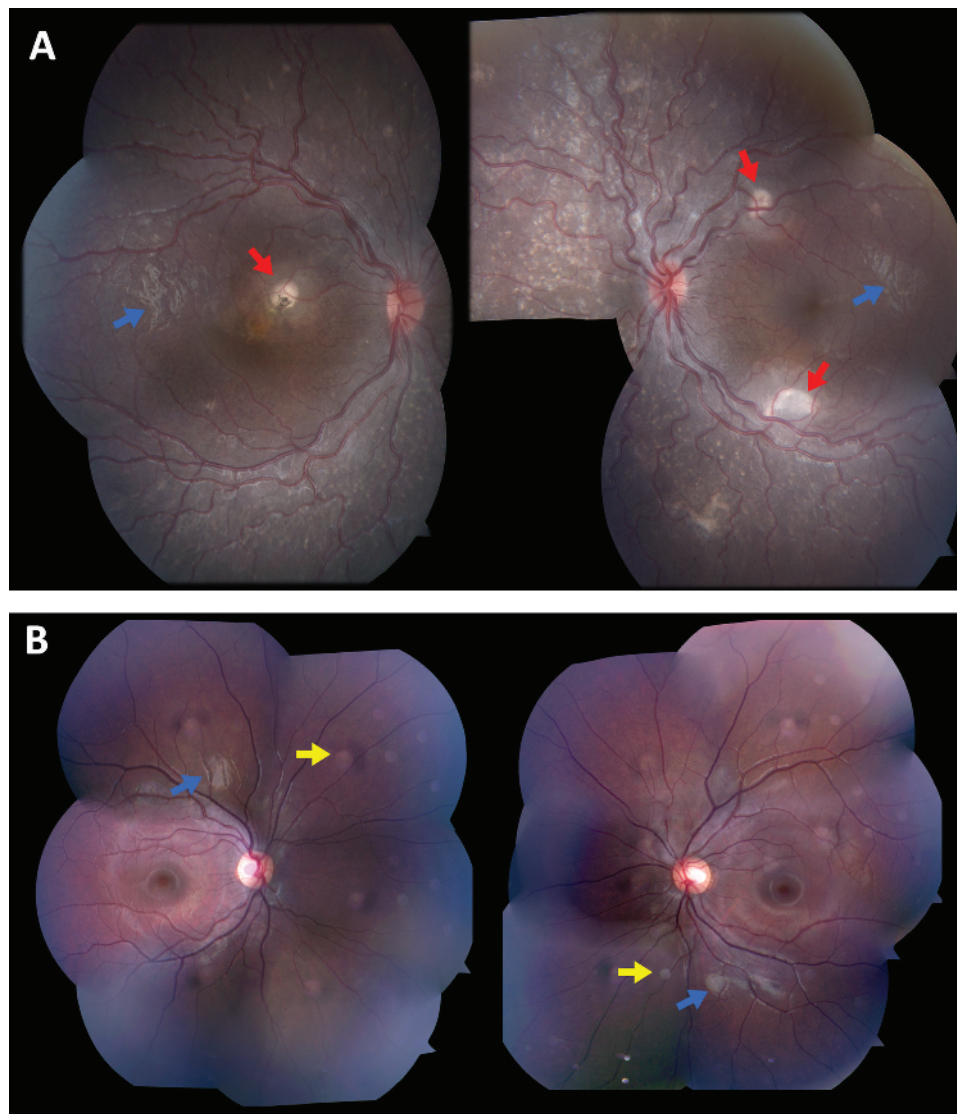
Clinical examination

Case 1

A 6-year-old boy presented with poor night vision since the age of 2. No history of prematurity or developmental abnormalities was noted, and past ocular history was also unremarkable. The patient is a product of consanguineous mating. Two months prior to presentation, the boy was suspected of having chorioretinitis after failing a standard vision screening at his elementary school. Serum examination was negative for inflammatory and infectious markers, including toxoplasmosis, toxocara, cat scratch disease, Lyme disease and syphilis.

On examination, visual acuity was 20/800 in the right eye and 20/40 in the left eye. The intraocular tension was 13 mm Hg in the right eye and 15 mm Hg in the left eye. The eye position was orthophoric with full motility. Biomicroscopy was unremarkable except for 1+ vitreous cells in both eyes. Dilated fundus examination of both eyes revealed multiple whitish subretinal deposits and several prominent lesions within the macula (fig 2A). Fundus autofluorescence imaging (FAF) showed hyperautofluorescence in the macula and mid-peripheral retina (fig 3A). Spectral-domain optical coherence tomography (OCT) showed intraretinal cystic changes surrounding the lesion and rosette-like lesions in the mid-peripheral retina, with loss of normal retinal lamination (fig 3B). There was no cystoid macular oedema or foveal schisis in the left eye. Fluorescein angiography showed hyperfluorescence that increased with time, suggesting chronic subretinal neovascularisation and fibrosis. There was no peripheral vascular leakage. Full-field ERG shows three characteristic findings: (1) no rod responses; (2) the waveforms of scotopic maximal response are identical to the transient photopic responses except the size (circles); (3) the amplitude of a wave in the transient photopic response is larger than the amplitude of photopic 30 Hz flicker. S-cone-specific ERG was of a remarkably high amplitude and confirmed the diagnosis of ESCS (fig 4).

Figure 2 (A) Composite fundus photographs of the right and left eyes of proband (case 1) showing multiple subretinal white deposits and prominent lesions in the macula (red arrows). (B) Composite fundus imaging of the right and left eyes of case 2 exhibiting a normal retina without subretinal deposit. There are several artefacts arising from photography (yellow arrows illustrate examples of artefacts from the camera lens; blue arrows show reflections of the nerve fibre layer).



Case 2

The proband's older brother was an asymptomatic 8-year-old boy. The best-corrected visual acuity was 20/20 (OU), and biomicroscopy was unremarkable. Dilated fundus examination of both eyes revealed a normal retinal appearance without white dots (fig 2B). FAF showed several increased hyperautofluorescence spots around the disc and arcades (fig 3C). OCT showed normal retinal lamination without rosette-like lesions (fig 3D). ERG results were normal (fig 4).

Cases 3 and 4

The proband's parents were first cousins, and both were beta-thalassemia carriers. Comprehensive ophthalmic evaluation was unremarkable, and there were no fundus white dots or hyperautofluorescence spots in either parent.

Examination of *Nr2e3^{rd7}* mutant mice

Dilated fundus photography from 5-week-old *Nr2e3^{rd7}* mutant mice showed diffuse subretinal white dots (fig 5B), and whole mount eyecup from age-matched *Nr2e3^{rd7}* mice demonstrated similar hyperautofluorescent spots (fig 5D). Images obtained from 8-week-old wild type C57BL/6J mice showed no white

dots in the retina (fig 5A) and no hyperautofluorescent spots (fig 5C). Autofluorescence imaging of retina from *Nr2e3^{rd7}* mice has chromophores with a wide spectrum of emission in the visible wavelengths with the highest intensity around 550 nm when excited at 436 nm (fig 5E).

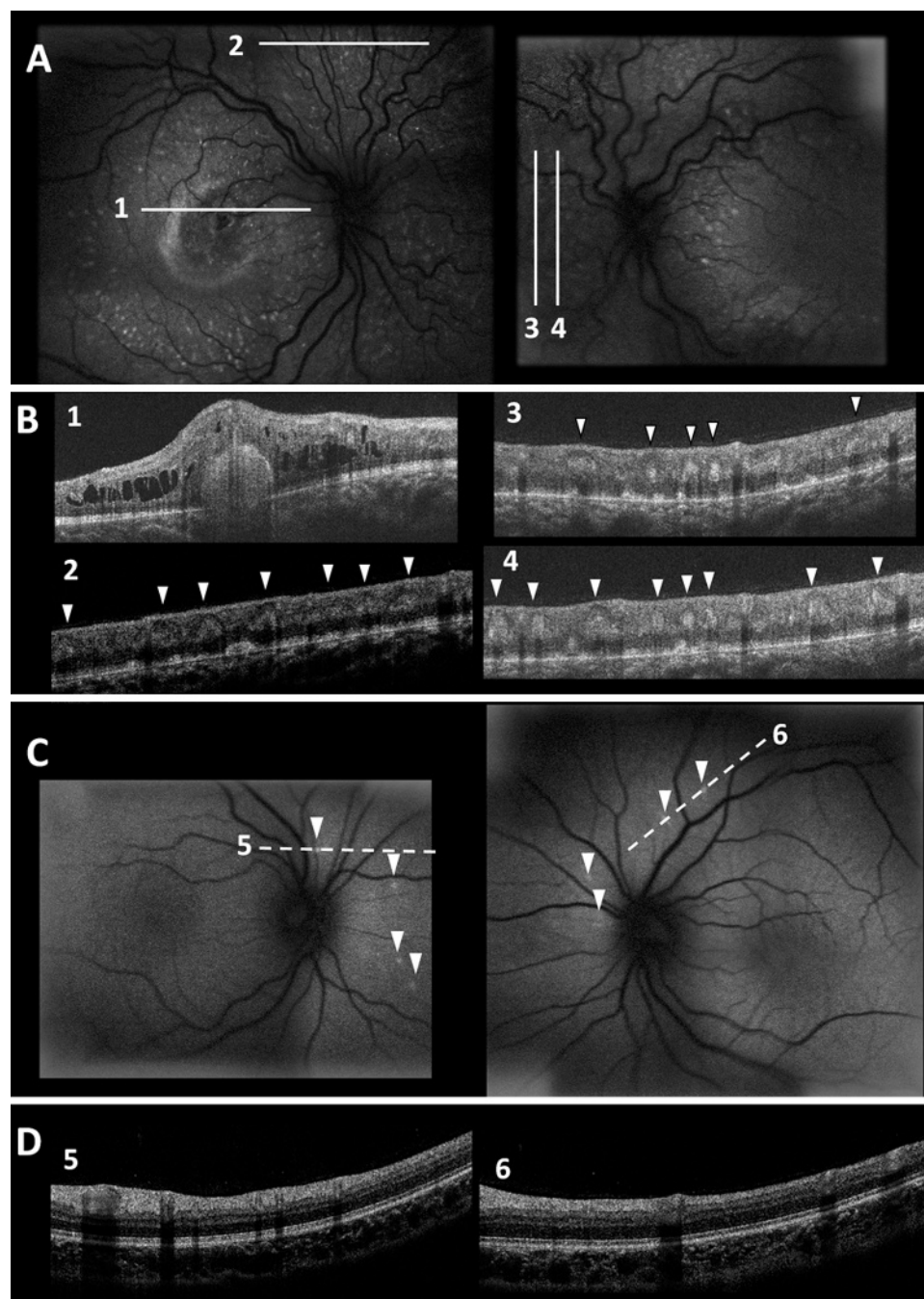
DAPI staining of retina from *Nr2e3^{rd7}* mice demonstrated rosette and whorl-like structures in the retina, and the autofluorescent materials were localised to the region between the outer nuclear layer (ONL) and retinal pigment epithelium (RPE), and mostly within the rosettes (fig 6A). IHC performed with the macrophage marker F4/80 demonstrated that the macrophages were within the rosettes, and the autofluorescent materials were in the cytoplasm of these macrophages (fig 6B).

DISCUSSION

Fundus examination

Nummular pigment clumping along the vascular arcades, the classical retinal phenotype seen in adult ESCS patients, is not observed in our proband. Findings from recent reports of young ESCS patients suggest that subtle pigmentary changes with white dots represent an early stage of the disease process,^{2 20} and these white dots progress to characteristic clumped retinopathy

Figure 3 (A) Fundus autofluorescence exam (FAF) of proband (case 1) showing hyperautofluorescent spots in the macular area and in the mid-peripheral retina. (B) Optical coherence tomography (OCT) 1, 2, 3, and 4 corresponding to scanning sections in (A). 1 showed cystic changes around the foveal lesion (OD). Note that the rosette-like lesions (arrowhead) correspond to hyperautofluorescent spots and loss of retinal lamination (2, 3 and 4). (C) FAF of case 2 showing several hyperautofluorescent spots around the disc and arcades. (D). (5,6) OCT sectioning of case 2 (lines 5 and 6 from (C)) showing normal retinal lamination without rosette-like lesions. Some shadows casted by retinal vessels are observed.



in late adulthood.² This phenomenon suggested why there were few reports describing similar fundus white dots from the ESCS patients. Although a normal fundus appearance without subretinal white dots has been reported in some case series with 6–10-year-old patients,^{12–21} those patients are homozygous for a missense mutation (R104W) that is different from the R311Q substitution, the most common ESCS allele, is found in ~45% of patients.³ Whether there is a genotype–phenotype correlation requires further studies to analyse younger ESCS patients to explain the clinical characteristics variability.

OCT

Foveal schisis has been reported in patients with ESCS.^{3–12–21} In case 1, there is no foveal schisis in the left eye, but there are intraretinal cysts around the lesion in the macula of the right eye (fig 3B).

Patients with ESCS have histologically dysmorphic retinas in the ONL,^{4–22–23} and our results demonstrate that spectral-domain OCT can detect such rosette formation in the ONL and can be used to monitor photoreceptor loss as the disease progresses.

AF imaging

The ring of increased AF in the macula area has been suggested to be associated with fundus white dots and retinal rosette.¹² In case 1, hyperautofluorescent spots are not limited in the macula area but also extended beyond the arcades. The hyperautofluorescent spots outside the macula area correspond to the fundus white dots (fig 3A), whereas the hyperautofluorescent spots within the macula do not correspond to the white dots or pigmentary clumps. In addition, the heterozygous brother (case 2) does not have white dots visible funduscopically but does have several hyperautofluorescent spots along the arcades.

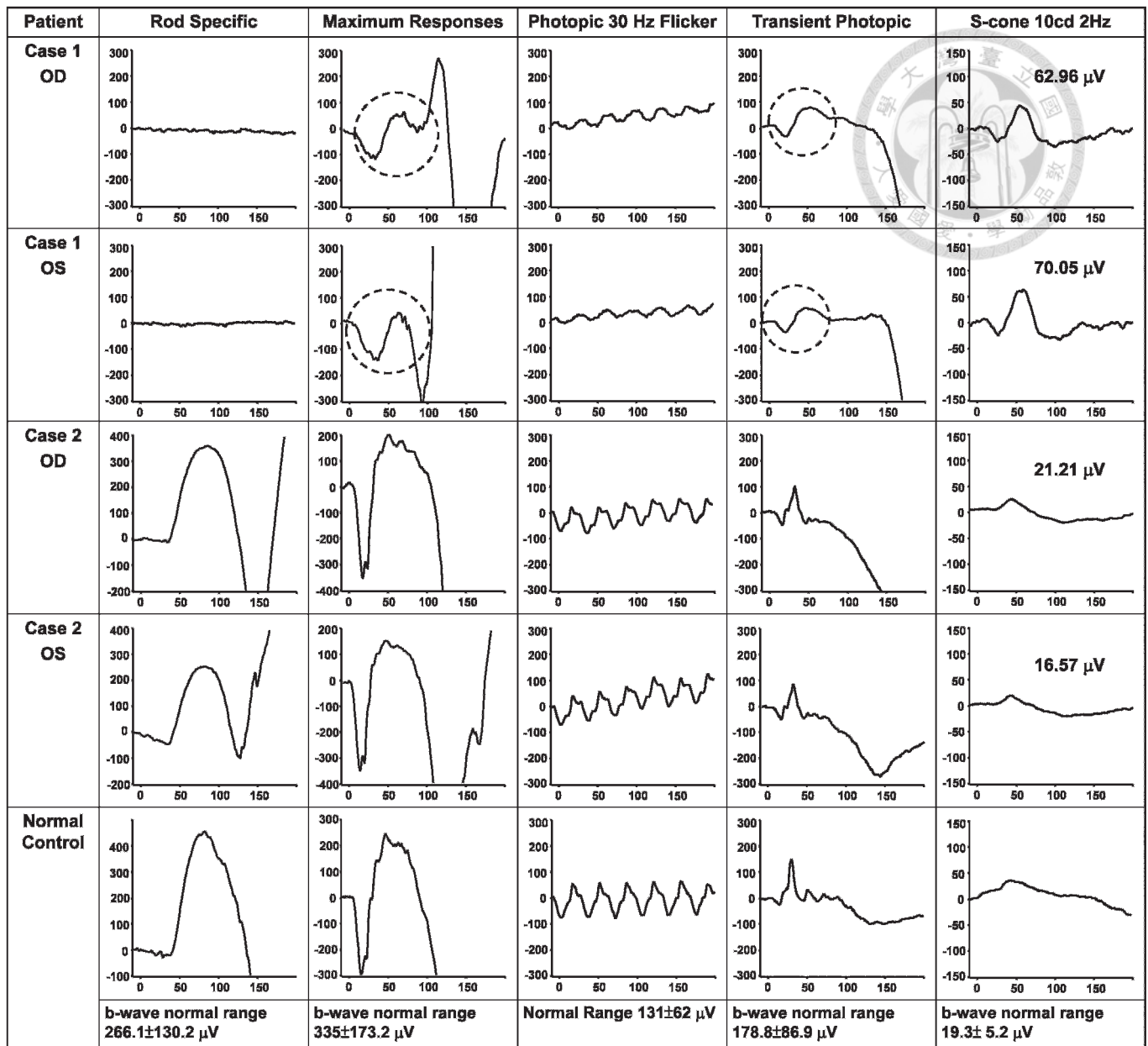


Figure 4 Electroretinogram (ERG) from case 1 revealing three characteristic findings: (1) no rod responses; (2) the waveforms of scotopic maximal response identical to the transient photopic responses except the size (circles); (3) amplitude of a wave in the transient photopic response larger than amplitude of photopic 30 Hz flicker. S-cone-specific ERG was of remarkably high amplitude (60–70 μV) and further confirmed the diagnosis of ESCS. ERG from case 2 was normal. OD, right eye; OS, left eye.

Thus, the hyperautofluorescent spots and fundus white dots may have different origins.

Figure 3C showed several hyperautofluorescence dots around the disc and arcades in case 2. Whether heterozygosity with the mutant *NR2E3* allele has any phenotypic manifestation is unknown; the absence of these hyperautofluorescent dots in the asymptomatic consanguineous parents suggests that they may be transient in nature and only detectable in heterozygous children.

Fundus white dots and retinal rosettes of *Nr2e3^{rd7}* mutant mice

Subretinal white dots¹⁰ and abnormal lamination of the ONL^{10 11} have been described in *Nr2e3^{rd7}* mutant mice. The *Nr2e3^{rd7}* mutant mice have numerous white dots over the entire retina at 1 month old that gradually decrease by 5 months of age and

disappear completely by 16 months.¹⁰ The concordance of the appearance and disappearance of the white spots observed over entire retina with the waves seen under histology suggests that these spots are associated with the retinal rosettes.¹⁰ Milam *et al* described an approximately twofold increase in total cones from a 70-year-old R311Q patient,⁴ and Haider *et al* described a 1.5–2.0-fold increase of S-cones in *Nr2e3^{rd7}* mice.¹¹ Whether the excessive numbers of S-cones contribute to rosette formation is uncertain.

Autofluorescent spots of *Nr2e3^{rd7}* mutant mice

In *Nr2e3^{rd7}* mice retina, we found that the autofluorescent materials were present in the cytoplasm of macrophages situated within and sometimes adjacent to the retinal rosettes

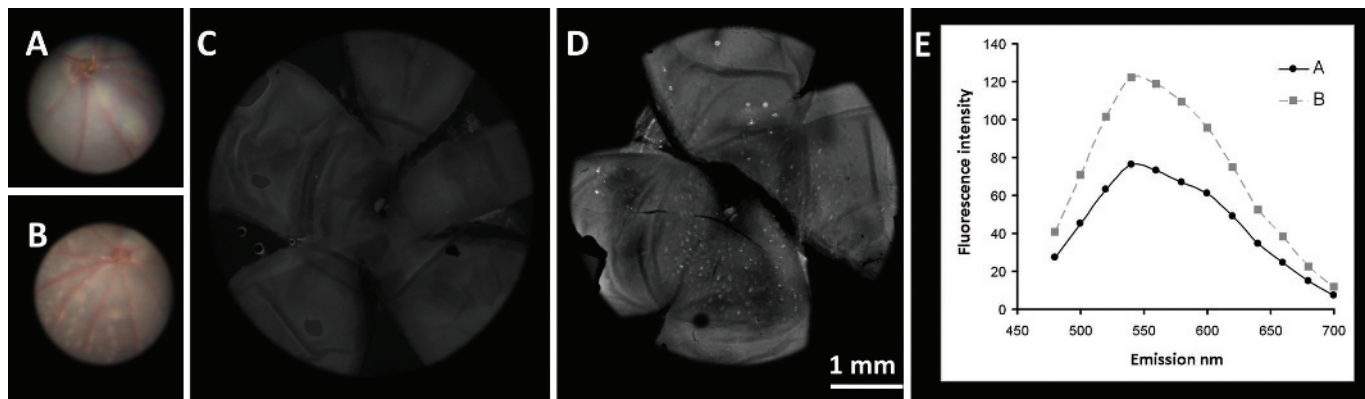


Figure 5 Colour fundus photographs from wild type mouse (A) showing normal retina, and image from *rd7* mouse (B) showing numerous subretinal white dots. The whole mount eyecup from wild type mouse (C) did not reveal hyperautofluorescence spots, whereas the image from *rd7* mouse (D) showed hyperautofluorescence spots. (E) Spectral fluorescence of hyperautofluorescence spots from *rd7* mouse retina demonstrating that the wavelength of highest fluorescence intensity was 540 nm to 560 nm when excited with light of 436 nm.

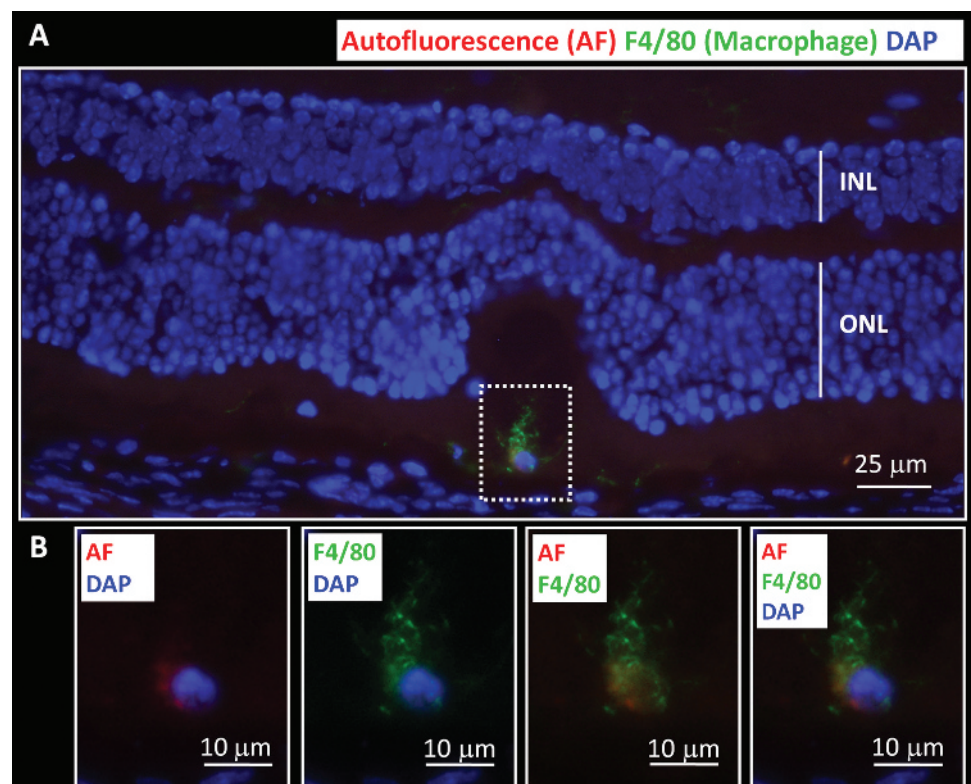
(fig 6). Immunolocalisation studies (fig 6) demonstrate that the chromophores are found within macrophages instead of RPE. In addition, the multiple spectral wavelength (fig 5) of the hyperautofluorescent spots from *Nr2e3^{rd7}* mutant mice suggests that these spots contain chromophores in addition to A2E, which has an emission maxima of 565 to 570 nm.²⁴ In a manner analogous to that seen in *Nr2e3^{rd7}* mutant mice, we can expect that hyperautofluorescent spots in our case may come not from RPE cells but from macrophages. Further *in vivo* studies on ESCS patients with different spectral wavelengths can help to determine the origin of these hyperautofluorescent spots.

There are two probable explanations for the presence of macrophages in *Nr2e3^{rd7}* mice retina. First, the macrophages are recruited into the retina to remove apoptotic photoreceptors

found as early as in P30 *Nr2e3^{rd7}* retina.²⁵ Second, photoreceptor outer segments within the rosettes are inefficiently phagocytosed by RPE due to the abnormal retinal structure, and the accumulation of outer segment debris may in turn trigger macrophage infiltration to remove the waste. However, our IHC studies suggest that these fluorophores within macrophages are derived from the outer segment, rather than apoptotic photoreceptors.

Similar accumulation of outer segment debris and macrophage infiltration has been associated with the development of age-related macular degeneration (AMD).²⁶ In photoreceptor damage or degeneration, macrophages invade the retina to support the role of RPE in phagocytosing outer segment debris.^{27 28} Thus, infiltration of macrophages can be used as a

Figure 6 (A) Immunohistochemistry of a frozen section from *rd7* mouse retina using anti-F4/80 antibodies (macrophage marker) showing one macrophage in the retinal rosette, or whorl lesion. (B) High magnification of white dots lined area from (A) showing images merging from different fluorescence channels. The autofluorescence (red) was colocalised with macrophage marker (green). AF, autofluorescence; DAP, DAPI staining; F4/80: macrophage marker; INL, inner nuclear layer; ONL, outer nuclear layer.



marker for early phases of various degenerative conditions, and their subsequent disappearance correlates with loss of hyperautofluorescent spots in later stages of retinal degeneration.

In summary, we discovered several novel features (fundus white dots, hyperautofluorescent spots and rosette-like retinal lesions) observed in a child homozygous for the R311Q allele in *NR2E3*. Findings from the *Nr2e3^{rd7}* mutant mice suggest that fundus hyperautofluorescent lesions are likely to be contributed by macrophages.

Acknowledgements: We would like to thank the medical imaging division at the Edward S. Harkness Eye Institute for their excellent work. We greatly appreciate the assistance of the members of the Brown Glaucoma laboratory for sharing ideas, and equipment, especially N Palmer.

Funding: Burroughs-Wellcome Program in Biomedical Sciences Fellow, Charles Culpeper Scholarship, Foundation Fighting Blindness, Hirschl Trust, Schneeweiss Stern Cell Fund, Sylvia Wright Retinal Research Trust, Joel Hoffmann Foundation, Jonas Family Fund, Crowley Research Fund, Jahnigen/Hartford/American Geriatrics Society, Eye Surgery Fund, Bernard Becker-Association of University Professors in Ophthalmology-Research to Prevent Blindness (RPB) and EY018213. NKW is supported by the Taiwan National Science Council NSC-096-2917-I-002-105 and the Chang Gung Memorial Hospital Fellowship CMRPG360571 & 360572.

Competing interests: None.

Ethics approval: Ethics approval was provided by institutional review board protocol #AAAB6560 at Columbia University.

Patient consent: Obtained.

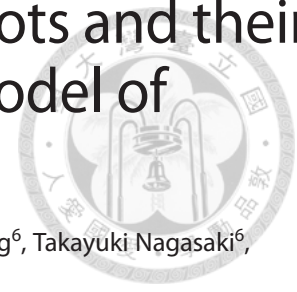
Provenance and peer review: Not commissioned; externally peer reviewed.

REFERENCES

1. **Chen J**, Rattner A, Nathans J. The rod photoreceptor-specific nuclear receptor Nr2e3 represses transcription of multiple cone-specific genes. *J Neurosci* 2005;**25**:118–29.
2. **Sharon D**, Sandberg MA, Caruso RC, *et al*. Shared mutations in NR2E3 in enhanced S-cone syndrome, Goldmann–Favre syndrome, and many cases of clumped pigmentary retinal degeneration. *Arch Ophthalmol* 2003;**121**:1316–23.
3. **Haider NB**, Jacobson SG, Cideciyan AV, *et al*. Mutation of a nuclear receptor gene, NR2E3, causes enhanced S cone syndrome, a disorder of retinal cell fate. *Nat Genet* 2000;**24**:127–31.
4. **Milam AH**, Rose L, Cideciyan AV, *et al*. The nuclear receptor NR2E3 plays a role in human retinal photoreceptor differentiation and degeneration. *Proc Natl Acad Sci USA* 2002;**99**:473–8.
5. **Wright AF**, Reddick AC, Schwartz SB, *et al*. Mutation analysis of NR2E3 and NRL genes in Enhanced S Cone Syndrome. *Hum Mutat* 2004;**24**:439.
6. **Coppieters F**, Leroy BP, Beyens D, *et al*. Recurrent mutation in the first zinc finger of the orphan nuclear receptor NR2E3 causes autosomal dominant retinitis pigmentosa. *Am J Hum Genet* 2007;**81**:147–57.
7. **Hayashi T**, Gekka T, Goto-Omoto S, *et al*. Novel NR2E3 mutations (R104Q, R334G) associated with a mild form of enhanced S-cone syndrome demonstrate compound heterozygosity. *Ophthalmology* 2005;**112**:2115.
8. **Chavala SH**, Sari A, Lewis H, *et al*. An Arg311Gln NR2E3 mutation in a family with classic Goldmann–Favre syndrome. *Br J Ophthalmol* 2005;**89**:1065–6.
9. **Gerber S**, Rozet JM, Takezawa SI, *et al*. The photoreceptor cell-specific nuclear receptor gene (PNR) accounts for retinitis pigmentosa in the Crypto-Jews from Portugal (Marranos), survivors from the Spanish Inquisition. *Hum Genet* 2000;**107**:276–84.
10. **Akhmedov NB**, Piriev NI, Chang B, *et al*. A deletion in a photoreceptor-specific nuclear receptor mRNA causes retinal degeneration in the rd7 mouse. *Proc Natl Acad Sci USA* 2000;**97**:5551–6.
11. **Haider NB**, Naggert JK, Nishina PM. Excess cone cell proliferation due to lack of a functional NR2E3 causes retinal dysplasia and degeneration in rd7/rd7 mice. *Hum Mol Genet* 2001;**10**:1619–26.
12. **Audo I**, Michaelides M, Robson AG, *et al*. Phenotypic variation in enhanced S-cone syndrome. *Invest Ophthalmol Vis Sci* 2008;**49**:2082–93.
13. **Robson AG**, Egan C, Holder GE, *et al*. Comparing rod and cone function with fundus autofluorescence images in retinitis pigmentosa. *Adv Exp Med Biol* 2003;**533**:41–7.
14. **Robson AG**, Saihan Z, Jenkins SA, *et al*. Functional characterisation and serial imaging of abnormal fundus autofluorescence in patients with retinitis pigmentosa and normal visual acuity. *Br J Ophthalmol* 2006;**90**:472–9.
15. **Tsang SH**, Vaclavik V, Bird AC, *et al*. Novel phenotypic and genotypic findings in X-linked retinoschisis. *Arch Ophthalmol* 2007;**125**:259–67.
16. **Tsui I**, Casper D, Chou CL, *et al*. Electronegative electroretinogram associated with topiramate toxicity and vitelliform maculopathy. *Doc Ophthalmol* 2008;**116**:57–60.
17. **Tsui I**, Fuchs BS, Chou CL, *et al*. Non-vascular vision loss in pseudoxanthoma elasticum. *Doc Ophthalmol* 2008;**117**:65–7.
18. **von Ruckmann A**, Fitzke FW, Bird AC. Distribution of fundus autofluorescence with a scanning laser ophthalmoscope. *Br J Ophthalmol* 1995;**79**:407–12.
19. **Holder GE**, Brigell MG, Hawlina M, *et al*. ISCEV standard for clinical pattern electroretinography—2007 update. *Doc Ophthalmol* 2007;**114**:111–16.
20. **Khan AO**, Aldahmesh M, Meyer B. The enhanced S-cone syndrome in children. *Br J Ophthalmol* 2007;**91**:394–6.
21. **Vaclavik V**, Chakarova C, Bhattacharya SS, *et al*. Bilateral giant macular schisis in a patient with enhanced S-cone syndrome from a family showing pseudo-dominant inheritance. *Br J Ophthalmol* 2008;**92**:299–300.
22. **Milam AH**, Jacobson SG. Photoreceptor rosettes with blue cone opsin immunoreactivity in retinitis pigmentosa. *Ophthalmology* 1990;**97**:1620–31.
23. **Peyman GA**, Fishman GA, Sanders DR, *et al*. Histopathology of Goldmann–Favre syndrome obtained by full-thickness eye-wall biopsy. *Ann Ophthalmol* 1977;**9**:479–84.
24. **Sparrow JR**, Parish CA, Hashimoto M, *et al*. A2E, a lipofuscin fluorophore, in human retinal pigmented epithelial cells in culture. *Invest Ophthalmol Vis Sci* 1999;**40**:2988–95.
25. **Haider NB**, Demarco P, Nystuen AM, *et al*. The transcription factor Nr2e3 functions in retinal progenitors to suppress cone cell generation. *Vis Neurosci* 2006;**23**:917–29.
26. **Wenzel A**, Grimm C, Samardzija M, *et al*. Molecular mechanisms of light-induced photoreceptor apoptosis and neuroprotection for retinal degeneration. *Prog Retin Eye Res* 2005;**24**:275–306.
27. **Hoppeler T**, Hendrickson P, Dietrich C, *et al*. Morphology and time-course of defined photochemical lesions in the rabbit retina. *Curr Eye Res* 1988;**7**:849–60.
28. **Gordon WC**, Casey DM, Lukiw WJ, *et al*. DNA damage and repair in light-induced photoreceptor degeneration. *Invest Ophthalmol Vis Sci* 2002;**43**:3511–21.

Origin of fundus hyperautofluorescent spots and their role in retinal degeneration in a mouse model of Goldmann-Favre syndrome

Nan-Kai Wang^{1,2,3}, Chi-Chun Lai^{1,2,3}, Chi-Hsiu Liu¹, Lung-Kun Yeh^{2,3}, Chai Lin Chou^{4,5,6}, Jian Kong⁶, Takayuki Nagasaki⁶, Stephen H. Tsang^{5,6,*} and Chung-Liang Chien^{1,*}



SUMMARY

Goldmann-Favre syndrome, also known as enhanced S-cone syndrome, is an inherited retinal degeneration disease in which a gain of photoreceptor cell types results in retinal dysplasia and degeneration. Although microglia have been implicated in the pathogenesis of many neurodegenerative diseases, the fundamental role of these cells in this disease is unknown. In the current study, sequential analyses suggest that microglia are recruited and appear after outer nuclear layer folding. By crossing *rd7* mice (a model for hereditary retinal degeneration owing to *Nr2e3* mutation) with mice carrying the macrophage Fas-induced apoptosis (Mafia) transgene, we generated double-mutant mice and studied the role of the resident retinal microglia. Microglial cells in these double-mutant mice express enhanced green fluorescent protein (EGFP) and a suicide gene that can trigger Fas-mediated apoptosis via systemic treatment with AP20187 (FK506 dimerizer). We demonstrated that more than 80% of the EGFP+ cells in retinas from *rd7/rd7;Tg/Tg* mice express Iba-1 (a microglial marker), and resident microglia are still present in the retina because AP20187 does not cross the blood-brain barrier. Hence, only circulating bone marrow (BM)-derived microglia are depleted. Depletion of circulating BM-derived microglia accelerates retinal degeneration in *rd7* mice. An increased number of autofluorescent (AF) spots is a consequence of resident microglia proliferation, which in turn establishes an inflammatory cytokine milieu via the upregulation of *IL-1β*, *IL-6* and *TNFα* expression. This inflammation is likely to accelerate retinal degeneration. This study not only identifies inflammation as a crucial step in the pathogenesis of retinal degeneration, but also highlights the involvement of specific cytokine genes that could serve as future treatment targets in retinal degenerations.

INTRODUCTION

Retinal degeneration in *rd7* mice is caused by a spontaneous mutation in the *Nr2e3* gene. In addition, this mouse strain is a model for Goldmann-Favre syndrome [also known as enhanced S-cone syndrome (ESCS); OMIM 268100 (<http://omim.org/entry/268100>)] (Akhmedov et al., 2000). In these mice, a gain of photoreceptor cell types results in retinal dysplasia and degeneration.

Recently, we described newly identified characteristics – including diffuse retinal white dots, hyperautofluorescent (hyper-AF) spots and retinal rosettes – in a 6-year-old boy with ESCS who carried a homozygous R311Q mutation in the *NR2E3* gene (Wang et al., 2009). His phenotypic manifestations were similar to those of ‘young’ *rd7* mice. We demonstrated that F4/80-positive microglia, rather than retinal pigment epithelium (RPE) cells, contributed to these AF spots.

Most of these cells were present inside retinal rosettes and presumably helped RPE cells phagocytose this outer segment (OS) debris within the rosettes. Although these data demonstrated the presence of comparable retinal characteristics in human ESCS and a mouse model of the disease, the fundamental role of microglia in retinal degeneration is unknown.

Microglia, which are part of the mononuclear phagocytic system, act as the first and main form of active immune defense in the central nervous system (CNS), including in the retina (Kreutzberg, 1996; Cuadros and Navascués, 1998; Hanisch and Kettenmann, 2007; Tambuyzer et al., 2009). Microglial activation is characterized by the expression of various microglial and/or macrophagic markers. In the retina, microglial activation has been demonstrated in injury (Ng and Streilein, 2001; Langmann, 2007; Joly et al., 2009), ischemia (Zhang et al., 2005; Ritter et al., 2006; Sivakumar et al., 2011) and degeneration (Langmann, 2007; Sasahara et al., 2008; Arroba et al., 2011). Microglial cells from two origins exist in the retina: resident microglia and circulating bone marrow (BM)-derived microglia, with the former entering from hyaloid vessels and being thought to be associated with neuronal death in retinal histogenesis (Ashwell et al., 1989), whereas the latter enter from the optic nerve after retinal vascularization (Caicedo et al., 2005; Hou et al., 2006). Although BM transplantation approaches have the potential to systemically remove macrophages in order to study their function *in vivo* in normal or disease models, pre-BM-transplantation irradiation damages resident microglia, which might change the immune environment of the retina (Amoakul et al., 1992; Kaneko et al., 2008).

Burnett and colleagues generated mice that carry the transgene for macrophage Fas-induced apoptosis (Mafia) (Burnett et al., 2004;

¹Department of Anatomy and Cell Biology, National Taiwan University, Taipei 100, Taiwan

²Department of Ophthalmology, Chang Gung Memorial Hospital, Linkou, Taoyuan 333, Taiwan

³Chang Gung University College of Medicine, Linkou, Taoyuan 333, Taiwan

⁴Faculty of Medicine, The University of British Columbia, Vancouver, BC V6T 1Z4 Canada

⁵Bernard and Shirlee Brown Glaucoma Laboratory, Department of Pathology and Cell Biology, Columbia University, New York, NY 10032, USA

⁶Edward S. Harkness Eye Institute, Columbia University, New York, NY 10032, USA

*These authors contributed equally to this work

†Authors for correspondence (sht2@columbia.edu; chien@ntu.edu.tw)

Received 15 February 2013; Accepted 15 May 2013

© 2013. Published by The Company of Biologists Ltd
This is an Open Access article distributed under the terms of the Creative Commons Attribution License (<http://creativecommons.org/licenses/by/3.0>), which permits unrestricted use, distribution and reproduction in any medium provided that the original work is properly attributed.

TRANSLATIONAL IMPACT

Clinical issue

Goldmann-Favre syndrome, also known as enhanced S-cone syndrome, is an inherited eye disorder characterized by retinal degeneration. Previously, this group reported the appearance of diffuse retinal white dots, hyperautofluorescent spots and retinal rosettes in young patients with Goldmann-Favre syndrome, and they recently showed that these features are also seen in young *rd7* (retinal degeneration) mice. Retinal microglial cells, of which there are two origins – resident microglia and circulating bone marrow (BM)-derived microglia – have been implicated in the pathogenesis of Goldmann-Favre syndrome and it was suggested that microglial cells contribute to the development of hyperautofluorescent spots. However, the fundamental role of microglial cells in Goldmann-Favre syndrome pathogenesis is unknown.

Results

Here, the authors exploited *Mafia* (macrophage Fas-induced apoptosis) transgenic mice to explore the contribution of microglial cells to Goldmann-Favre syndrome. Temporal control of a circulating BM-derived microglia population was achieved by introducing the *Mafia* transgene into the *rd7* mouse model of Goldmann-Favre syndrome. Systemic ablation of BM-derived microglia can be induced by treatment with a synthetic dimerizer, AP20187. Because this compound does not cross the blood-brain barrier, resident retinal microglia are spared but circulating BM-derived microglia are ablated after AP20187 administration. After systemic depletion of circulating BM-derived microglia in young mice, characteristics that mimicked those of later stages of retinal degeneration in *rd7* mice were observed in cilioretinal flatmounts. Moreover, analyses of the outer nuclear layer revealed a decreased nuclei count in photoreceptors. Inflammatory cytokines IL-1 β , IL-6, TNF α and monocyte chemoattractant protein (MCP-1) were upregulated, whereas the anti-inflammatory cytokine TGF-1 was found to be downregulated in the retina.

Implications and future directions

These data suggest that circulating BM-derived microglia have a role in suppressing intraocular inflammation. Loss of the microglial population can thereby enhance inflammatory pathways and accelerate retinal degeneration. This study highlights the opposing roles of resident microglia, which are still present in the retina of mutant mice, and circulating BM-derived microglia in retinal degeneration. Future studies dedicated to the search for therapeutic agents that intervene in the inflammatory processes involved could provide a novel treatment strategy for inherited retinal degeneration and other diseases characterized by degeneration of neurons, such as Alzheimer's disease.

Burnett et al., 2006). This transgene (*Tg: Csf1r-EGFP-NGFR/FKBP1A/TNFRSF6*) is under the control of the *c-fms* promoter, which drives the expression of the CSF-1 receptor in cells of the mononuclear phagocytic system, including monocytes, macrophages, dendritic cells (DC), Kupffer cells, Langerhans cells, osteoclasts and microglial cells (Cecchini et al., 1994). In *Mafia* mice, cells of the macrophage lineage express the EGFP and a membrane-bound suicide protein that can be activated by the covalently linked dimerizing reagent AP20187. Henceforth, we will use 'Tg/Tg' to refer to mice that are homozygous for this transgene.

In the current study, we took advantage of *Mafia* transgenic mice to mark the origin of AF spots with the EGFP reporter in *rd7* mice.

RESULTS

Spatial and temporal distribution of AF spots and rosettes in *rd7* mice

Our previous study showed that retinal rosettes corresponded to retinal folds, and that AF spots corresponded to microglial cells

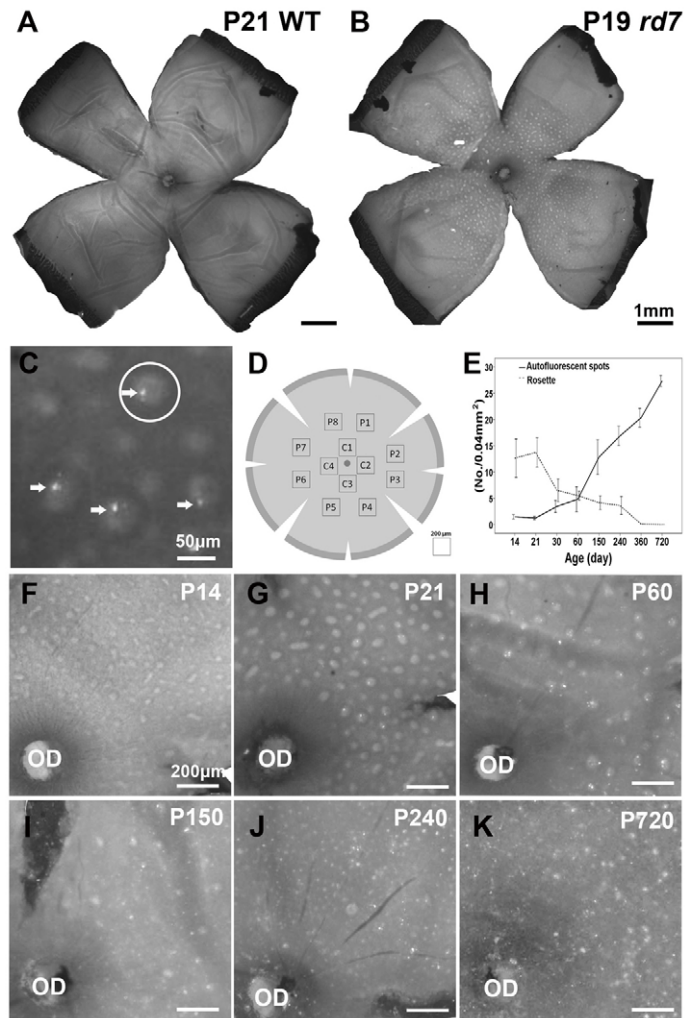


Fig. 1. Spatial and temporal distribution of autofluorescent (AF) spots and rosettes in *rd7* mice. (A,B) Cilioretinal flatmount of P21 wild-type (WT; A) and P19 *rd7* (B) mice. (C) Higher magnification of the boxed area from panel B shows examples of AF spots (arrows) and rosettes (circular halos; an example is circled). Note that the AF spots were located inside the rosettes. (D) Scheme of a cilioretinal flatmount showing the areas in which the AF spots and rosettes were counted. C, central; P, peripheral. (E) The number of AF spots and rosettes in the cilioretinal flatmount (mean \pm s.d.) was determined at P14 ($n=4$), P21 ($n=3$), P30 ($n=3$), P60 ($n=4$), P150 ($n=3$), P240 ($n=3$), P360 ($n=2$) and P720 ($n=2$). (F) By P14, rosettes were distributed throughout the cilioretinal flatmount. Note that AF spots were absent. (G) By P21, some AF spots were located inside rosettes; the AF spots were not distributed along the retinal vessels. (G-K and E) The number of rosettes decreased gradually, whereas the number of AF spots increased. OD, optic disc.

located between the neural retina and the RPE (Wang et al., 2009). To investigate the relationship between autofluorescence, microglial infiltration and retinal degeneration, we counted the AF spots and rosettes in the cilioretinal flatmounts of *rd7* mice between postnatal day 14 (P14) and P720 (Fig. 1). Fig. 1A,B show the cilioretinal flatmounts of P21 wild-type (WT; A) and P19 *rd7* (B) mice. Fig. 1C shows examples of AF spots (arrows) and rosettes (circular halos). Although the number of retinal rosettes increased from P14 to P21, the number of rosettes decreased progressively from P21 through

to P720. In contrast, AF spots that were absent at P14 were first detected as early as P21 (Fig. 1G), and the number increased gradually with age (Fig. 1F-K). We found that the AF spots were not distributed along the retinal vessels, but rather were correlated with rosettes between P21 and P60.

Abnormal accumulation of material in the OS of *rd7* mice

Previously, abnormal accumulation of material at the photoreceptor-RPE interface was documented in *Nrl*^{-/-} mice, another mouse model of ESCS (Mustafi et al., 2011). In addition, in our previous study, we found cells that were stained positively for F4/80 inside the retinal rosettes (Wang et al., 2009). To characterize these cells further, we performed an immunohistochemical analysis of retinas in *rd7* mice. Confocal images taken from the cilioretinal flatmounts of 2-month-old *rd7* mouse retinas probed with anti-F4/80 antibodies revealed the presence of ramified microglia 'lying' above the RPE layer (Fig. 2). These cells were colocalized with F4/80 (green, Fig. 2B) and autofluorescent material (red, Fig. 2C). Crosshairs and high-magnification viewing revealed the presence of autofluorescent material within the cytoplasm of an F4/80-positive cell (Fig. 2E).

To characterize the autofluorescent material further, we performed a histological analysis of *rd7* and WT (C57BL/6) mouse photoreceptors. Abnormal folding at the outer nuclear layer (ONL), OS and inner segment was noted in P60 *rd7* mice (Fig. 3A), whereas this folding was not found in P60 WT mouse retinas (Fig. 3B). To confirm this finding, we examined the retinas of *rd7* and WT mice by using transmission electron microscopy (TEM) (Fig. 3C-H). In *rd7* mouse retinas, some microglia (different to RPE cells) were detected between the OS and the RPE (asterisks in Fig. 3E,F). A

higher-magnification view of the TEM images showed the accumulation of lysosomes inside microglial cells (arrow in Fig. 3G), and microglial cells were more likely to be found under retinal rosettes (Fig. 3E,F). No microglia were found in WT mouse retinas (Fig. 3D).

Distribution of microglia in *rd7/rd7;Tg/Tg* mice

To investigate the role of circulating BM-derived microglia in *rd7* mice, we generated *rd7/rd7;Tg/Tg* double homozygotes via a two-generation outcross-intercross series. Theoretically, the transgene is under the control of the *c-fms* promoter and is expressed in macrophages, monocytes, microglia and DCs (Burnett et al., 2004; Burnett et al., 2006). Previously, microglia were classified into various subtypes (Zhang et al., 2005). To investigate further whether EGFP was expressed in these microglia and whether EGFP expression colocalized with microglial markers, we performed an immunohistochemical analysis of the retinas of

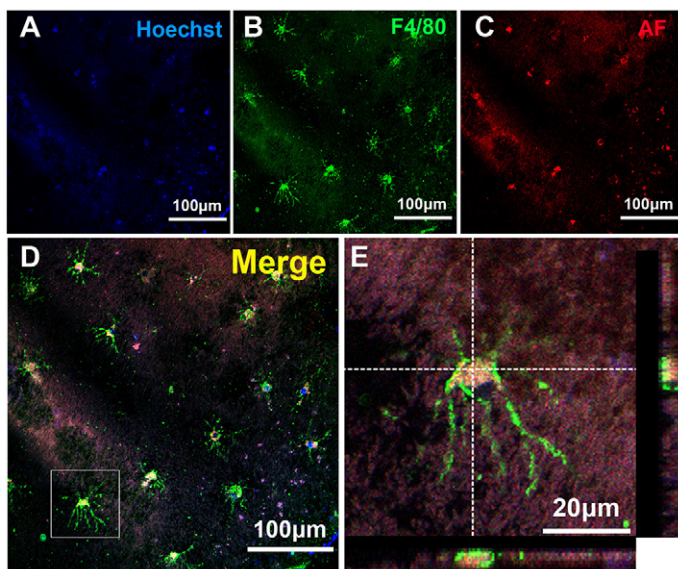


Fig. 2. Immunohistochemistry of the cilioretinal flatmounts from 2-month-old *rd7* mouse retinas using anti-F4/80 antibodies. (A-D) Confocal images taken from the cilioretinal flatmounts showed the presence of several ramified microglia 'lying' above the RPE layer. These cells were colocalized with F4/80 (green) and autofluorescent material (red). (E) Crosshairs and high-magnification viewing of single cells located inside the boxed area from panel D show the presence of autofluorescent material within the cytoplasm of an F4/80-positive cell. F4/80, microglial marker; AF, autofluorescence.

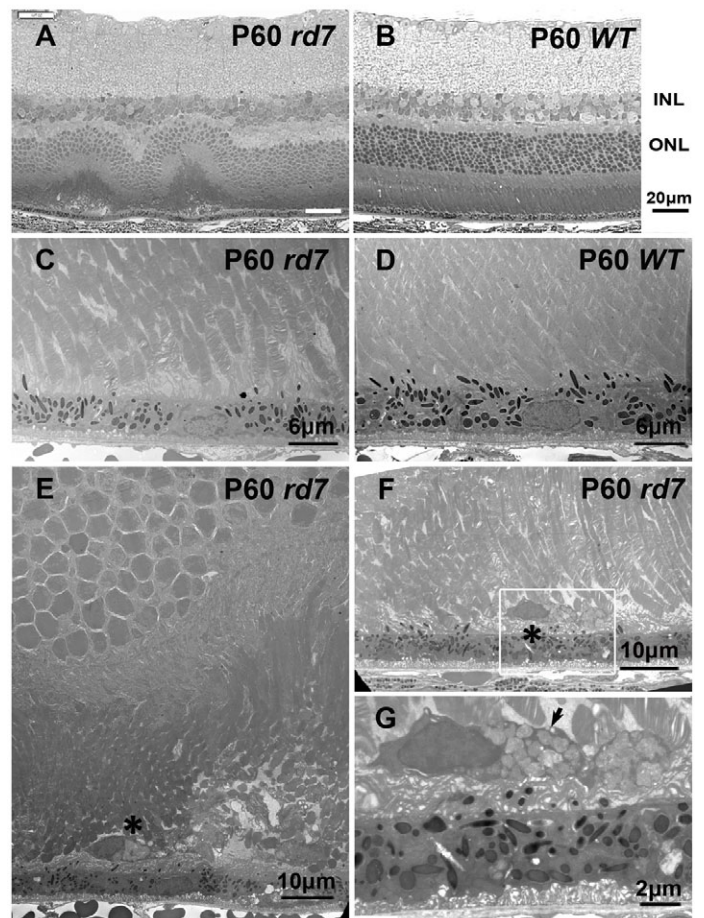


Fig. 3. Histology and electron microscopy of P60 *rd7* mouse retinas compared with P60 wild-type mouse retinas. (A) Semi-thin section of an *rd7* mouse retina showing outer nuclear layer foldings. (B) Control: semi-thin section of a WT mouse retina. INL, inner nuclear layer; ONL, outer nuclear layer. (C,D) Ultrathin section of retinas of *rd7* and WT mice, showing the junction between the outer segment (OS) and RPE. (E,F) The ultrastructural analysis of the retina of *rd7* mice revealed the presence of microglial cells between the OS and the RPE. Asterisks indicate microglia. (G) Higher magnification of the boxed area from panel F, showing the accumulation of lysosomes inside a microglial cell (arrow).

rd7/rd7;Tg/Tg mice. Among the EGFP+ cells, 45.4±9.5% expressed F4/80, 47.7±10.4% expressed CD68, 84.2±8.0% expressed Iba-1 and 39.7±7.7% expressed MHC class II (MHC-II). Less than 10% of the EGFP+ cells expressed vimentin. We also found that the EGFP+ cells were distributed in the ganglion cell layer (GCL), inner plexiform layer (IPL), inner nuclear layer (INL), outer plexiform layer (OPL), and between the OS and the RPE (Fig. 4). In summary, the majority of EGFP+ cells (>80%) in *rd7/rd7;Tg/Tg* mice expressed Iba-1, and few EGFP+ cells were labeled by vimentin.

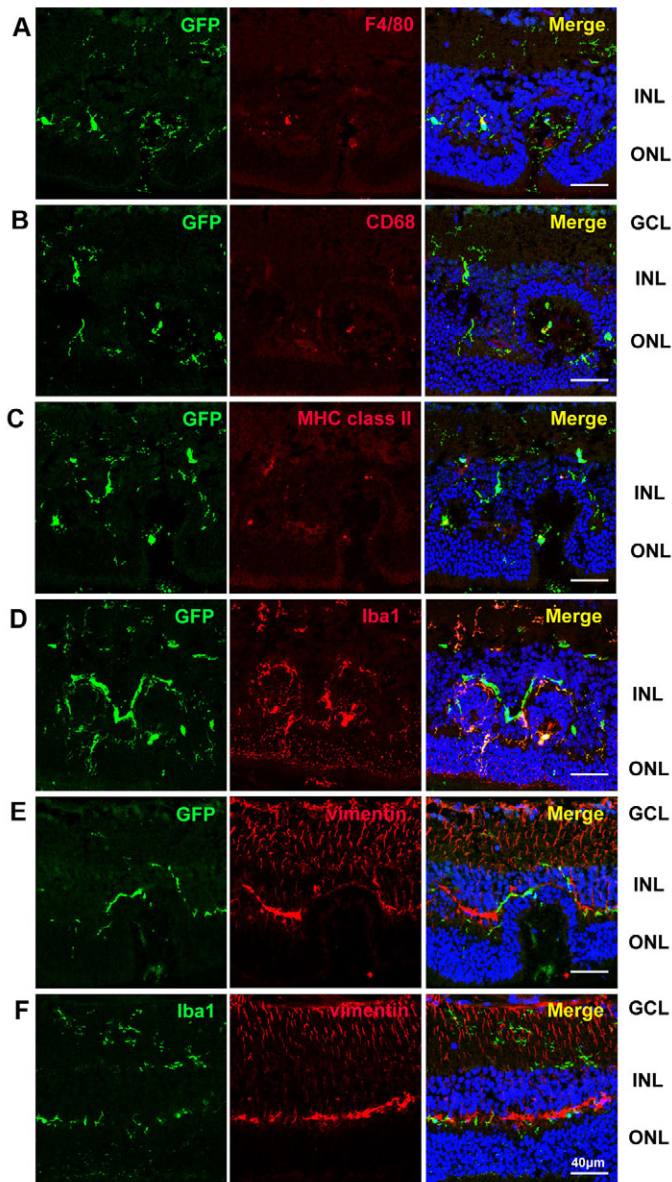


Fig. 4. Confocal images showing the distribution of EGFP, F4/80, CD68, MHC-II, Iba-1 and vimentin labeling in the retina of a 3-month-old *rd7/rd7;Tg/Tg* mouse. Of the EGFP+ cells, 45.4±9.5% expressed F4/80 (A), 47.7±10.4% expressed CD68 (B), 39.7±7.7% expressed MHC class II (C) and 84.2±8.0% expressed Iba-1 (D). Less than 10% of the EGFP+ cells expressed vimentin (E). GCL, ganglion cell layer; INL, inner nuclear layer; ONL, outer nuclear layer.

Circulating BM-derived microglia deficiency in *rd7* mice

We introduced inducible circulating BM-derived microglia deficiency into the mouse model of ESCS by crossbreeding *rd7* onto the *Mafia* mice. The *rd7/rd7;Tg/Tg* mice had similar physical characteristics as those of *rd7* mice and survived more than 1 year, when allowed. The growth of *rd7/rd7;Tg/Tg* mice was similar to that of *rd7* mice. However, after circulating BM-derived microglia ablation using AP20187, the body weight in the AP20187 mice did not increase as fast as in the vehicle-treated animals (supplementary material Fig. S1).

To investigate whether AP20187 can systemically deplete circulating BM-derived microglia in *rd7/rd7;Tg/Tg* mice, we injected AP20187 intravenously at a dose of 10 mg/kg of body weight for 5 consecutive days, and then twice weekly at a reduced dose of 1 mg/kg of body weight. We found a marked decrease in EGFP expression in peritoneal cells, suggesting that AP20187 can deplete circulating BM-derived microglia in *rd7/rd7;Tg/Tg* mice (supplementary material Fig. S2A). An enlarged spleen was noted in *rd7/rd7;Tg/Tg* mice injected with AP20187 compared with the vehicle-injected mice (supplementary material Fig. S2G,D). We stained apoptotic cells selectively in the spleen section using an anti-active-caspase-3 antibody and TUNEL, and found a marked increase in apoptotic cells in AP20187-injected *rd7/rd7;Tg/Tg* mice (supplementary material Fig. S2B,C,E,F). Our hematoxylin and eosin analysis demonstrated an increase in the nucleus:cytoplasm ratio and loss of red pulp in the spleen (data not shown), suggesting the presence of extramedullary hematopoiesis in *rd7/rd7;Tg/Tg* mice after long-term depletion of circulating BM-derived microglia.

Acceleration of retinal degeneration in *rd7/rd7;Tg/Tg* mice after systemic depletion of circulating BM-derived microglia

To confirm the role of circulating BM-derived microglia in *rd7/rd7;Tg/Tg* mice, we investigated the morphological changes in the retinal rosettes and AF spots after AP20187 injection (Fig. 5A-G). We found a marked and rapid decrease in the number of retinal rosettes, which was accompanied by an increase in the number of AF spots (Fig. 5L,I). As mentioned above, increasing numbers of AF spots and decreased numbers of rosettes resemble the characteristics found in older *rd7* mice, suggesting an acceleration of retinal degeneration. For this reason, we counted the number of nuclei in the photoreceptors of *rd7/rd7;Tg/Tg* mice after 5 months of AP20187 injections, as well as that for the vehicle-injected mice (Fig. 5L). There was a significant decrease in the number of nuclei in the ONL in *rd7/rd7;Tg/Tg* mice injected with AP20187 compared with vehicle-injected mice (posterior pole, $P=0.022$; midperipheral area, $P=0.031$; $n=3$) (Fig. 5D,H,K). These data suggest that the systemic depletion of circulating BM-derived microglia accelerates retinal degeneration in *rd7/rd7;Tg/Tg* mice.

Changes in the number of proliferative cells after systemic depletion of circulating BM-derived microglia in *rd7/rd7;Tg/Tg* mice

To investigate whether retinal resident microglia proliferation accounts for the significantly increased number of AF spots observed in *rd7/rd7;Tg/Tg* mice injected with AP20187, we performed EdU labeling and Iba-1 immunostaining in *rd7/rd7;Tg/Tg* mice 1 month after treatment with AP20187 or vehicle. Compared with retinas from vehicle-injected *rd7/rd7;Tg/Tg* mice, there were significantly more labeled dividing resident

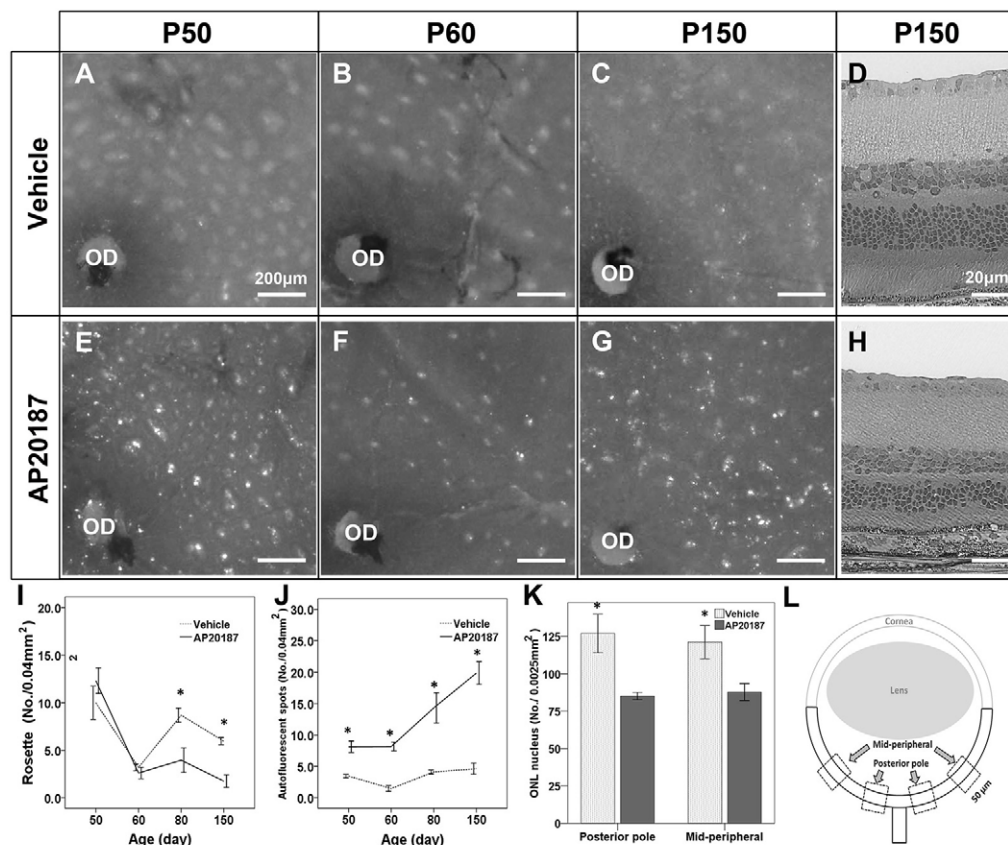


Fig. 5. Accelerated retinal degeneration after systemic depletion of circulating BM-derived microglia in *rd7/rd7;Tg/Tg* mice. (A-D) The cilioretinal flatmounts and histology from *rd7/rd7;Tg/Tg* mice treated with vehicle at P50 (A), P60 (B) and P150 (C,D). (E-H) The cilioretinal flatmounts and histology from *rd7/rd7;Tg/Tg* mice treated with AP20187 at P50 (E), P60 (F) and P150 (G,H). (I) The number of rosettes in the cilioretinal flatmounts (mean \pm s.d.) was determined at P50 ($n=8$), P60 ($n=11$), P80 ($n=3$) and P150 ($n=4$). (J) The number of AF spots in the cilioretinal flatmounts (mean \pm s.d.) was determined at P50 ($n=8$), P60 ($n=11$), P80 ($n=3$) and P150 ($n=4$). (K) The number of nuclei in the outer nuclear layer (ONL) was significantly decreased in mice injected with AP20187 for 5 months compared with mice injected with vehicle. (L) Scheme of an eye section, showing the areas in which the ONL nuclei were counted. OD, optic disc. * $p<0.05$.

microglial cells in retinas from AP20187-injected mice (Fig. 6), demonstrating an essential role for the resident microglia after the systemic depletion of circulating BM-derived microglia.

Changes in the expression of retinal cytokines/chemokines after systemic depletion of circulating BM-derived microglia in *rd7/rd7;Tg/Tg* mice

Next, we investigated the mechanism underlying the retinal degeneration observed after circulating BM-derived microglia depletion. Retinas from WT mice (C57BL/6), *rd7/rd7;Tg/Tg* mice treated with AP20187, and *rd7/rd7;Tg/Tg* mice treated with vehicle were extracted using lysis buffer and were subjected to quantitative real-time PCR (qRT-PCR; $n=3$ in each group). The genes that encode the inflammatory cytokines interleukin-1 β (IL-1 β), IL-6, tumor necrosis factor- α (TNF α) and monocyte chemoattractant protein (MCP-1) were upregulated after systemic depletion of circulating BM-derived microglia; however, the gene that encodes the anti-inflammatory cytokine TGF β 1 was downregulated (Fig. 7). TNF α was chosen for its role as the classical activator and initiator of cytotoxicity, as well as a sustainer of macrophage responses. We thus concluded that resident microglia play an essential role in, and that their proliferation upregulates, the expression of the IL-1 β , IL-6 and TNF α genes in the retina, after circulating BM-derived microglia depletion.

DISCUSSION

Microglia have been reported to play a central role in chronic degenerative conditions of the CNS, including Alzheimer's and

Parkinson's diseases, and amyotrophic lateral sclerosis (Block et al., 2007; Gentleman, 2013). In the present study, we reported the opposing roles of resident microglia and circulating BM-derived microglia in retinal degeneration.

Sequential appearance of AF spots, rosettes and microglial cells

In a previous study, we found microglia inside the ONL folding, which appeared as white dots in funduscopy and retinal rosettes in cilioretinal flatmounts (Wang et al., 2009). In the current study, TEM and immunochemical analyses demonstrated the presence of lysosomes inside these microglia, which appeared as AF spots in the cilioretinal flatmounts. Sequential analyses of the retinal rosettes and AF spots indicated that the retinal rosettes appeared earlier than the AF spots, suggesting that microglia are recruited and appear after ONL folding. The increased number of AF spots found in the older *rd7* mice might be related to an increase in activated-lysosome-laden microglia, which represent a later stage of retinal degeneration.

Based on the spatial and temporal distribution of the AF spots and rosettes, we found that microglial cells are not simply bystanders in *rd7* mice, but might contribute to the degenerative process. We hypothesize that microglia play a positive role in maintaining the environment of photoreceptors by initially cleaning up debris between photoreceptors and the RPE. A similar symbiosis between microglia and photoreceptors was found in other studies (Banerjee and Lund, 1992; Ritter et al., 2006; Sasahara et al., 2008; Joly et al., 2009; Arroba et al., 2011). Another study demonstrated that BM-derived cells can eliminate amyloid

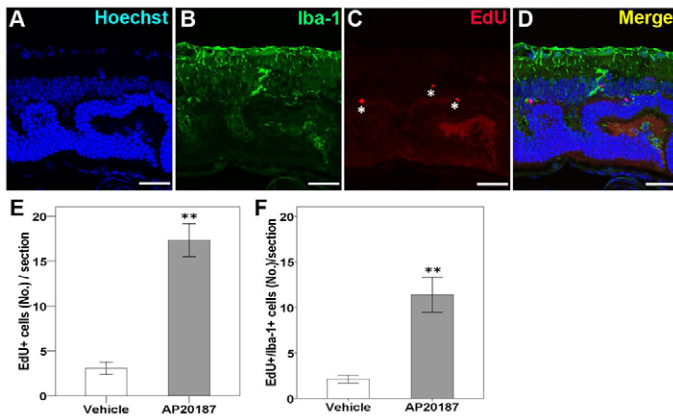


Fig. 6. Confocal images showing proliferative resident microglia in the retina of *rd7/rd7;tg/tg* mice after 4 weeks of injection of AP20187. (A-D) Proliferative cells located in the outer plexiform layer (OPL), outer nuclear layer (ONL) or ganglion cell layer exhibited EdU labeling (asterisks in C). Colocalized labeling of EdU and Iba-1 was detected (D). (E,F) The number of EdU-labeled cells was significantly increased in mice injected with AP20187 for 1 month compared with mice injected with vehicle ($n=3$ in each group). The majority of the EdU-labeled cells were colocalized with Iba-1 (F). Asterisks indicate significant difference: $**P<0.001$. Scale bars: 30 μm .

deposits in Alzheimer's disease via a cell-specific phagocytic mechanism (Simard et al., 2006).

Advantages of Mafia mice compared with BM chimeric mice

An advantage of our murine model of circulating BM-derived microglia deficiency in retinal degeneration is that, in contrast to most published macrophage-deficiency models, on which BM transplantations were performed after systemic irradiation, in our model, the resident microglia are not ablated after systemic depletion of BM-derived microglia. This helped us investigate the role of resident and circulating BM-derived microglia in retinal degeneration. Although many researchers have used BM transplantation to investigate the role of BM-derived microglia, the number of migrating BM-derived cells in normal retinas remains controversial. Xu et al. reported that a majority of retinal microglia/macrophages are replenished from circulating BM-derived cells over 6 months, with very little *in situ* proliferation (i.e. insufficient to account for renewal) (Xu et al., 2007). Kaneko et al. observed bulk BM-derived cell migration to the retina only after the induction of retinal damage (Kaneko et al., 2008). Conversely, systemic irradiation before BM transplantation might ablate resident microglia in the retina, thereby inducing additional BM-derived cell migration. In the current study, we demonstrated that AP20187 efficiently depleted circulating EGFP+ BM-derived cells in *rd7/rd7;Tg/Tg* mice (supplementary material Fig. S2), thus providing better results than BM transplantation, without damaging resident retinal microglial cells. However, we only injected AP20187 after P14 because injection is technically easier at the tail vein after this stage; as such, we could not determine the number of circulating BM-derived cells that migrated to the retina before P14 in *rd7/rd7;Tg/Tg* mice. It is noteworthy that the variance in the number of AF spots in *rd7* mice (Fig. 1E) and *rd7/rd7;Tg/Tg* mice treated with vehicle (Fig. 5) might not be identical because of an

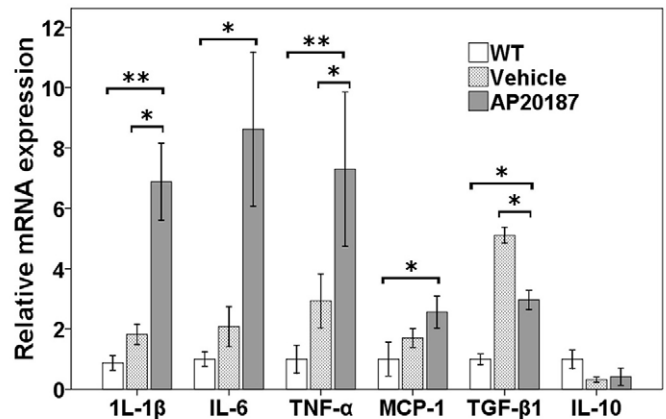


Fig. 7. Relative gene expression after systemic depletion of circulating BM-derived microglia. Quantification of gene expression changes by qRT-PCR at P60 (4 weeks after being treated with AP20187 or vehicle; $n=3$ in each group), expressed as mean fold change in comparison with wild type (WT) ± 1 s.d., showing a trend of downregulation of the gene encoding the anti-inflammatory cytokine TGF β 1, and upregulation of genes encoding the inflammatory cytokines IL-1 β , IL-6, TNF α and monocyte chemoattractant protein (MCP-1). Asterisks indicate significant difference: $*P<0.05$, $**P<0.01$, $***P<0.001$.

effect of the genetic background and/or the use of ethanol as a vehicle for AP20187 intraperitoneal injection.

In this study, we demonstrated the presence of heterogeneous populations of microglia in the retina that exhibited distinct morphological characteristics, location and distribution in *rd7/rd7;Tg/Tg* mice. Iba-1+ ramified cells have delicate processes, are located in the inner layers of the retina and are considered to be a marker of resident microglia (Sasahara et al., 2008; Joly et al., 2009). CD68 is a cytoplasmic lysosomal antigen and CD68+ amoeboid cells can represent blood-borne macrophages (Milligan et al., 1991). MHC-II+ spindle cells are regarded as antigen-presenting cells and are not present in the normal retina (Zhang et al., 2005). The intermediate filament vimentin is expressed ubiquitously in Müller cells of many mammalian species (Kivelä et al., 1986). However, although different subgroups of microglia might express different markers, we found that, not only do more than 80% of the EGFP+ cells also express Iba-1 in *rd7/rd7;Tg/Tg* mice but, also, these EGFP+ cells are different from Müller cells.

Distribution of microglia in *rd7/rd7;Tg/Tg* mice

BM-derived cells have been observed along optic nerves and retinal vessels, where activated astrocytes are present, after 24 hours of retinal degeneration induced by N-methyl-N-nitrosourea (MNU) (Kaneko et al., 2008). Similar findings of the presence of BM-derived cells in the ciliary body and in the optic nerve have also been reported in other studies that used BM transplantation (Hou et al., 2006; Xu et al., 2007). In the present study, microglial cells in *rd7* and *rd7/rd7;Tg/Tg* mice were distributed throughout the retina. Additionally, we did not find the pattern that was observed during retinal development (i.e. waves of radial migration along optic nerves and retinal vessels) in *rd7/rd7;Tg/Tg* mice treated with AP20187. One explanation for this finding is that the processes of retinal degeneration in *rd7* and *rd7/rd7;Tg/Tg* mice (with or

without AP20187) are subtle and are different from the abrupt degeneration induced by drugs or potential damage during pre-BM-transplantation irradiation. Another explanation is that AP20187 depleted most of the circulating BM-derived cells, resulting in few cells being left in circulation.

In *rd7/rd7;Tg/Tg* mice injected with AP20187, we observed the presence of EGFP+ ramified microglial cells distributed evenly and superficially in the cilioretinal flatmounts. Burnett et al. found no significant EGFP+ cell depletion in brain tissues after AP20187 injection in Mafia mice, and assumed that AP20187 cannot cross the blood-brain barrier (Burnett et al., 2004). Our immunohistochemical findings that Iba-1+ cells were distributed in the GCL and that residual ramified microglial cells remained in the cilioretinal flatmounts after AP20187 injection suggest that these EGFP+ ramified cells are resident microglia and that the dimerizing reagent AP20187 cannot effectively penetrate the blood-retina barrier. However, it should be noted that we could only inject AP20187 through the tail vein or intraperitoneally because AP20187 powder needs to dissolve in ethanol during preparation, which might cause retinal toxicity if injected intravitreally. We attempted retrobulbar injection of AP20187, but injections repeatedly resulted in eyeball ischemia and fibrosis. Additional studies are needed to optimize the dimerizer-treatment protocol to achieve depletion of microglial cells in the CNS and in the retina.

Inflammation was seen after systemic depletion of circulating BM-derived microglia

Unexpectedly, accelerated retinal degeneration occurred after the observation of the systemic depletion of circulating BM-derived microglia in the ESCS model (Fig. 5). Macrophages and microglial cells become classically activated (M1) or alternatively activated (M2) when affected by Th1- and Th2-derived cytokines, respectively. Several studies have indicated that M1 cells have strong cytotoxic activity, whereas M2 cells promote cell survival and angiogenesis, and suppress destructive immunity (Gratchev et al., 2001; Gratchev et al., 2005; Kzhyshkowska et al., 2006; Kigerl et al., 2009; Seledtsov and Seledtsova, 2012). In the retina, M2 cells secrete neurotrophic factors that promote the survival of neurons during retinal degeneration (Carwile et al., 1998; Harada et al., 2002; Arroba et al., 2011) and vascular repair in a model of ischemic retinopathy (Ritter et al., 2006). Conversely, M1 cells can induce ganglion cell and photoreceptor death by releasing cytotoxic factors (Roque et al., 1999; Zeng et al., 2005; Sivakumar et al., 2011). Inflammatory cytokines related to M1 cells include TNF α , IL-1 β and IL-6, whereas cytokines related to M2 cells include IL-10 and TGF β 1. In *rd* mice, the TNF α produced by activated microglia has been found to be neurotoxic (Zeng et al., 2005). In hypoxic neonatal retinas, TNF α and IL-1 β also seem to induce retinal ganglion cell death (Sivakumar et al., 2011).

Joly et al. have shown that both resident and BM-derived microglia cooperate to remove dead photoreceptors from retinal lesions (Joly et al., 2009). Therefore, resident microglia initially play a positive role in maintaining the environment of photoreceptors by cleaning up debris between photoreceptors and the RPE. Without the cooperation of circulating BM-derived microglia, resident microglia secrete a monocyte chemotactic protein to try to recruit additional monocytes, as seen in Fig. 7. In addition, resident microglia can proliferate and produce high levels of TNF α and IL-1 β , which subsequently lead to the acceleration of retinal degeneration.

In summary, our study demonstrates the sequence of events during the retinal degenerative process in *rd7* mice. Taking advantage of the unique characteristics of Mafia mice, we demonstrated that more than 80% of EGFP+ cells in the retina of *rd7/rd7;Tg/Tg* mice expressed Iba-1, and that resident microglia are still present in the retina because AP20187 does not cross the blood-brain barrier. For this reason, only circulating BM-derived microglia are depleted. After the systemic depletion of circulating BM-derived microglia, the cilioretinal flatmounts from *rd7/rd7;Tg/Tg* mice exhibited characteristics that mimicked those of later stages of retinal degeneration in *rd7* mice. Moreover, ONL analyses confirmed the decrease in the number of nuclei in this region in *rd7/rd7;Tg/Tg* mice. Our finding suggests that the increased number of AF spots is related to resident microglia proliferation, which established a cytokine milieu that was skewed to inflammation by upregulating the expression of the *IL-1 β* , *IL-6* and *TNF α* genes, which subsequently accelerated retinal degeneration. Future studies dedicated to the search for therapeutic agents to intervene in the inflammatory processes involved in retinal degeneration should investigate the molecular signals that act between microglial activation and photoreceptor loss.

MATERIALS AND METHODS

Mouse strains

All mice were handled in accordance with the Statement for the Use of Animals in Ophthalmic and Vision Research of the Association for Research in Vision and Ophthalmology, and all experiments were approved by the Institutional Animal Care and Use Committee of the Chang Gung Memorial Hospital.

C57BL/6, B6.Cg-*Nr2e3*^{rd7/rd7} (*rd7*) and Mafia (Tg/Tg) mice were purchased from the Jackson Laboratory (Bar Harbor, ME) and were housed at a local animal facility under a 12-hour light/12-hour dark cycle. All mice used in this study were in the B6 background. *rd7* mice were outcrossed to Tg/Tg mice, with F₁ offspring from each of these outcrosses being intercrossed to generate F₂ mice. The two-generation outcross-intercross series was used to generate *rd7/rd7;Tg/Tg* double homozygotes for the *Nr2e3*^{rd7/rd7} mutation and Tg/Tg, as described previously (Haider et al., 2001). The offspring from an intercross of *rd7/rd7;Tg/Tg* mice were used in this study.

Screening for the transgene in Mafia mice and for the *Nr2e3* gene in *rd7* mice

Genomic DNA was extracted from mouse tails using the QuickExtract kit (Epicentre, Madison, WI). To detect the transgene in Mafia mice, the following EGFP primers were used: 5'-AAGTTCATCTGCACCACCG-3' (forward) and 5'-TCCTTGAA-GAAGATGGTTCG-3' (reverse). Homozygous *rd7* animals were differentiated from heterozygous and WT controls via PCR analysis of genomic DNA using primers designed for the *Nr2e3* gene. A forward primer located in exon 4 (5'-GTAGCCTCTCCT-GCTCTGGCAG-3') and a reverse primer located in exon 5 (5'-CAGGTTGAAAACACAGGCAAG-3') were used to amplify a 339 bp fragment in WT animals and a 239 bp fragment in *rd7* mutants and in heterozygotes harboring the deletion. The fragments were amplified using 5 μ l of DNA extract in a 50.0 μ l PCR reaction. The cycling conditions were an initial 10 minutes incubation at 94°C, followed by ten cycles of 94°C for 10 seconds, 60°C for 30 seconds

and 68°C for 60 seconds, and 20 cycles of 94°C for 10 seconds, 55°C for 30 seconds and 68°C for 60 seconds, and a final extension at 68°C for 7 minutes. PCR products were electrophoresed on 2% agarose gels (Seakem LE, Lonza Rockland, Rockland, ME) and visualized via ethidium bromide staining. The homozygosity of *Tg* mice was determined by calculating the Δ Ct using real-time PCR with primers for *EGFP* (test gene) and *ApoB* (reference gene).

Cilioretinal flatmount and histochemical analyses

Eyes were enucleated and placed in 4% paraformaldehyde for 1 hour at room temperature (RT). The cornea and lens were removed from each eye under a surgical microscope. Whole eyecups were flattened using four to eight radial cuts and mounted with mounting medium (VECTASHIELD, Burlingame, CA). Autofluorescence was detected using standard fluorescence microscopy, as described previously (Wang et al., 2009). Immunostaining was performed as described previously (Wang et al., 2009; Wang et al., 2010).

After fixation as described above, eyes were frozen in optimum cutting temperature compound (Tissue-Tek OCT; Miles Laboratories, Elkhart, IN). Frozen eyes were cryosectioned at a thickness of 10 μ m. Blocking was performed using 10% normal blocking serum in PBS with 0.3% Triton X-100 (blocking solution) for 30 minutes at RT. Sections were then incubated with primary antibodies diluted in 4% normal blocking serum in PBS with 0.1% Triton X-100 for 2 hours at RT. The samples were subsequently incubated for 40 minutes at RT with secondary antibodies diluted in PBS with 0.1% Triton X-100. The primary antibodies used were anti-EGFP (1:2000, Novus Biologicals, Littleton, CO), anti-F4/80 (1:100, Abcam, Cambridge, MA), anti-CD68 (1:200, Abcam, Cambridge, MA), anti-ionized calcium-binding adaptor molecule 1 (Iba-1; 1:1000, Wako, Osaka, Japan), anti-major histocompatibility complex (MHC) class II (1:100, BD Pharmingen, San Jose, CA), anti-vimentin (1:200, Sigma-Aldrich, St Louis, MO) and anti-active caspase 3 (1:200, BD Pharmingen, San Jose, CA). The secondary antibodies used were Alexa-Fluor-488- or -555-conjugated antibodies (dilution, 1:1000; Invitrogen, Carlsbad, CA). After being washed three times with PBS, the sections were mounted with mounting medium containing the nuclear dye Hoechst (Invitrogen, Carlsbad, CA) and viewed using a Leica TCS SP5 confocal microscope (Leica Microsystems GmbH, Wetzlar, Germany). Images were merged digitally to assess triple labeling.

The Click-iT 5-ethynyl-2'-deoxyuridine (EdU) labeling kit was used to perform EdU labeling (Invitrogen, Carlsbad, CA). Timed, *rd7/rd7;Tg/Tg* mice were injected with EdU solution (30 μ g/g of body weight) continuously for 2 days, and then killed on the third day. Eyes were collected, fixed and processed according to the immunostaining protocol mentioned above. EdU staining was performed according to the protocol provided by the kit.

Transmission electron microscopy

For TEM, P60 *rd7* and P60 WT mice were first perfused transcardially with 2% glutaraldehyde and 2% paraformaldehyde in phosphate buffer. Subsequently, the eyes of animals were enucleated and placed in 3% glutaraldehyde with 2% paraformaldehyde for 2 hours at 4°C. The cornea was cut and the lens was removed, to allow further fixation for 1 hour. After refixation in 1% osmium tetroxide for 4 hours at room temperature, the eye samples were prepared as described previously (Yeh et al., 2008). After fixation,

the eye samples were washed in phosphate buffer, dehydrated and embedded in Epon 812 epoxy resin. Serial semi-thin sections were obtained along the long axis and stained with toluidine blue. Ultrathin sections from selected areas were collected on 75 mesh copper grids and stained with uranyl acetate and lead citrate, and images were photographed with an Hitachi 7100 transmission electron microscope (Hitachi, Tokyo, Japan) equipped with an AMT digital camera.

qRT-PCR

Total mRNA was prepared from freshly dissected whole mouse retinas using the TRIzol reagent (Molecular Research Center, Cincinnati, OH). The mRNA was transcribed using SuperScript III Reverse Transcriptase (Invitrogen, Carlsbad, CA) and qRT-PCR assays were performed using the KAPA SYBR® FAST qPCR Kit (Kapa Biosystems, Woburn, MA). Amplified products were run on the Mx3000P™ instrument (Stratagene) in a final reaction volume of 10 μ l. The following thermocycling profile was used: denaturation at 95°C for 3 minutes and 40 cycles of 95°C for 3 seconds, 55°C for 20 seconds and 72°C for 1 second. The MxPro software was used to set baselines and CT values according to the guidelines provided by Stratagene. The expression levels of each gene were normalized to the PCR products of β -actin. The following primers were used for qRT-PCR: IL-1 β , 5'-TGTGAAATGCCACCTTTTGA-3' and 5'-CTGCCTGAAGCTCTTGTGTTGA-3'; IL-6, 5'-TGTGCAATGGCAATTCTGAT-3' and 5'-CTCTGAAGGACTCTGGC-TTTG-3'; IL-10, 5'-TGGCCCAGAAATCAAGGAGC-3' and 5'-CAGCAGACTCAATACACACT-3'; TNF α , 5'-CCACCACGCTCTTCTGTCTA-3' and 5'-CACTTGGTGGTTTGCTACGA-3'; TGF- β 1, 5'-TTGCTTCAGCTCCACAGAGA-3' and 5'-TGGTTGTAGAGGGCAAGGAC-3'; MCP-1, 5'-TCTCTTCC-TCCACC ACTATGCA-3' and 5'-GGCTGAGACAGCACGTGGAT-3'; β -actin, 5'-TCATGAAGTGTGACGTTGACATCCGT-3' and 5'-CCTAGAAGCATTGCGGTGCAGGATG-3'.

Ablation of BM-derived microglia in transgenic mice

The depletion protocol used here was as described previously (Burnett et al., 2004; Qualls et al., 2006). AP20187 (Ariad Pharmaceuticals, Cambridge, MA) was injected (i.v.) into P14 *rd7/rd7;Tg/Tg* mice once daily at a dose of 10 mg/kg of body weight for 5 consecutive days, for initial cell depletion. This depletion protocol has been shown to cause 80-95% depletion of monocytes, macrophages and DCs in many tissues (Burnett et al., 2004). Depletion can be prolonged by subsequent injection of AP20187 twice weekly at a reduced dose of 1 mg/kg of body weight (Qualls et al., 2006).

Flow cytometry to determine macrophage and DC depletion

Flow cytometric analysis and sorting were performed on a BD FACSCalibur flow cytometer (BD Biosciences, San Jose, CA) and the data collected were analyzed using the Flowjo software. Peritoneal lavage was performed under anesthesia using 5 ml of PBS and peripheral blood was collected from the tail vein. The preparations were resuspended in tenfold ACK lysis buffer (Lonza Walkersville, Walkersville, MD), spun and processed using flow cytometry. Histograms were graphed from events gated by forward and side scatter (FSC and SSC, respectively) to the region where macrophages and lymphocytes would be found.

Quantification and statistical analyses

In Fig. 1H, the number of AF spots and rosettes within fields of 200×200 μm (the average of four fields from the central retina and eight fields from the peripheral retina) was determined and processed statistically from montage images of the cilioretinal flatmounts. To compare the EdU-labeled cells in *rd7/rd7;Tg/Tg* mice injected with AP20187 or vehicle, the number of EdU-labeled cells was counted and averaged from 15 serial sections cut around the optic nerve head in each mouse ($n=3$ in each group).

All experimental data were assessed by an operator blinded to the treatment condition. Significance was determined using a paired *t*-test. $P<0.05$ was considered significant. All analyses were performed using the SPSS 15.0 software (SPSS, Chicago, IL).

ACKNOWLEDGEMENTS

We greatly appreciate Tsai-Ling Liao and Sheng-Chieh Huang for their excellent technical assistance throughout the course of this study, and Professor Kuo-Shyan Lu, Professor June-Hong Lue and Professor Chang-Hao Yang for their critical comments on the manuscript. We also thank Hui-Chun Kung and Ya-Ling Chen from Microscope Core Laboratory, Chang Gung Memorial Hospital, Linkou, for the preparation of the TEM studies. Facilities provided by grants from the Ministry of Education, Taiwan, to the Center of Genomic Medicine in National Taiwan University are also acknowledged.

COMPETING INTERESTS

The authors declare that they do not have any competing or financial interests.

AUTHOR CONTRIBUTIONS

N.-K.W., S.H.T. and C.-L.C. conceived and designed the experiments. N.-K.W., C.-L.C., C.-H.L. and L.-K.Y. performed the experiments. N.-K.W., S.H.T. and C.L.C. analyzed the data. N.-K.W., J.K. and T.N. contributed reagents/materials/analysis tools. N.-K.W., C.-H.L., S.H.T. and C.-L.C. wrote the paper.

FUNDING

This work was supported by grants from the Taiwan National Science Council (NSC-99-2314-B-182A-029-MY3 to N.-K.W. and NSC-100-2320-B-002-085 to C.-L.C.), Chang Gung Memorial Hospital (CMRPG 381561~381563 and 391801~391802 to N.-K.W.), the National Eye Institute/NIH [Bethesda, MD (EY018213 to S.H.T.) and Core Support for Vision Research, Columbia University (P30EY019007)], Foundation Fighting Blindness (Owings Mills, MD), Department of Defense (TS080017), and unrestricted funds from Research to Prevent Blindness (New York, NY). S.H.T. is a Burroughs-Wellcome Program in Biomedical Sciences Fellow, and is also supported by the Charles E. Culpeper- Partnership for Cures 07-CS3, Crowley Research Fund, Schneeweiss Stem Cell Fund, New York State N09G-302 and Joel Hoffmann Scholarship. The funders had no role in study design, data collection and analysis, decision to publish, or preparation of the manuscript.

SUPPLEMENTARY MATERIAL

Supplementary material for this article is available at <http://dmm.biologists.org/lookup/suppl/doi:10.1242/dmm.012112/-/DC1>

REFERENCES

- Akhmedov, N. B., Piriev, N. I., Chang, B., Rapoport, A. L., Hawes, N. L., Nishina, P. M., Nusinowitz, S., Heckenlively, J. R., Roderick, T. H., Kozak, C. A. et al. (2000). A deletion in a photoreceptor-specific nuclear receptor mRNA causes retinal degeneration in the *rd7* mouse. *Proc. Natl. Acad. Sci. USA* **97**, 5551-5556.
- Amoakul, W. M., Mahon, G. J., Gardiner, T. A., Frew, L. and Archer, D. B. (1992). Late ultrastructural changes in the retina of the rat following low-dose X-irradiation. *Graefes Arch. Clin. Exp. Ophthalmol.* **230**, 569-574.
- Arroba, A. I., Alvarez-Lindo, N., van Rooijen, N. and de la Rosa, E. J. (2011). Microglia-mediated IGF-1 neuroprotection in the *rd10* mouse model of retinitis pigmentosa. *Invest. Ophthalmol. Vis. Sci.* **52**, 9124-9130.
- Ashwell, K. W., Holländer, H., Streit, W. and Stone, J. (1989). The appearance and distribution of microglia in the developing retina of the rat. *Vis. Neurosci.* **2**, 437-448.
- Banerjee, R. and Lund, R. D. (1992). A role for microglia in the maintenance of photoreceptors in retinal transplants lacking pigment epithelium. *J. Neurocytol.* **21**, 235-243.
- Block, M. L., Zecca, L. and Hong, J. S. (2007). Microglia-mediated neurotoxicity: uncovering the molecular mechanisms. *Nat. Rev. Neurosci.* **8**, 57-69.
- Burnett, S. H., Kershen, E. J., Zhang, J., Zeng, L., Straley, S. C., Kaplan, A. M. and Cohen, D. A. (2004). Conditional macrophage ablation in transgenic mice expressing a Fas-based suicide gene. *J. Leukoc. Biol.* **75**, 612-623.
- Burnett, S. H., Beus, B. J., Avdiushko, R., Qualls, J., Kaplan, A. M. and Cohen, D. A. (2006). Development of peritoneal adhesions in macrophage depleted mice. *J. Surg. Res.* **131**, 296-301.
- Caicedo, A., Espinosa-Heidmann, D. G., Piña, Y., Hernandez, E. P. and Cousins, S. W. (2005). Blood-derived macrophages infiltrate the retina and activate Muller glial cells under experimental choroidal neovascularization. *Exp. Eye Res.* **81**, 38-47.
- Carwile, M. E., Culbert, R. B., Sturdivant, R. L. and Kraft, T. W. (1998). Rod outer segment maintenance is enhanced in the presence of bFGF, CNTF and GDNF. *Exp. Eye Res.* **66**, 791-805.
- Cecchini, M. G., Dominguez, M. G., Mocci, S., Wetterwald, A., Felix, R., Fleisch, H., Chisholm, O., Hofstetter, W., Pollard, J. W. and Stanley, E. R. (1994). Role of colony stimulating factor-1 in the establishment and regulation of tissue macrophages during postnatal development of the mouse. *Development* **120**, 1357-1372.
- Cuadros, M. A. and Navascués, J. (1998). The origin and differentiation of microglial cells during development. *Prog. Neurobiol.* **56**, 173-189.
- Gentleman, S. M. (2013). Review: microglia in protein aggregation disorders: friend or foe? *Neuropathol. Appl. Neurobiol.* **39**, 45-50.
- Gratchev, A., Guillot, P., Hakiy, N., Politz, O., Orfanos, C. E., Schledzewski, K. and Goerdit, S. (2001). Alternatively activated macrophages differentially express fibronectin and its splice variants and the extracellular matrix protein betaG-H3. *Scand. J. Immunol.* **53**, 386-392.
- Gratchev, A., Kzhyshkowska, J., Utikal, J. and Goerdit, S. (2005). Interleukin-4 and dexamethasone counterregulate extracellular matrix remodelling and phagocytosis in type-2 macrophages. *Scand. J. Immunol.* **61**, 10-17.
- Haider, N. B., Naggert, J. K. and Nishina, P. M. (2001). Excess cone cell proliferation due to lack of a functional NR2E3 causes retinal dysplasia and degeneration in *rd7/rd7* mice. *Hum. Mol. Genet.* **10**, 1619-1626.
- Hanisch, U. K. and Kettenmann, H. (2007). Microglia: active sensor and versatile effector cells in the normal and pathologic brain. *Nat. Neurosci.* **10**, 1387-1394.
- Harada, T., Harada, C., Kohsaka, S., Wada, E., Yoshida, K., Ohno, S., Mamada, H., Tanaka, K., Parada, L. F. and Wada, K. (2002). Microglia-Müller glia cell interactions control neurotrophic factor production during light-induced retinal degeneration. *J. Neurosci.* **22**, 9228-9236.
- Hou, H. Y., Wang, Y. S., Xu, J. F., Wang, Y. C. and Liu, J. P. (2006). The dynamic conduct of bone marrow-derived cells in the choroidal neovascularization microenvironment. *Curr. Eye Res.* **31**, 1051-1061.
- Joly, S., Francke, M., Ulbricht, E., Beck, S., Seeliger, M., Hirrlinger, P., Hirrlinger, J., Lang, K. S., Zinkernagel, M., Odermatt, B. et al. (2009). Cooperative phagocytes: resident microglia and bone marrow immigrants remove dead photoreceptors in retinal lesions. *Am. J. Pathol.* **174**, 2310-2323.
- Kaneko, H., Nishiguchi, K. M., Nakamura, M., Kachi, S. and Terasaki, H. (2008). Characteristics of bone marrow-derived microglia in the normal and injured retina. *Invest. Ophthalmol. Vis. Sci.* **49**, 4162-4168.
- Kigerl, K. A., Gensel, J. C., Ankeny, D. P., Alexander, J. K., Donnelly, D. J. and Popovich, P. G. (2009). Identification of two distinct macrophage subsets with divergent effects causing either neurotoxicity or regeneration in the injured mouse spinal cord. *J. Neurosci.* **29**, 13435-13444.
- Kivelä, T., Tarkkanen, A. and Virtanen, I. (1986). Intermediate filaments in the human retina and retinoblastoma. An immunohistochemical study of vimentin, glial fibrillary acidic protein, and neurofilaments. *Invest. Ophthalmol. Vis. Sci.* **27**, 1075-1084.
- Kreutzberg, G. W. (1996). Microglia: a sensor for pathological events in the CNS. *Trends Neurosci.* **19**, 312-318.
- Kzhyshkowska, J., Workman, G., Cardó-Vila, M., Arap, W., Pasqualini, R., Gratchev, A., Krusell, L., Goerdit, S. and Sage, E. H. (2006). Novel function of alternatively activated macrophages: stabilin-1-mediated clearance of SPARC. *J. Immunol.* **176**, 5825-5832.
- Langmann, T. (2007). Microglia activation in retinal degeneration. *J. Leukoc. Biol.* **81**, 1345-1351.
- Milligan, C. E., Cunningham, T. J. and Levitt, P. (1991). Differential immunochemical markers reveal the normal distribution of brain macrophages and microglia in the developing rat brain. *J. Comp. Neurol.* **314**, 125-135.
- Mustafi, D., Kevany, B. M., Genoud, C., Okano, K., Cideciyan, A. V., Sumaroka, A., Roman, A. J., Jacobson, S. G., Engel, A., Adams, M. D. et al. (2011). Defective photoreceptor phagocytosis in a mouse model of enhanced S-cone syndrome causes progressive retinal degeneration. *FASEB J.* **25**, 3157-3176.
- Ng, T. F. and Streilein, J. W. (2001). Light-induced migration of retinal microglia into the subretinal space. *Invest. Ophthalmol. Vis. Sci.* **42**, 3301-3310.
- Qualls, J. E., Kaplan, A. M., van Rooijen, N. and Cohen, D. A. (2006). Suppression of experimental colitis by intestinal mononuclear phagocytes. *J. Leukoc. Biol.* **80**, 802-815.
- Ritter, M. R., Banin, E., Moreno, S. K., Aguilar, E., Dorrell, M. I. and Friedlander, M. (2006). Myeloid progenitors differentiate into microglia and promote vascular repair in a model of ischemic retinopathy. *J. Clin. Invest.* **116**, 3266-3276.

- Roque, R. S., Rosales, A. A., Jingjing, L., Agarwal, N. and Al-Ubaidi, M. R.** (1999). Retina-derived microglial cells induce photoreceptor cell death in vitro. *Brain Res.* **836**, 110-119.
- Sasahara, M., Otani, A., Oishi, A., Kojima, H., Yodoi, Y., Kameda, T., Nakamura, H. and Yoshimura, N.** (2008). Activation of bone marrow-derived microglia promotes photoreceptor survival in inherited retinal degeneration. *Am. J. Pathol.* **172**, 1693-1703.
- Seledtsov, V. I. and Seledtsova, G. V.** (2012). A balance between tissue-destructive and tissue-protective immunities: a role of toll-like receptors in regulation of adaptive immunity. *Immunobiology* **217**, 430-435.
- Simard, A. R., Soulet, D., Gowing, G., Julien, J. P. and Rivest, S.** (2006). Bone marrow-derived microglia play a critical role in restricting senile plaque formation in Alzheimer's disease. *Neuron* **49**, 489-502.
- Sivakumar, V., Foulds, W. S., Luu, C. D., Ling, E. A. and Kaur, C.** (2011). Retinal ganglion cell death is induced by microglia derived pro-inflammatory cytokines in the hypoxic neonatal retina. *J. Pathol.* **224**, 245-260.
- Tambuyzer, B. R., Ponsaerts, P. and Nouwen, E. J.** (2009). Microglia: gatekeepers of central nervous system immunology. *J. Leukoc. Biol.* **85**, 352-370.
- Wang, N. K., Fine, H. F., Chang, S., Chou, C. L., Cella, W., Tosi, J., Lin, C. S., Nagasaki, T. and Tsang, S. H.** (2009). Cellular origin of fundus autofluorescence in patients and mice with a defective NR2E3 gene. *Br. J. Ophthalmol.* **93**, 1234-1240.
- Wang, N. K., Tosi, J., Kasanuki, J. M., Chou, C. L., Kong, J., Parmalee, N., Wert, K. J., Allikmets, R., Lai, C. C., Chien, C. L. et al.** (2010). Transplantation of reprogrammed embryonic stem cells improves visual function in a mouse model for retinitis pigmentosa. *Transplantation* **89**, 911-919.
- Xu, H., Chen, M., Mayer, E. J., Forrester, J. V. and Dick, A. D.** (2007). Turnover of resident retinal microglia in the normal adult mouse. *Glia* **55**, 1189-1198.
- Yeh, L. K., Liu, C. Y., Chien, C. L., Converse, R. L., Kao, W. W., Chen, M. S., Hu, F. R., Hsieh, F. J. and Wang, I. J.** (2008). Molecular analysis and characterization of zebrafish keratocan (*zKera*) gene. *J. Biol. Chem.* **283**, 506-517.
- Zeng, H. Y., Zhu, X. A., Zhang, C., Yang, L. P., Wu, L. M. and Tso, M. O.** (2005). Identification of sequential events and factors associated with microglial activation, migration, and cytotoxicity in retinal degeneration in rd mice. *Invest. Ophthalmol. Vis. Sci.* **46**, 2992-2999.
- Zhang, C., Lam, T. T. and Tso, M. O.** (2005). Heterogeneous populations of microglia/macrophages in the retina and their activation after retinal ischemia and reperfusion injury. *Exp. Eye Res.* **81**, 700-709.



1 **SUPPLEMENTARY FIGURE LEGENDS**

2 **Figure S1. Body weight changes after systemic depletion of circulating BM-derived**
3 **microglia.**

4 **A and B:** After systemic macrophage ablation using AP20187, body weight didn't increase as
5 fast in the AP20187 mice than in the vehicle treated animal.

6

7 **Figure S2. Systemic Depletion of Circulating BM-derived Microglia**

8 **A:** Peritoneal cells from an *rd7/rd7;Tg/Tg* mouse were analyzed for EGFP expression using
9 cytometric analysis after treatment with AP20187 (i.v.) for 3 weeks and 6 weeks. Histograms
10 were graphed from events gated by forward and side scatter (FSC and SSC, respectively) to
11 the region where macrophages and lymphocytes would be found. Immunostaining of spleens
12 of *rd7/rd7;Tg/Tg* mice 8 weeks after being injected with vehicle (**B** and **C**) and AP20187 (**E**
13 and **F**) showed more apoptotic cells (brown, active caspase 3; green, TUNEL) in
14 AP20187-injected groups. Nuclei are stained with Hoechst (**C** and **F**). Enlarged spleens were
15 noted in *rd7/rd7;Tg/Tg* mice 8 weeks after injection with AP20187 (**G**) compared with
16 animals injected with vehicle (**D**). Scale bar: (**B**, **C**, **E**, **F**) 20 μm .

17

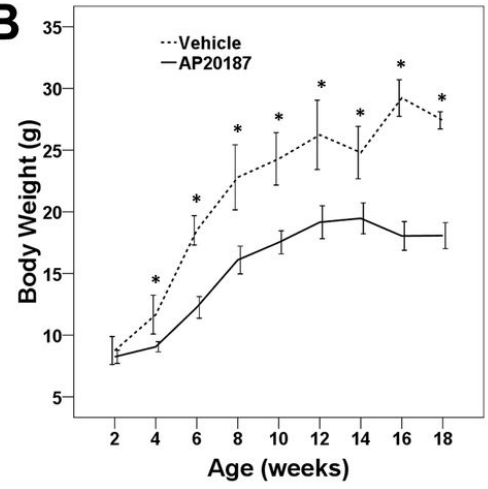
A

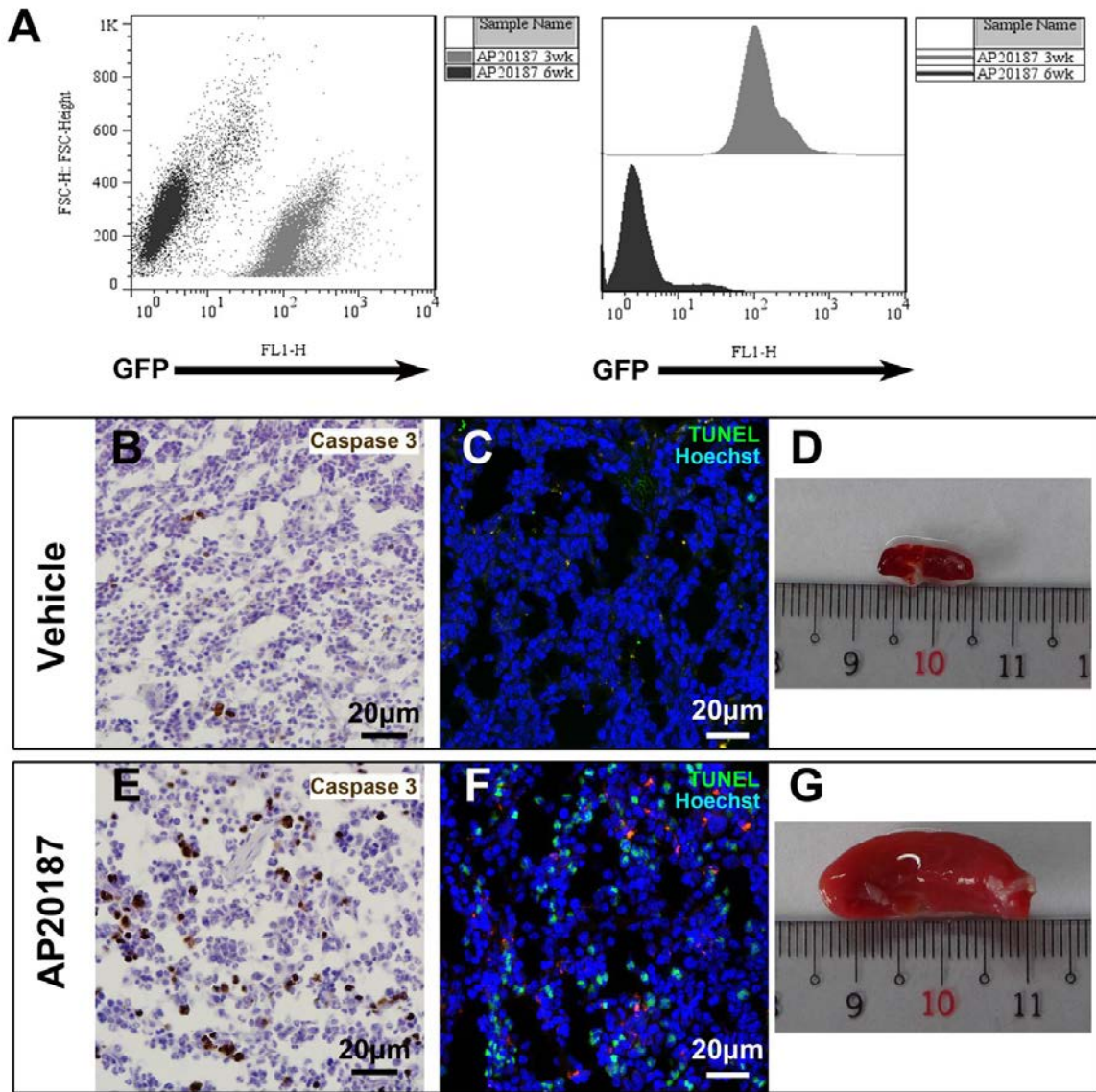
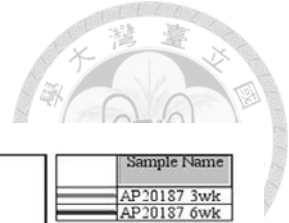
	AP20187 (No.)	Vehicle (No.)	P Value
BW 2 wks, gm	8.25 ± 1.02 (15)	8.76 ± 1.79 (10)	0.375
BW 4 wks, gm	9.06 ± 0.80 (15)	11.67 ± 2.49 (10)	0.009
BW 6 wks, gm	12.25 ± 1.70 (15)	18.50 ± 1.88 (10)	<0.001
BW 8 wks, gm	16.10 ± 2.18 (15)	22.80 ± 4.17 (10)	0.001
BW 10 wks, gm	17.52 ± 1.75 (14)	24.30 ± 3.36 (10)	<0.001
BW 12 wks, gm	19.15 ± 2.31 (12)	26.24 ± 3.97 (8)	0.001
BW 14 wks, gm	19.47 ± 1.98 (10)	24.80 ± 2.81 (7)	<0.001
BW 16 wks, gm	18.04 ± 1.53 (7)	29.22 ± 1.82 (6)	<0.001
BW 18 wks, gm	18.07 ± 1.18 (5)	27.42 ± 0.86 (6)	<0.001

BW: body weight; No.: number.

19

B





21
22